Stony Brook University

Andes Virus Regulation of Cellular MicroRNAs Contributes to Hantavirus–Induced Endothelial Cell Permeability

A Dissertation Presented

by

Timothy Pepini

to

The Graduate School

in Partial Fulfillment of the

Requirements

for the Degree of

Doctor of Philosophy

In

Molecular and Cellular Biology

Stony Brook University

December 2010

Stony Brook University
The Graduate School

Timothy Pepini

We, the dissertation committee for the above candidate for the degree of Doctor of Philosophy, hereby recommend acceptance of this dissertation.

Erich R. Mackow – Dissertation Advisor
Professor – Department of Molecular Genetics and Microbiology

Patrick Hearing – Chairperson of Defense
Professor – Department of Molecular Genetics and Microbiology

Janet Hearing
Associate Professor – Department of Molecular Genetics and Microbiology

David Thanassi
Professor – Department of Molecular Genetics and Microbiology

Eckard Wimmer
Distinguished Professor – Department of Molecular Genetics and Microbiology

This dissertation is accepted by the Graduate School

Lawrence Martin
Dean of the Graduate School

Abstract of the Dissertation

Andes Virus Regulation of Cellular MicroRNAs Contributes to Hantavirus–Induced Endothelial Cell Permeability

by

Timothy Pepini

Doctor of Philosophy

in

Molecular and Cellular Biology

Stony Brook University

2010

Hantaviruses infect human endothelial cells (ECs) and cause two diseases marked by vascular permeability defects: hemorrhagic fever with renal syndrome (HFRS) and hantavirus pulmonary syndrome (HPS). Vascular permeability occurs in the absence of EC lysis suggesting that hantaviruses alter normal EC fluid barrier functions. Hantavirus–infected endothelial cells are hyper–responsive to vascular endothelial growth factor (VEGF) which directs changes in EC adherens junctions and induces paracellular permeability. However, VEGF–directed responses are regulated by cellular microRNAs (miRNAs). The hantavirus nucleocapsid (N) protein binds cellular and viral RNA and reportedly co–localizes with P–bodies where miRNAs mature. These findings suggest that

hantaviruses may modify miRNA regulation of EC protein expression. Here we analyzed miRNAs within endothelial cells infected by the HPS–causing Andes hantavirus (ANDV). The levels of 352 human miRNAs were evaluated within ANDV–infected ECs using quantitative RT–PCR arrays. Fourteen miRNAs were upregulated >4–fold following infection by ANDV, including 6 miRNAs that are associated with changes in vascular integrity. These findings suggest that ANDV alters EC miRNAs that regulate cellular permeability. Nine miRNAs were downregulated >3–fold following ANDV infection. The level of miR–410 was decreased by 3,400–fold in ANDV infected cells, although the role of miR–410 in regulating EC functions is currently unknown. We evaluated ANDV–induced changes in miR–126, an endothelial cell–specific miRNA, which regulates vascular integrity by downregulating SPRED1 and PIK3R2 mRNAs. However, the level of miR–126 was only increased 2–fold by ANDV infection and, in contrast to miR–126 changes, SPRED1 and PIK3R2 mRNA levels increased 10– and 7–fold, respectively, in ANDV infected ECs but remained unchanged in ECs infected by a nonpathogenic hantavirus, Tula (TULV). Since SPRED1 increases EC permeability, we evaluated the effect of SPRED1 siRNAs on ANDV induced EC permeability. SiRNA knockdown of SPRED1 dramatically decreased the permeability of ANDV–infected ECs in response to VEGF suggesting that increased SPRED1 levels contribute to EC permeability during ANDV infection. These findings suggest the potential for ANDV to interfere with miR–126

directed downregulation of SPRED1, resulting in the enhanced EC permeability of ANDV infected cells. These results suggest that ANDV infection alters the function of specific endothelial cell miRNAs that contribute to EC barrier functions and paracellular permeability.

Table of Contents

List of Abbreviations

AJ	Adherens Junction
ANDV	Andes Virus
Ang1	Angiopoietin 1
BSA	Bovine Serum Albumin
BSL	Biosafety Level
BUN	Bunyamwera Virus
C_t	Threshold Cycle
DMEM	Dulbecco's Modified Eagle Medium
EBM–2	Essential Basal Medium–2
EC	Endothelial Cell
ECM	Extracellular Matrix
ECMO	Extracorporeal Membrane Oxygenation
FCS	Fetal Calf Serum
GAPDH	Glyceraldehyde–3–Phosphate Dehydrogenase
GFP	Green Fluorescent Protein
G_N–T	G_N Cytoplasmic Tail
GPC	Glycoprotein Precursor
HFRS	Hemorrhagic Fever with Renal Syndrome
HPS	Hantavirus Pulmonary Syndrome
HRP	Horse Radish Peroxidase
HUVEC	Human Umbilical Vein Endothelial Cell
IFN	Interferon
IRES	Internal Ribosomal Entry Site
IRF–3	Interferon Regulatory Factor 3
ISG56	Interferon Stimulated Gene 56
ISRE	Interferon Stimulated Response Element
KHF	Korean Hemorrhagic Fever
L	Large Segment
M	Medium Segment
MiRNA	MicroRNA
MxA	Myxovirus Resistance A
N	Nucleocapsid
NA	Neuraminidase
NE	Nephropathia Epidemica
NSs	Non–Structural Protein Encoded by the S Segment
ORF	Open Reading Frame
PAGE	Polyacrylamide Gel Electrophoresis
P–bodies	Processing Bodies
PBS	Phosphate–Buffered Saline

PHV	Prospect Hill Virus
PIK3R2	Phosphoinositide–3–Kinase, Regulatory Subunit 2
P.I.	Post Infection
Pol I	RNA Polymerase I
Pol II	RNA Polymerase II
Pol	ANDV Polymerase
PSI	Plexin–Semaphorin–Integrin
RIG–I	Retinoic Acid Inducible Gene–I
RNP	Ribonucleoprotein
S	Small Segment
S.E.M.	Standard Error of the Mean
S1P	Sphingosine–1–Phosphate
SDM	Site–Directed Mutagenesis
SDS	Sodium Dodecyl Sulfate
SEOV	Seoul Virus
SNV	Sin Nombre Virus
SPRED1	Sprouty–Related EVH1 Domain Containing Protein 1
SV40	Simian Virus 40
TBK1	TANK Binding Kinase 1
TESK1	Testis–Specific Protein Kinase 1
TRAF3	TNF Receptor–Associated Factor 3
TULV	Tula Virus
VE–cadherin	Vascular Endothelial Cadherin
VEGF	Vascular Endothelial Growth Factor
VEGFR2	Vascular Endothelial Growth Factor Receptor 2

List of Tables

List of Figures

Chapter 1:

Hantaviruses

Historical Perspective

The first hantavirus infections resulting in hemorrhagic disease were documented by Japanese physicians in the 1930s. The disease was subsequently identified as resulting from hantavirus infection and termed Hemorrhagic Fever with Renal Syndrome (HFRS). Field troops were afflicted with a hemorrhagic fever accompanied by renal complications resulting in a 10% mortality rate (96). American physicians first encountered the disease during the Korean War (1951–1954) when over 3,000 troops were afflicted an acute febrile illness with organ failure, which was named Korean Hemorrhagic Fever (KHF) (29, 175)

It was not until 1976 that the causative agent of KHF was isolated from its host, *Apodemus agrarius*, the striped field mouse. The virus was named Hantaan virus after the Hantaan River in Korea near where the virus was isolated (116). Following identification of Hantaan virus, the etiological agents of other HFRS–causing diseases were discovered throughout Eurasia including Seoul virus (Asia), Dobrava virus (Eastern Europe), and Puumala virus (Scandinavia) (17, 116, 125, 179). Hantaan and Dobrava viruses result in severe HFRS while Puumala virus results in a milder form termed nephropathia epidemica (NE) (29, 96).

Hantaviruses were first recognized in the Americas (Figure 1) in the Four Corners region of the Southwestern United States following a 1993 outbreak of a severe respiratory illness. Flu–like symptoms were experienced early during

hantavirus infection followed by rapid onset of acute pulmonary edema and thrombocytopenia. Patients succumbed to acute respiratory distress with a 75% mortality rate (148, 179).

Unexpectedly, examination of patient sera revealed cross–reactivity with hantavirus antigens (175). The causative agent was quickly identified as an novel hantavirus that caused a clinically–distinct disease from Eurasian hantaviruses, and was called Hantavirus Pulmonary Syndrome (HPS). The newly–identified hantavirus was named Sin Nombre virus (SNV) and was found to be carried by the common deer mouse (*Peromyscus maniculatus*) (96, 179). Subsequent to the discovery of SNV in the American Southwest, a number of other hantaviruses were described throughout the Americas (43, 95, 96) (Table 1). The occurrence of HPS is far lower than HFRS in Eurasia (approximately 1,000 cases have been documented in the United States since 1993). HPS continues to result in a high mortality rate (~45%) even with treatment (150, 161).

Although pathogenic hantaviruses constitute the majority of known hantaviruses, at least 2 nonpathogenic hantaviruses have been discovered. Nonpathogenic Tula virus (TULV) is found throughout Europe and carried by *Microtus arvalis* (common vole). A second nonpathogenic hantavirus was isolated in the United States in Prospect Hill, Maryland carried by *Microtus pennsylvanicus* (meadow vole) and called Prospect Hill virus (PHV) (Table 1).

Hosts and Transmission

Hantaviruses constitute a distinct genus within the Bunyavirus family, which also includes Orthobunyavirues, Nairoviruses, Phleboviruses and Tospoviruses. Hantaviruses are the only family members primarily transmitted by small mammal hosts while other family members are arthropod–borne (132, 175, 179). Hantaviruses found throughout Europe and Asia are predominantly carried by Murinae (rats and mice) and Arvicolinae (voles and lemmings), while hantaviruses in the Americas are predominantly carried by Sigmodontinae, Oligoryzomys, and Peromyscus species (hamster and vole–like rodents) (163) (Table 1).

Hantaviruses establish a persistent, asymptomatic infection within specific (or a few closely related) small mammal hosts (163, 175). The co–evolution of hantaviruses with specific hosts is the basis for their geographic distribution and coincident with their phylogeny (132, 163). As a result of evolution in isolated geographic settings, hantaviruses are genetically diverse and reassortment of pathogenic and nonpathogenic hantavirus gene segments has not been documented. Hantavirus hosts secrete virus for long periods of time and the viruses are transmitted horizontally primarily by inhalation of aerosolized excreta (176) and biting (63). Excreted hantaviruses are highly stable in dry environments (179).

Hantaviruses do not establish persistent infections in humans and thus human hantavirus infection is a genetic "dead–end" (163). Hantavirus infection of humans results from inhalation of aerosolized viral particles excreted in feces and urine. Hantaviruses are not generally transmitted between humans; however, person–to–person transmission has been documented between family members and physicians for the South American Andes virus (ANDV) (21, 153, 207).

Hantavirus Disease

Hantaviruses predominantly infect endothelial cells (ECs) present in vast glomerular and pulmonary capillary beds (175, 215, 216). Increased vascular permeability resulting in hypotension, edema, vasodilatation, and acute thrombocytopenia (rapid decrease in platelet number) in the absence of endothelial cell lysis are common clinical manifestations of HPS and HFRS. In fact, both HPS and HFRS infections may have renal or pulmonary sequelae. (161, 175, 179).

Clinical Features of HFRS

HFRS (5–15% mortality rate) cases progress through five stages. Following an approximately two week incubation time, patients enter a febrile phase (3–5 days) marked by acute onset of flu–like symptoms including high fever, chills, myalgia, and nausea. Early indications of HFRS include flushing of the face and conjunctival injection. Acute thrombocytopenia is a common symptom observed in all cases of HFRS at early time points during the disease.

In addition to platelet loss, platelet dysfunction is also common. Patients next enter a hypotensive stage (hours to days) during which edema, falling blood pressure, and acute shock are evident. During this phase nearly one–third of deaths occur as a result of vascular hemorrhage. Kidney output is decreased during this stage leading to proteinuria, hematuria, as well as other indications of kidney dysfunction. In the oliguric phase (days to two weeks) patients are often treated by hemodialysis as a result of hypervolemia. Nearly 50% of HFRS patient fatalities occur during this phase as a result of hemorrhage and/or renal dysfunction. Renal function begins to stabilize during the diuretic phase; however patients may still succumb as a result of shock or pulmonary dysfunction. Patients who survive enter a convalescent phase that can last 6–12 months before full recovery (33, 132, 175, 179).

Clinical Features of HPS

HPS (30–50% mortality rate) patients exhibit symptoms ranging from mild low blood oxygen to respiratory and cardiac failure. After a 7–14 day incubation period early symptoms of HPS infection begin and last 3 to 6 days including: fever, myalgia, nausea, abdominal pain, and diarrhea. Subsequently patients suddenly enter a stage of respiratory insufficiency highlighted by tachypnea, tachycardia, and hypotension. Rapid development of pulmonary edema and respiratory failure in some patients necessitates the use of mechanical ventilation. During the cardiopulmonary phase, which lasts 2 to 4 days, patients

also suffer from heart failure and a high level of pulmonary and cardiopulmonary edema. In patients who survive, pulmonary edema decreases and respiratory functions are restored in a diuretic phase. Patients finally enter a lengthy convalescent phase during which most patients exhibit degrees of weakness and fatigue (33, 132, 175, 179).

Treatment

Treatment of HFRS and HPS remains largely supportive in nature; generally consisting of management of fluid and electrolyte levels and, particularly in the case of severe HPS cases, extracorporeal membrane oxygenation (ECMO) (96, 128). Ribavirin is currently the only antiviral agent that has been effective in blocking HFRS; but only when administered prophylactically or during early stages of the disease progression (83, 181). Ribavirin has shown little efficacy in treating HPS (200). Hantaviruses are sensitive to the addition of interferon; but only when provided prophylactically with little or no effect once HPS or HFRS symptoms appear (98).

Animal Model of Hantavirus Disease – the Syrian Hamster

The study of hantavirus pathogenesis has been hindered by the lack of an animal model. Hantaviruses cause persistent infections within their natural hosts (voles, hamsters, and rats [SEOV]), where they do not cause disease. Laboratory mice (*Mus musculus*) are infected by HTNV but infection is not pathogenic. Lab mice are not productively infected by other HPS– or HFRS–causing hantaviruses

and, therefore, mice and knockout mice are not suitable for studying pathogenesis (13, 165). Experiments performed in Syrian hamsters revealed that ANDV infection resulted in HPS–like disease (82). ANDV was found to replicate within ECs of pulmonary capillary beds and disease progression in Syrian hamsters is very similar to human HPS patients in time, symptoms, and lethality. Approximately 14 days after infection there is a rapid onset of symptoms including the presence of virus within the blood, increased white blood cell counts, and localized pulmonary edema. At late stages of disease (12–14 days post–infection) hamsters develop a lethal pulmonary edema with a 90% mortality rate (81, 203). Curiously, other HPS– and HFRS–causing hantaviruses fail to cause disease in Syrian hamsters. As a result, ANDV infection of Syrian hamsters remains the only animal model of hantavirus disease. This model is currently used to study aspects of hantavirus pathogenesis and for the development of therapeutics and vaccines (82).

Genome and Life Cycle

Hantaviruses, like other members of the *Bunyaviridae* family, are spherical in shape and 90–100 nm in diameter (150). The genome consists of three negative–sense, single–stranded RNA segments designated large (L), medium (M), and small (S) according to nucleotide length (Figure 2). The 3` ends of each gene segment contain a conserved sequence which is complementary

to 5` ends and form panhandle structures which likely facilitate transcription and replication of viral RNAs (132).

The L segment (6,530–6,562 nucleotides [nt]) encodes an RNA–dependent RNA polymerase (Pol, approximately 240 kD) responsible for replication and transcription of the viral genome. Given the high mutation rate of hantaviruses, the polymerase is not thought to have proofreading or repair functions. Cap splicing activity has recently been reported for hantaviruses and suggested to be a function of the polymerase although there is no demonstration of this hantavirus polymerase function (96, 110).

The M segment (3,600–3,700 nt) encodes a glycoprotein precursor (GPC) which is co–translationally cleaved into the G_N (68–76 kD) and G_C (52–58 kD) surface glycoproteins (158, 159). Cleavage of the precursor by a yet–to–be defined cellular signal peptidase appears to be directed by the conserved pentapeptide sequence "WAASA." The hantavirus glycoproteins are Type I integral membrane proteins with their N–termini present in the ER lumen and their C–termini in the cytoplasm (122, 183). G_N contains a predicted signal sequence at its N–terminus followed by multiple transmembrane domains, RING– and zinc–finger domains, and a cytoplasmic tail 142 amino acids in length that contains an ITAM motif (61, 62). The cytoplasmic tail of pathogenic hantaviruses has been shown to block cellular interferon responses (3, 4) and

contains a degron motif which in some hantavirus directs proteasomal degradation of G_N (180). The cytoplasmic tail of G_C is <10 residues in length.

When expressed individually G_N and G_C localize to the ER (158). Co–expression of the glycoproteins, however, results in the formation of heterodimers within the ER that are required for translocation of G_N and G_C to the cis–Golgi (183). The G_N cytoplasmic tail has recently been shown to interact with the nucleocapsid (N) protein (encoded by the S segment), presumably to direct viral assembly (71, 72). Mature virions bud into the lumen of the Golgi and are translocated to the plasma membrane by an aberrant secretory mechanism (Figure 3) (187). G_NG_C heterodimer oligomerize and are present on the surface of mature virions and presumably mediate attachment to cellular receptors. pH–dependent conformational changes in G_C result in the release of the viral genome into the cytoplasm (93, 193).

The S segment (1,700–2,100 nt) encodes the N protein (50–54 kD) (132, 179). The N protein is detected as early as six hours post–infection and is the most abundant hantavirus protein and the major viral antigen. The nucleocapsid protein binds and stabilizes viral RNAs and nucleates virus assembly through interactions with the G_N cytoplasmic tail (72, 134, 187). The N protein contains N–terminal coiled–coil motifs that facilitate trimerization of the N protein. Moreover, the trimeric form has been shown to bind with high specificity and affinity to gene segment panhandles (134, 136).

Recent studies suggest that the hantavirus N protein supplants the cellular eIF4F complex to direct viral protein translation. The N protein binds cellular mRNA caps, directly linking the 43S pre–initiation complex, and replaces the helicase activity of eIF4A (135, 137). These functions are reported to be localized to cytoplasmic processing bodies (P–bodies) where cellular microRNAs and mRNAs are localized (45, 133).

Hantaviruses carried by members of the Arvicolinae (moles and lemmings) and Sigmodontinae (New World mice and rats) families (i.e., Tula and Puumala) also express a non–structural protein encoded within the S segment (NSs). The NSs protein expressed by members of the related orthobunyaviruses has been shown to reduce cellular interferon responses 10–30% within infected cells (106, 206). It was revealed that the NSs protein expressed by TULV and PUUV also reduces cellular interferon responses and increased successive passage of TULV within interferon–competent cells compared to a naturally occurring TULV containing a truncated NSs ORF (89, 90). A functional NSs ORF has not yet been described for other hantaviruses.

Hantavirus Regulation of Cellular Interferon Responses

Like other viruses, hantaviruses need to evade cellular interferon responses in order to establish an infection. Nonpathogenic PHV has been shown to induce a robust interferon (IFN) response one day post–infection (p.i.) of human endothelial cells while pathogenic NY–1V (HPS) and HTNV (HFRS) do

not (62, 107). Further studies indicate that the NY–1V G_N cytoplasmic tail blocks retinoic acid inducible gene–I (RIG–I) and TANK binding kinase 1 (TBK1) directed transcription from interferon stimulated response element (ISRE) and beta interferon (IFN–β) containing promoters. Additionally, since neither NY–1V nor PHV G_N tails inhibited transcriptional responses by a constitutively active interferon regulatory factor 3 (IRF–3 5D) mutant, these findings suggest NY–1V G_N regulates EC interferon responses at the level of the TBK1 complex (3).

TBK1 forms a complex with TNF receptor–associated factor 3 (TRAF3) which is required for the phosphorylation and subsequent activation of IRF–3. This results in the induction of IFN–β and activation of ISRE–responsive genes (76, 77). Co–immunoprecipitation experiments have revealed that NY–1V G_N tail binds to TRAF3 but not to TBK1 and that the interaction occurs through the N–terminus of TRAF3. Furthermore, expression of NY–1V G_N tail or infection with NY–1V both blocked TBK1 co–immunoprecipitation of TRAF3. In contrast, expression of the G_N tail from nonpathogenic PHV or following PHV infection had no effect on TBK1–TRAF3 complexes (3, 4).

While PHV induces a robust interferon response at early times post infection, nonpathogenic TULV replicates to titers similar to those of pathogenic hantaviruses in human endothelial cells (57). This points out a fundamental difference in endothelial cell regulation by nonpathogenic TULV and PHV, and

suggests that TULV has the ability to regulate IFN induction within human endothelial cells (130).

Hantavirus Receptors

While both pathogenic and nonpathogenic hantaviruses can enter endothelial cells, only pathogenic hantaviruses cause vascular permeability; suggesting that viral entry into endothelial cells alone is not a determinant of hantavirus pathogenesis (126, 161). Pathogenic hantaviruses bind the β_3 integrin subunit present in bent, inactive $\alpha_v\beta_3$ and $\alpha_{IIb}\beta_3$ integrins (Figure 4) which are abundantly expressed on the surface of human ECs and platelets. Hantaviruses enter cells by an exceptionally slow endocytic process (55, 59, 93). In contrast, nonpathogenic hantaviruses bind $\alpha_5\beta_1$ integrins (55, 59).

$\alpha_v\beta_3$ integrins are highly expressed on the surface of cells of the vasculature. They are equally distributed between the luminal and basolateral surface of ECs and are also present in adherens junctions (AJs). Vitronectin, a component of the extracellular matrix (ECM), is the $\alpha_v\beta_3$ integrin high–affinity ligand (19). Binding of vitronectin, and other ligands, to $\alpha_v\beta_3$ results in the activation of signaling responses that facilitate interactions of endothelial cells with the ECM, directs cell–cell adherence, and directs endothelial cell migration (19, 152, 210). $\alpha_v\beta_3$ integrins are also important regulators of vascular permeability and contribute to capillary integrity, recruitment of immune cells,

immune cell extravasation, endothelial cell migration and angiogenesis (19, 152). Knocking out β_3 integrins enhances capillary permeability in response to VEGF and β_3 ectodomains normally form complexes with VEGFR2 (vascular endothelial growth factor receptor 2) which regulate VEGF directed EC permeability.

Integrins are a family of heterodimeric cell surface receptors that bind components of the extracellular matrix (ECM). Integrins exist in two conformations: an extended, active conformation and a bent, inactive conformation (189, 214). In the inactive conformation, the Plexin–Semaphorin–Intergin (PSI) domain, located at the N–terminus of β subunits, is at the apex of the bent integrin dimer (213). Interestingly, pathogenic hantaviruses have been shown to bind to the PSI domain of bent, inactive $\alpha_v\beta_3$ integrins (Figure 4). Consistent with this, only pathogenic hantaviruses inhibit $\alpha_v\beta_3$ directed migration and enhance VEGFR2 signaling responses and EC permeability (55, 59, 169).

Hantaviruses Direct Enhanced EC Permeability in Response to VEGF

The primary fluid barrier of endothelial cells is formed by adherens junctions and responses of VEGFR2, an endothelial cell–specific receptor, control AJ disassembly (Figure 5) (9, 152, 202). A key AJ constituent is vascular endothelial cadherin (VE–cadherin), another endothelial cell–specific transmembrane protein, which is the major determinant of paracellular permeability within the vasculature (112-114). Binding of VEGF to VEGFR2

results in receptor dimerization and phosphorylation which activates a signaling cascade resulting in VE–cadherin endocytosis and AJ disassembly (Figure 5), which increases inter–endothelial cell permeability (9, 152, 202). VEGF is released by ECs, platelets, epithelial, and immune cells under hypoxic conditions (11, 27, 49, 141, 190). It acts locally on ECs through the autocrine or paracrine activation of VEGFR2. This interaction results in the disassembly of endothelial cell AJs; increasing the availability of nutrients to tissues and facilitating leukocyte diapedesis (Figure 6) (9, 152, 202).

Interestingly, tissue edema and hypoxia are common findings in both HPS and HFRS patients (36, 150, 153, 216), and the ability of pathogenic hantaviruses to infect human endothelial cells provides a means for hantaviruses to directly alter normal VEGF–VE–cadherin regulation. Endothelial cells are not lysed or permeabilized by hantavirus infection alone. However, Gavrilovskaya et al (57) have shown that pathogenic NY–1V, ANDV, and HTNV enhance endothelial cell permeability in response to VEGF and that maximal effects are observed three days post–infection. In contrast, nonpathogenic PHV and TULV failed to enhance EC permeability in the presence or absence of VEGF. Treatment of ANDV– or HTNV–infected cells with Ang1 (angiopoietin 1), an EC–specific growth factor, and S1P (sphingosine–1–phosphate), a platelet–derived lipid mediator, blocked hantavirus–directed endothelial cell permeability at physiologic concentrations, suggesting their potential use as hantavirus therapeutics (57).

Further work revealed that pathogenic ANDV and HTNV induce the disassembly of EC adherens junctions by directing VEGFR2 hyperphosphorylation and the internalization of VE–cadherin (66). Treatment of ECs with VEGF three days post ANDV or HTNV infection resulted in a 3– to 4–fold increase in VEGFR2 phosphorylation over mock– or TULV–infected controls. Since VEGFR2 activation results in the subsequent internalization of VE–cadherin and disassembly of AJs, Gorbunova et al (66) investigated the localization of VE–cadherin following VEGF stimulation of human ECs infected by pathogenic ANDV, HTNV, or nonpathogenic TULV. It was observed that >70% of ECs infected with either ANDV or HTNV and treated with VEGF contained internalized VE–cadherin while only 10–15% of VE–cadherin was intracellularly localized in mock– or TULV–infected controls (66). Hantavirus–directed internalization of VE–cadherin was also inhibited by Ang1 and S1P, consistent with their ability to block paracellular permeability of hantavirus infected endothelial cells (57). These findings rationalize studies of how hantavirus interactions with cellular VEGFR2–VE–cadherin signaling pathways contributes to hantavirus–induced permeability.

Chapter 2:

Experimental Procedures

Cells and Virus

VeroE6 cells (African Green monkey kidney epithelial cells; ATCC CRL–1586) were grown in Dulbecco's Modified Eagle Medium (DMEM) containing 10% fetal calf serum (FCS, 56°C inactivated; Clonetics), penicillin (100 mg/ml), streptomycin sulfate (100 mg/ml), and amphotericin B (50 µg/ml) (GIBCO). Human umbilical vein endothelial cells (HUVECs) were purchased from Clonetics (Walkersville, MD) and grown in endothelial cell basal medium–2 (EBM–2; Clonetics) supplemented with gentamicin (50 µg/ml), amphotericin B (50 µg/ml), and 2% FCS. Andes virus (CHI–7913; ANDV) (131) was kindly provided by Dr. B. Hjelle (Department of Pathology, School of Medicine, University of New Mexico–Albuquerque). ANDV and Tula virus (TULV; Tula/Moravia/MA 5302V/94) (57) were cultivated on VeroE6 cells as previously described (57) in a Biosafety Level 3 (BSL3) facility. Virus was adsorbed onto VeroE6 monolayers for 1 hour at 37°C, washed with media, and cells maintained in DMEM containing 2% FCS. All experiments requiring virus infection was performed in collaboration with Dr. Gavrilovskaya and Dr. Gorbunova in the lab.

Bacterial strains

The following bacterial strains were used:

XL1–Blue: *recA1 endoA1 gyrA96 thi–1 hsd R17 supE44 relA1 lac* [F' *proAB lacI*^{q}*PZΔM15* Tn*10* (Tet^{r})] (Stratagene).

XL10–Gold: Tet^r Δ(*mcrA*)*183* Δ(*mcrCB–hsdSMR–mrr*)*173 endA1 supE44 thi–1 recA1 gyrA96 relA1 lac* Hte [F′ *proAB lacI*^{q}*Z*Δ*M15* Tn*10* (Tet^r) Amy Cam^r] (Stratagene).

Immunoperoxidase Staining of Hantavirus–Infected Endothelial Cells

In order to monitor hantavirus infections, rabbit polyclonal anti–nucleocapsid serum directed against the NY–1V nucleocapsid protein was used to detect N protein from both ANDV and TULV as previously described (55, 59). Infected endothelial cell monolayers were fixed with 100% methanol and incubated with anti–nucleocapsid serum (1:5,000) in phosphate–buffered saline (PBS) containing 1% bovine serum albumin (BSA) (EMD Chemicals). Cells were then washed with PBS and incubated with horseradish peroxidase–conjugated goat anti–rabbit antibody (1:5,000) (Amersham Biosciences). Monolayers were washed with PBS and the number of infected cells quantitated following staining with 3–amino–9–ethylcarbazole (0.026%) in 0.1M sodium acetate, pH5.2 and 0.03% H_2O_2 for 5 minutes. The number of nucleocapsid protein expressing infected cells present was compared to mock–infected controls using an Olympus IX51 microscope.

Infection and Cell Lysis

HUVEC monolayers in 6–well plates were mock infected or infected with ANDV or TULV as described above at a multiplicity of infection of 1 (57). Seventy–two hours post–infection (p.i.) cells were lysed using 600 µl/well TRIzol Reagent (Invitrogen) for miRNA array analysis or Buffer RLT (RNeasy Mini Kit, Invitrogen) for total RNA extraction and RNA purified as described below (3). Trizol–treated samples were incubated for 5 minutes at room temperature. Following incubation, 1.2 ml of chloroform was added, incubated 2 minutes at room temperature, and samples centrifuged at 12,000 x g for 15 minutes at 4ºC. The aqueous phase was transferred to a new microcentrifuge tube, mixed with 300 µl isopropanol, and incubated for 10 minutes at room temperature. Samples were centrifuged at 12,000 x g for 15 minutes at 4ºC and the RNA pellet rinsed with 600 µl of 75% ethanol. RNA precipitates were subsequently dissolved in RNase–free water.

MicroRNA and Total RNA Purification

MicroRNAs were purified from mock–infected and ANDV–infected HUVECs using the RT² qPCR–Grade miRNA Isolation Kit (SA Biosciences). The aqueous phase from chloroform extracted lysates was diluted in 100% ethanol and applied to spin columns to remove large RNA. Eluates were then diluted in a second volume of 100% ethanol and applied to a second spin column.

After centrifugation, columns were rinsed in Washing Buffer, centrifuged, washed with 70% ethanol, and small RNA eluted in RNase–free water (160).

Total cellular RNA was extracted from mock–, ANDV–, and TULV–infected HUVECs using RNeasy Mini Kit (Qiagen) according to the manufacturer's protocol (3). Cells were lysed with 600 µL of Buffer RLT containing 1% β–mercaptoethanol and lysates passed through a 20–gauge needle and diluted in one volume of 70% ethanol. The samples were applied to RNeasy spin columns and RNA bound to the column by centrifugation. Columns were successively washed with Buffer RW1 and twice with Buffer RPE and RNAs eluted with RNase–free water.

cDNA Synthesis

Purified microRNA (100 ng) was reverse transcribed using the RT² miRNA First Strand Kit (SA Biosciences). Small RNA, a proprietary mix of miRNA RT primer plus External RNA control, miRNA RT buffer, miRNA RT Enzyme mix, dithiothreitol (10mM), and RNase–free water were combined and incubated at 37°C for two hours. The reactions were then incubated for five minutes at 95°C to degrade the RNA and inactivate the reverse transcriptase. Samples were placed on ice and subsequently diluted 1:10 in RNase–free water prior to analysis by RT–PCR.

Purified total RNA (1 μg) was reverse transcribed using the Transcriptor First Strand cDNA Synthesis Kit (Roche) using oligo–$(dT)_{18}$ primer (25°C for 10 min., 55°C for 30 min., 85°C for 5 min.). cDNAs were diluted 1:10 in distilled water prior to analysis by RT–PCR or amplification by PCR.

MicroRNA Array Real–Time PCR

Diluted miRNA cDNAs were used as templates for real–time PCR using the Human Genome miRNA PCR Array (SA Biosciences). cDNA, RT^2 SYBR Green PCR master mix, and double–distilled H_2O (ddH_2O) were combined and aliquoted into each well of the PCR array consisting of four 96–well plates representing 352 human miRNAs. Each well contains a proprietary universal primer and miRNA–specific primer resulting in amplification of a specific miRNA per well. Real–time PCR was performed using the following thermocycling parameters: 1 cycle of 95°C for 10 min, then 95°C for 15 sec, 60°C for 40 sec, and 72°C for 30 sec for a total of 40 cycles.

Quantitative Real–Time PCR of Cellular mRNAs

TaqMan primers for human SPRED1, PIK3R2, and GAPDH (glyceraldehyde–3–phosphate dehydrogenase) were purchased from Applied Biosystems. SPRED1 and PIK3R2 mRNA levels were determined relative to those of mock infected controls. Real–time PCR was performed using an Applied

Biosystems 7300 RT–PCR machine. Thermocycling parameters were as follows: 50°C for 2 min, 95°C for 10 min, 95°C for 15 sec, and 60°C for 1 min for 40 cycles. GAPDH mRNA levels were used as an internal RNA reference to normalize samples. Each reaction was performed in duplicate. Specific primers for MxA (Forward primer: 5'–TGATCCAGCTGCTGCATCCC–3'; Reverse primer: 5'–GGCGCACCTTCTCCTCATAC–3') and GAPDH (Forward primer: 5'–GGAAGCTCACTGGCATGGC–3'; Reverse primer: 5'–TAGACGGCAGGTCAGGTCCA–3') were previously described (3) or obtained from Applied Biosystems (ISG56) and mRNA levels were similarly analyzed as described above.

MicroRNA Array Real–Time PCR Analysis

Fold changes in miRNA expression levels were calculated using the RT² miRNA PCR Array Data analysis web–based software (SA Biosciences; http://www.sabiosciences.com/pcr/arrayanalysis.php). The threshold cycle (C_t), the cycle along the amplification curve when the exponential growth of the PCR products is maximal, of each miRNA from ANDV–infected and mock–infected samples was normalized to that of U6 RNA (ΔC_t). Expression levels of normalized miRNA C_t values was calculated using the $2^{-\Delta Ct}$ method (108). The fold change in expression levels of each miRNA was determined from the

expression levels of ANDV–infected and mock–infected HUVECs. Graphs were plotted using GraphPad Prism 5 software.

Real–Time PCR Analysis

Fold changes in SPRED1 and PIK3R2 mRNA levels were calculated using the $2^{-\Delta Ct}$ method (108). The C_t value of each mRNA was normalized to those of GAPDH. Changes in the C_t values between ANDV–infected and mock–infected samples (ΔC_t) were then calculated. Fold changes were determined ($2^{-\Delta Ct}$) and plotted (± S.E.M.) using GraphPad Prism 5 software.

siRNA Transfection

SPRED1 and PIK3R2 knockdown experiments were performed using small interfering RNAs purchased from SA Biosciences. Briefly, thirty–six µl of 2 µM SureSilencing siRNAs against SPRED1, PIK3R2, or negative control siRNA (si–NEG2) were combined with serum–free DMEM (200 µl) and SureFECT reagent (6 µl) (SA Biosciences). Complexes were allowed to form for 20 minutes at room temperature and then added to HUVECs. Total RNA for RT–PCR analysis was purified as described above and analyzed by qRT–PCR (62).

Endothelial Cell Permeability Assay (57)

HUVECs were plated on Costar Transwell plates (3 μm pores; Corning) and confluent monolayers were infected with pathogenic ANDV at an MOI of 0.5 in a BSL–3 facility or mock–infected. Three days p.i. monolayer permeability was assayed by adding 0.5 mg/ml of FITC–dextran and VEGF (100 ng/ml) to the upper chamber of each well. Media taken from the lower chamber (100 μl) 5 minutes or 2 hours later was assayed for the presence of FITC–dextran and expressed as the fold change in monolayer permeability over basal permeability controls. Hantavirus infections were monitored by immunoperoxidase staining as described above (55, 59).

Western Blot Analysis

Cofilin and Phospho–cofilin:

Western blot analysis was performed as previously described (60, 61). HUVECs were infected with TULV or ANDV and cells treated with VEGF as described above (57). Three days post infection cells were lysed at various times after VEGF addition using Brugge buffer (0.1% NP40, 150 mM NaCl, 40 mM Tris–Cl, 2 mM EDTA, 10% glycerol, 5 nM sodium fluoride, 1 mM sodium pyrophosphate, 1 mM sodium orthovanadate) containing 0.1% sodium dodecyl sulfate and protease inhibitor cocktail (Sigma). Total protein levels were determined by a bicinchoninic acid assay (Pierce) and 20 μg protein was diluted

in 5X sample buffer (250 mM Tris–Cl, 500 mM dithiothreitol, 10% SDS, 0.5% bromophenol blue, 50% glycerol) and separated by 15% sodium dodecyl sulfate (SDS)–polyacrylamide gel electrophoresis (PAGE) using a Mini–PROTEAN Tetra Cell (Bio–Rad) at 100V. Proteins were transferred for 1 hour at 100V to nitrocellulose using a Tris–Glycine transfer buffer containing 30% methanol in a Novex Xcell electroblotter, blocked in PBS containing 5% bovine serum albumin, and cofilin was detected using polyclonal anti–cofilin antibody (1:1,000; cofilin, #3312; Cell Signaling) followed by anti–rabbit horse radish peroxidase (HRP)–conjugated antibody (1:2,000; Amersham). Western blots were developed using enhanced chemiluminescence reagent (Amersham) and exposed to HyBlot CL autoradiography film (Denville Scientific). Western blotting was performed in duplicate with similar results.

To assess the level of phospho–cofilin, cofilin western blots were stripped (2% sodium dodecyl sulfate, 62.5 mM Tris–Cl, 100 mM beta–mercaptoethanol) and re–probed using polyclonal anti–phospho–cofilin antibody (1:1,000; phospho–cofilin, #3311; Cell Signaling). Blots were developed as described above. Densitometric analysis of cofilin and phospho–cofilin levels was performed using ImageJ (NIH) software and data plotted ± S.E.M. and statistical analysis performed using GraphPad Prism 5 software.

Andes Virus G_C Protein:

The expression of G_C protein from pT7HR1–ANDV–M and pTM1–ANDV–M was detected following co–transfection of either plasmid with the T7 RNA polymerase expression plasmid pCAGGS–T7 (155) or transfection of pCAGGS–T7 alone into VeroE6 cells. Thirty–six hours post transfection cells were lysed using Brugge buffer and total protein levels determined as described above. Twenty µg protein was diluted in 5X sample buffer and separated by 12% SDS–PAGE. Proteins were transferred to nitrocellulose as above and blocked in 5% bovine serum albumin and G_C was detected using polyclonal anti–Gc antibody (1:2,000; U.S. Biological) followed by anti–rabbit horse radish peroxidase (HRP)–conjugated antibody (1:2,000; Amersham). Blots were developed as described above.

Polymerase Chain Reaction

Amplification of PCR products were performed in an Eppendorf Mastercycler Personal. Each reaction contained: 1X buffer (50 mM Tris–HCl, pH 9.0; 20 mM $(NH4)_2SO_4$; 2.5 mM $MgCl_2$; 0.2 mM dNTPs), 1 U *Tfl* polymerase (Epicentre), 100 ng forward and reverse primers (Table 2), and 10–100 ng template. Annealing temperatures used varied from 50–60°C depending on template DNA and oligo. The following thermocycling parameters were used for amplifying PCR products: 95°C for 30 seconds, 50–60°C for 30 seconds, 72°C

for 1min/kb of PCR product (with modification as required for specific PCR products).

Restriction Digestion

Digestion of vectors and PCR products was performed in 50 µl reactions. Restriction enzymes and supplied buffers (New England BioLabs) were used according to manufacturer's protocols. For cloning reactions, 2 µg of DNA was digested with 10 U of restriction enzyme for 1 hour at 37°C or 55°C as required by the specific enzyme used. To screen for positive clones, 2 U of enzyme was used per µg of vector and reactions were digested for 1 hour at 37°C.

Gel Purification

Digested vectors and PCR products were resolved on 1% agarose gels (Ultrapure Agarose, Invitrogen) containing 0.5 µg/µl ethidium bromide (Sigma–Aldrich) in TAE buffer (40mM Tris acetate and 10mM EDTA, pH 8.0) at 100 V. Following separation, bands corresponding to digested products were excised and DNA extracted and purified using the QIAquick Gel Extraction Kit (Qiagen) according to manufacturer's instructions. Gel slices were immersed in QG buffer and dissolved at 50°C for 10 minutes. The mixture was diluted with isopropanol and DNA bound to a spin column by centrifugation at >10,000 rpm for 1 minute.

Columns were washed with Buffer PE and the bound DNA was eluted with Buffer EB (10 mM Tris·Cl, pH 8.5) or water.

DNA Ligation

Twenty µl ligation reactions were prepared containing the following: linearized vector, digested insert, 1X T4 DNA ligase buffer (50mM Tris–HCl [pH 7.5], 10mM $MgCl_2$, 10 mM DTT, 1 mM ATP), and T4 DNA ligase (1U; New England BioLabs). Reactions were mixed and allowed to incubate overnight at 16°C.

Bacterial Transformation

Frozen XL1–Blue competent cells were thawed on ice, 2 µl (~0.1–10 ng) DNA added, and the mixture transferred to a pre–chilled 0.1 ml cuvette (Invitrogen). Cells were electroporated using a Bio–Rad Gene Pulser (200 ohms, 25 µF, 1.25 kV) and 600 µl of pre–warmed (37°C) LB was immediately added. Cells were incubated at 37°C for 1 hour with shaking for recovery, plated on LB agar plates containing the appropriate antibiotic, and plates incubated at 37°C overnight.

Site–Directed Mutagenesis

Mutations present in cloning products were corrected using the QuikChange Site–Directed Mutagenesis (SDM) kit (or QuikChange XL kit for large templates, >6 kb; Stratagene) according to manufacturer's protocols. Reactions contained 5 µl of 10X Reaction buffer (1X reaction: 10 mM KCl, 10 mM $(NH_4)_2SO_4$, 20 mM Tris–HCl (pH8.8), 2 mM $MgSO_4$, 0.1% Triton X–100, 0.1 mg/ml BSA), 50 ng template DNA, 125 ng forward primer and reverse primers, 1 µl dNTP mix, and 1 µl (2.5 U) *PfuTurbo* DNA polymerase (note: XL kit reactions also contained 3 µl of QuikSolution). Cycling parameters were as follows: 1 cycle at 95°C for 30 sec; followed by 16 cycles of 95°C for 30 sec; 55°C for 1 min, and 68°C for 1 min/kb of template. For XL kit reactions cycling parameters were as follows: 1 cycle at 95°C for 1 min; followed by 18 cycles of 95°C for 50 sec, 60°C for 50 sec, and 68°C for 1 min/kb of template; and 1 cycle at 68°C for 7 min. Following PCR, amplification products were digested with 10 U *Dpn* I at 37°C for 1 hour to remove template DNA. Chemically competent XL1–Blue cells were transformed with 1 µl of *Dpn* I–digested amplification products by the heat–shock: DNA and cells were incubated on ice for 30 min, transferred to 42°C for 45 seconds, and then quickly placed on ice for 2 minutes. Following recovery, cells were diluted in 500 µl LB, incubated for 1 hour at 37°C, and plated on LB agar plates containing appropriate antibiotic(s).

Preparation of Plasmid DNA

Alkaline Lysis Mini Prep:

A 5 ml bacterial culture was grown at 37°C with shaking overnight. Pelleted cells (>12,000 rpm; 3 min) were resuspended in 100 µl of Solution I and subsequently lysed in 200 µl of Solution II for 5 minutes at room temperature. Lysed cells were neutralized using 150 µl of Solution III and lysate cleared by centrifugation for 10 min at >12,000 rpm. Clarified lysate was extracted with phenol:chloroform and phases separated by centrifugation at >12,000 rpm. The upper, aqueous phase was transferred to a clean tube and ethanol precipitated ($1/10^{th}$ volume 3 M sodium acetate, pH 5.2; 2.5 volumes ethanol). Samples were vortexed, placed at –80°C for 10 minutes, and DNA pelleted by centrifugation (14,000 rpm; 10 min). The DNA pellet was rinsed using 70% ethanol and resuspended in 50 µl dH_2O containing 1 µl RNase A (10 mg/ml).

Cesium Chloride Maxi Prep:

An LB culture (500 mL) containing appropriate antibiotics was grown at 37°C with shaking overnight. Pelleted cells (5,000 x g; 5 min) were resuspended in 6.7 ml of Solution I (50 mM glucose; 25 mM Tris, pH 8.0; 10 mM EDTA) and subsequently lysed in 13.4 ml of Solution II (200 mM NaOH; 1% SDS) for 5 minutes on ice. Lysed cells were neutralized using 10 ml of Solution III (5 M Potassium Acetate: 3 M Potassium, 5 M Acetate) and lysate cleared by centrifugation for 30 min at 3,500 rpm. The pellet was rinsed with 70% ethanol,

dried, and resuspended in 4 ml of Tris–EDTA, pH 8.0. Cesium chloride (4.4 g) and 10 µl of ethidium bromide (10 mg/ml) was added and the mixture was subsequently sealed in a polyallomer Quick–Seal tube (Beckman). The sample was centrifuged at 50,000 rpm overnight in a Beckman LS–70 ultracentrifuge using a VTi 65 rotor. Bands corresponding to plasmid DNA were harvested by side puncture using a 20 gauge needle and ethidium bromide extracted from collected bands using successive washes of butanol–saturated water. Samples were dialyzed overnight in Tris–EDTA, pH 8.0 using 14 kD MWCO dialysis tubing and DNA isolated by ethanol precipitation.

Plasmids

All vectors were verified by sequencing. Template DNA (500 ng), oligonucleotide, and dH_2O were combined and analyzed on an Applied Biosystems 3730 Genetic Analyzer (DNA Sequencing Facility, Stony Brook University).

Andes Virus Gene Segment Vectors:

To generate Andes virus anti–genomic RNAs within transfected cells two approaches were utilized. In the first approach, a vector (pT7HR2) containing a 5' T7 RNA polymerase promoter and Hammerhead ribozyme (5'–CTGATGAGGCCGAAAGGCCGAAACTCCGTAAGGAGTC–3'; Figure 17A) (177) elements and a 3' Hepatitis Delta ribozyme (5'–GGGTCGGCATGGCATCTCCACCTCCTCGCGGTCCGACCTGGGCATCTT

CGGATGGCTAAGGGAGCAAGCT–3'; Figure 17B) (25) flanking BsmBI restriction sites was created. A cassette consisting of four ligated oligonucleotides (Figure 17C) containing the T7 RNA polymerase promoter, Hammerhead ribozyme, Hepatitis Delta ribozyme, and cloning sites was synthesized and ligated into a BglI–EcoRI digested pET30a vector (Invitrogen). In the second approach, the pT7HR1 vector was similarly constructed except the Hammerhead ribozyme was not incorporated into the ligated oligonucleotide cassette (Figure 17D). Andes virus L (GenBank Accession: AY228239.1), M (GenBank Accession: AY228238.1), and S (GenBank Accession: AY228237.1) anti–genomic cDNAs were generated by PCR using segment–specific oligonucleotides (Table II) containing a BsmBI restriction site on the 5' and 3' ends, digested with BsmBI, and cloned into pT7HR2 or pT7HR1 which had been linearized with BsmBI (pT7HR2– or pT7HR1–ANDV–Segment, respectively). To generate vectors to be used as templates for in vitro transcription (pT7HR1–ANDV–Segment–ApaI), site–directed mutagenesis using oligonucleotides containing an ApaI restriction site (Table II) was performed to insert the ApaI between the 3' UTR of each gene segment and the Hepatitis Delta ribozyme.

Andes Virus Protein Expression Vectors:

To generate plasmids expressing ANDV proteins, gene segment open reading frames (ORFs) were generated by PCR using segment–specific oligonucleotides (nucleocapsid; Table II) containing appropriate restriction sites

flanking the ORFs, sub–cloned from existing vectors (polymerase), or purchased from Blue Heron Biotechnology (glycoproteins and codon–optimized polymerase). For the N protein vector (pTM1–ANDV–S), PCR products were digested with NcoI and BamHI and cloned into similarly digested pTM1 vector (140) downstream of a T7 RNA polymerase promoter and in–frame with an encephalomyocarditis virus internal ribosomal entry site (IRES) (Figure 17E).

To generate a non–optimized ANDV polymerase expression vector (pTM1–ANDV–L), SDM (Table II) was used to introduce an NcoI site in–frame with the polymerase ORF start codon using pT7HR1–ANDV–L as the template. The clone was subsequently digested with NcoI and EcoRI and the released fragment containing the polymerase ORF ligated into similarly digested pTM1.

To generate codon–optimized ANDV polymerase and glycoprotein expression vectors (pTM1–ANDV–L–Opt and pTM1–ANDV–M–Opt, respectively), codon–optimized polymerase and Gn/Gc ORF sequences were designed and purchased from Blue Heron Biotechnology. Sequences were flanked by BsmBI restriction sites to facilitate the creation of NcoI and BamHI overhangs for sub–cloning of the ORFs into NcoI–BamHI digested pTM1.

In Vitro Transcription

To generate Andes virus gene segment cRNAs in vitro, 10 µg pT7HR1–ANDV–Segment–ApaI vectors were linearized using 2 U of ApaI. Restrictions

reactions were terminated by addition of 2 volumes of ethanol. Diluted reactions were placed at –20°C for 15 minutes and DNA pelleted by centrifugation (14,000 rpm; 15 min). Linearized vector was resuspended in dH_2O. Purified DNA (1 μg) was used as templates for in vitro transcription using the mMessage mMachine T7 kit (Ambion). Linearized DNA templates combined with nuclease–free dH_2O, NTPs, Reaction Buffer, and Enzyme Mix according to the manufacturer's instructions and incubated at 37°C for 1 hour. Reactions were terminated Ammonium Acetate Stop Solution (Ambion), diluted in nuclease–free dH_2O, and extracted with an equal volume of phenol:chloroform. RNA from the aqueous phase was precipitated by addition of 1 volume of isopropanol, incubation at –20°C for 15 min., and centrifugation for at 14,000 rpm for 15 min at 4°C. Pelleted RNAs were resuspended in nuclease–free dH_2O.

In Vitro Transcription/Translation

ANDV nucleocapsid protein was generated in vitro from linearized pT7HR1–ANDV–S–Marker templates using the TNT Quick Coupled Transcription/Translation System (Promega) according to the manufacturer's protocol. Briefly, 1 μg linearized template, TNT Quick Master Mix, 1 mM methionine, and dH_20 were combined and incubated at 30°C for 90 minutes. An aliquot (10%) of the reaction was diluted in 5X sample buffer and resolved by

12% SDS–PAGE. The presence of nucleocapsid protein was evaluated by Western blot as described above using anti–nucleocapsid sera.

Transfection of Mammalian Cells

Transfections were performed on ~75–95% or ~50–70% confluent cell monolayers in 6–well plates (Corning, Inc) using Lipofectamine 2000 (Invitrogen) or FuGENE 6 (Roche), respectively, according to the manufacturers' instructions (169, 180). Cells were transfected using 3 µl of transfection reagent per µg of plasmid DNA (or RNA) per well. Six (Lipofectamine 2000) or sixteen (FuGENE 6) hours post–transfection monolayers were washed with 1X PBS and grown in complete DMEM (10% FCS).

Chapter 3:

Andes Virus Regulation of Cellular MicroRNAs Contributes to Hantavirus–Induced Endothelial Cell Permeability

Introduction:

Pathogenic hantaviruses predominantly infect endothelial cells (176) and cause one of two vascular permeability–based diseases: Hemorrhagic Fever with Renal Syndrome (HFRS) and Hantavirus Pulmonary Syndrome (HPS) (176). Both diseases are characterized by acute thrombocytopenia, edema, and the loss of vascular integrity following endothelial cell infection (22, 32, 33, 150, 175, 176, 216). However, hantaviruses are not lytic, indicating that hantaviruses alter normal endothelial cell functions that maintain vascular integrity (150, 175, 216).

Hantaviruses are enveloped viruses containing a tri–segmented, negative–sense RNA genome encoding 4 viral proteins (176). Hantaviruses replicate in the cytoplasm, mature by budding into the lumen of the cis–Golgi, and exit cells by an aberrant secretory process (176). Pathogenic hantaviruses attach to cells by binding inactive conformations of β_3 integrin receptors present on endothelial cells and platelets (55, 56, 59, 131, 169). At late times post–infection, hantaviruses remain cell associated through interactions with $\alpha_v\beta_3$ and bound virus directs the adherence of quiescent platelets to the endothelial cell surface (55, 56, 59). β_3 integrins on platelets and endothelial cells play a central role in the regulation of vascular integrity (6, 14, 30, 79, 86, 170, 171). On endothelial cells, β_3 integrins normally regulate the permeabilizing effects of VEGF by forming a complex with VEGFR2 (14, 185). In fact, β_3 integrin knockouts are hyper–responsive to the permeabilizing effects of VEGF (79, 170, 171).

Consistent with this, pathogenic hantaviruses block $\alpha_v\beta_3$ directed endothelial cell migration and enhance endothelial cell permeability in response to VEGF 3 days post infection (57, 58, 66, 169). These findings suggest that pathogenic hantaviruses alter VEGFR2–directed signaling responses at late times after endothelial cell infection, although the mechanism by which hantaviruses enhance VEGFR2 responses remains to be defined (57, 66).

VEGFR2 responses are regulated by redundant receptors and signaling pathways that rapidly alter the barrier function of endothelial cell adherens junctions in order to control vascular integrity (35, 37, 53, 114). Within ECs, VEGFR2 phosphorylation at tyrosine 951 recruits Src kinases which activate a Src/Rac/PAK signaling pathway that results in VE–cadherin internalization, disassembly of inter–endothelial AJs, and increased inter–endothelial cell permeability. The hyperpermeabilization of ANDV–infected ECs in response to VEGF suggests that VEGFR2–Src signaling responses direct ANDV–induced permeability (111, 129, 152).

Recently, endothelial cell–specific microRNAs have been shown to regulate VEGF–induced responses and serve as key determinants of vascular permeability (47, 108, 197, 204, 205). As a result, changes in miRNA regulation could contribute to enhanced EC permeability following pathogenic hantavirus infection. MicroRNAs are short, non–coding RNAs, ~21 nucleotides in length, which are highly conserved (8, 23, 45, 69, 102, 211) and selectively expressed in

specific cells and tissues (99, 108, 204). MiRNAs regulate protein expression of specific mRNAs at a post–transcriptional level, either by directing the degradation of target mRNAs or by repressing mRNA translation (156). MiR–126 is an endothelial cell specific miRNA that is responsible for maintaining vascular integrity and knocking out miR–126 results in increased capillary permeability and edema in mice (46, 109). MiR–126 functions by repressing the expression of SPRED1 (sprouty–related EVH1 domain containing protein 1) and PIK3R2 (phosphoinositide–3–kinase, regulatory subunit 2), which are tied to downstream signaling responses directed by VEGFR2 activation (46, 94, 109, 204). Similar to knocking out miR–126, over–expressing SPRED1 alone increases VEGF–induced endothelial cell permeability, and as a result miR–126 normally enhances endothelial cell barrier functions by repressing SPRED1 activity (46, 109, 204, 205).

MiR–126 and SPRED1 regulate capillary integrity by determining the phosphorylation state of cofilin (46, 94). SPRED1 is a negative regulator of the LIM family kinase TESK1 (testis–specific protein kinase 1) and SPRED1 binding to TESK1 inhibits cofilin phosphorylation (46, 94) (Figure 7). Unphosphorylated cofilin severs actin filaments and disrupts adherens junctions by dissociating VE–cadherin from its cytoskeletal anchor (188). In contrast, TESK1 phosphorylation of cofilin inactivates cofilin, stabilizing actin filaments and inter–endothelial cell adherens junctions (105, 195). Since adherens junctions form the primary fluid

barrier of the endothelium (35, 53), the state of cofilin phosphorylation contributes to the regulation of endothelial cell permeability.

The hantavirus nucleocapsid protein reportedly binds mRNA caps and facilitates translation of viral proteins (133, 135). Interestingly, the nucleocapsid protein was also reported to localize to P–bodies (133) where miRNAs mature and regulate mRNA expression (8, 23, 45, 69, 102, 211). The ability of the nucleocapsid protein to bind cellular RNAs and localize to miRNA–containing P–bodies provides a strong rationale for hantaviruses to alter miRNA regulation within infected endothelial cells and thereby endothelial cell permeability in response to VEGF (57).

Results:

Src Knockdown Decreases ANDV–Induced Endothelial Cell Permeability

The VEGFR2 cytoplasmic tail recruits Src kinases which activate a Src–RAC–PAK signaling cascade that results in VE–cadherin internalization and increased paracellular permeability of endothelial cells (Figure 5). ANDV–infected endothelial cells are hyperpermeabilized by VEGF suggesting that VEGFR2–Src signaling responses direct ANDV–induced permeability. Here we determine if knocking down Src blocks endothelial cell permeability induced by ANDV infection.

We transfected endothelial cells with control or Src–specific siRNAs and assayed ANDV–induced EC permeability 3 days post–infection. Quantitative RT–PCR analysis indicates that endothelial cells transfected with Src siRNAs specifically reduced Src mRNA levels by ~70% (Figure 8A). ECs similarly transfected with Src or control siRNAs were subsequently analyzed for their effect on ANDV–induced permeability (57, 160). We found that siRNAs to Src reduced the hyperpermeability of ANDV–infected ECs 55–65% compared to control siRNA at all time points after VEGF addition (Figure 8B). These findings suggest that ANDV–induced hyperpermeability occurs via the VEGFR2–Src pathway and suggests that inhibiting Src is a viable mechanism for reducing ANDV–induced endothelial cell permeability. In addition, these findings further suggest that chemical inhibitors of VEGFR2 and Src kinases may similarly inhibit ANDV–induced EC permeability. These findings have led us to test the ability of Src kinase inhibitors to block ANDV induced endothelial cell permeability. These studies have been continued by Dr. Gavrilovskaya and Dr. Gorbunova in the lab and recently submitted for publication (65).

ANDV Regulation of Cellular MicroRNAs

The ability of the hantavirus nucleocapsid protein to bind cellular mRNA and localize to cytoplasmic P–bodies (133) suggests that pathogenic hantaviruses may alter the function of endothelial cell miRNAs and the ability of miRNAs to

regulate cognate mRNA targets. Here we determined whether ANDV infection of endothelial cells alters the synthesis of cellular miRNAs (Figure 9A–D).

Human endothelial cells were infected with ANDV and 3 days post infection small cellular RNAs were purified. The level of specific endothelial cell miRNAs was analyzed using a qRT–PCR microarray and compared to mock infected controls. Analysis of 352 human miRNAs revealed that ANDV upregulated the expression of 14 miRNAs greater than 4–fold (Figure 10A). The level of 3 miRNAs increased >10 fold in ANDV versus mock infected endothelial cells including miR–let7d, miR–423–3p, and miR–146b–5p. In contrast, ANDV infection resulted in the downregulation of 9 miRNAs (≥3–fold) (Figure 10B), including miR–410, miR–218, and miR–503 which were reduced approximately 3,400–, 129–, and 77–fold, respectively. These findings demonstrate that ANDV infection of endothelial cells results in a dramatic change in the level of specific endothelial cell miRNAs and fundamentally alters the constellation of miRNAs present within its primary cellular target.

Several miRNAs are reported to be highly expressed in endothelial cells (108). Figure 11 confirms the high level expression of 16 miRNAs within mock infected endothelial cells and evaluates changes in these miRNAs resulting from ANDV infection. The level of the most highly expressed EC miRNA, miR–503, was decreased approximately 77–fold following ANDV infection (Figure 11). Despite this, miR–503 remains the most abundant miRNA present within ANDV–

infected endothelial cells. The level of miR–126, which has a known function in regulating vascular permeability, increased approximately 2–fold following ANDV infection (Figure 11). In contrast, we observed a striking 3,400–fold reduction in the level of miR–410 following ANDV infection. Although miR–410 specific mRNA targets have yet to be defined, miR–410 expression was recently associated with enhancing cellular secretion (70). These findings indicate that ANDV substantially alters the level of endothelial cell–specific miRNAs and further suggests that changes in miRNA regulation may contribute to altered endothelial cell functions following infection.

MiRNAs have been reported to play critical roles in the regulation of angiogenesis and endothelial cell permeability (204, 205). Analysis of microarray data revealed that 6 miRNAs involved in angiogenesis (miR–155, –320, –27b, –222, –21, and –378) were upregulated approximately 3–7 fold following ANDV infection (Figure 12). While the mechanism by which a number of these miRNAs regulate angiogenesis and endothelial cell functions has not been determined, miR–155, miR–320, and miR–222 have been shown to have important roles in the regulation of endothelial cell responses to growth factors, including VEGF, or are linked to the maintenance of capillary integrity (47, 149, 205). These findings indicate that ANDV infection alters miRNAs which regulate endothelial cell integrity and this further suggests the importance of analyzing endothelial cell

miRNAs and miRNA targets in understanding hantavirus regulation of the endothelium.

SPRED1 and PIK3R2 mRNA Levels are Increased Following ANDV Infection

MiR–126 is an endothelial cell–specific miRNA that normally inhibits VEGF–directed vascular permeability. MiR–126 functions by downregulating mRNAs encoding SPRED1 and PIK3R2, effectively blocking SPRED1 and PIK3R2 functions (46). Although we observed a 2–fold increase in miR–126 levels following ANDV infection (Figure 11), it was unclear whether this change resulted in altered levels of cellular mRNAs. In order to determine if hantaviruses alter miR–126 function, we analyzed the level of SPRED1 and PIK3R2 mRNAs within endothelial cells infected by pathogenic ANDV and nonpathogenic TULV, 3 days post infection. Using qRT–PCR we found that SPRED1 and PIK3R2 mRNA levels were induced 10– and 7–fold, respectively, following ANDV infection (Figure 13). In contrast, no changes in the levels of SPRED1 or PIK3R2 mRNAs were observed following infection with TULV (Figure 13). This data indicates that ANDV infection increased SPRED1 and PIK3R2 mRNA levels without decreasing miR–126. As a result, ANDV interferes with the normal function of miR–126 in regulating its cognate mRNAs and this finding demonstrates that ANDV induces cellular transcriptional responses associated with enhancing endothelial cell permeability.

ANDV Infection Decreases Phosphorylation of Cofilin

SPRED1 binding to TESK1 inhibits cofilin phosphorylation and enhances the dissociation of adherens junctions and endothelial cell permeability (94). In order to determine if increased SPRED1 mRNA levels were functionally significant (Figure 13), we determined whether there was an effect on cofilin phosphorylation following pathogenic ANDV or nonpathogenic TULV infection of endothelial cells. The level of phospho–cofilin was substantially lower in ANDV versus TULV infected endothelial cells 30 and 60 minutes after VEGF addition (Figure 14A, B), and quantitatively resulted in a 30–50% decrease in phospho–cofilin levels in ANDV infected cells (Figure 14B). These findings are consistent with increased SPRED1 function within ANDV infected cells and suggest that SPRED1 induction may contribute to the enhanced permeability of ANDV infected endothelial cells in response to VEGF.

Knockdown of Endogenous SPRED1 Decreased ANDV Induced Endothelial Cell Permeability

SPRED1 overexpression results in increased vascular permeability (46) and from our findings both SPRED1 levels and SPRED1 functions are increased in ANDV–infected endothelial cells. In order to determine if SPRED1 induction contributes to the enhanced permeability of hantavirus infected cells, we transfected endothelial cells with SPRED1 siRNAs and assayed ANDV induced endothelial cell permeability. Endothelial cells transfected with SPRED1 or

PIK3R2 siRNAs specifically reduced SPRED1 or PIK3R2 mRNAs, respectively, by 60–65% (Figure 15A). Interestingly, siRNA knockdown of SPRED1 inhibited ANDV–induced permeability in response to VEGF by 30–60% compared to endothelial cells transfected with a control siRNA or siRNA to PIK3R2 (Figure 15B). These findings demonstrate that the induction of SPRED1 within ANDV infected cells contributes to the enhanced permeability of ANDV–infected endothelial cells and further suggests a specific target for regulating ANDV–induced permeability.

Discussion:

Pulmonary edema and hypoxia are hallmarks of HPS disease and linked to VEGFR2–directed responses within endothelial cells which are the primary targets of hantavirus infection. Hypoxia induces the secretion of VEGF, a factor which was first called vascular permeability factor for its potent ability to permeabilize capillaries and cause edema (37). Hyper–oxygenation of patients has been used to reduce HPS mortality to 40% (20). In vitro, endothelial cells infected by HFRS and HPS causing hantaviruses, but not nonpathogenic TULV, results in a dramatic enhancement of permeability in response to VEGF (57). ANDV–enhanced endothelial cell permeability results from the hyper–activation of VEGFR2 signaling pathways, VE–cadherin internalization, and the dissociation of AJs which normally maintain vascular integrity (57, 66, 152).

Our results suggest that inhibition of VEGFR2–Src signaling responses is able to block ANDV–induced EC permeability. Here we demonstrate that knockdown of Src within endothelial cells inhibits ANDV–induced permeability in response to VEGF. While there are currently no therapeutics for HFRS and HPS, this finding rationalizes the use of chemical inhibitors of Src to inhibit ANDV–induced EC permeability. The VEGFR2–Src signaling pathway has been a prominent target of anti–cancer therapies. These clinically available compounds may similarly regulate ANDV–induced permeability and have therapeutic utility against HPS. Recent results suggest that small molecule Src inhibitors are able to block ANDV induced endothelial cell permeability (65).

MiRNAs are emerging as prominent regulatory molecules that play important roles in cancer, angiogenesis, and cell type specificity (26, 67, 73, 85, 99, 144, 149, 174, 197). Discrete miRNAs are required for viral infection of specific cell types and thereby contribute to the cell and tissue tropism of viruses and their sequelae (46, 47, 173, 174, 204, 205). Endothelial cells contain a unique constellation of miRNAs that contribute to the cell type specific expression of cellular proteins within the endothelium and regulate endothelial cell functions which control vascular permeability (108). Several endothelial cell miRNAs are associated with regulating angiogenesis, growth factor activated pathways, or cell–cell interactions that control endothelial cell fluid barrier functions (46, 47, 173, 204, 205).

Tissue edema is a hallmark of pathogenic hantavirus infections regardless of whether infection results in HFRS or HPS (22, 32, 33, 150, 175, 176, 216). Pathogenic hantaviruses infect the endothelial cell lining of capillaries and enhance the permeability of endothelial cells in response to VEGF at late times post–infection (57). Hantaviruses traffic the RNA–binding nucleocapsid protein to cellular P–bodies (133), where miRNAs mature (8, 23, 45), suggesting that hantaviruses might alter endothelial cell functions by interfering with normal miRNA regulatory functions. To examine this, we studied the effects of ANDV on miRNA expression within infected endothelial cells. Our results indicate that ANDV infection alters the expression of a number of endothelial cell miRNAs, including a subset that play an important role in endothelial cell migration, adherence, and angiogenesis.

ANDV infection increased the level of six miRNAs which have recently been shown to play roles in regulating angiogenesis or vascular integrity including miR–155, miR–320, and miR–222 (Figure 12) (46, 47, 173, 204, 205). These miRNAs reportedly regulate adherens junction disassembly, cell migration, and cell morphology which contribute to changes in vascular permeability (47, 149, 205). However, the role of these miRNAs in hantavirus infection of endothelial cells remains to be defined.

ANDV infection of endothelial cells resulted in a dramatic 3,400–fold downregulation of miR–410 (Figure 10B). The function of miR–410 is only

beginning to be disclosed and this miRNA has not been studied in endothelial cells. However, knockdown of miR–410 decreases cellular secretion while increased miR–410 appears to increase secretory responses (70). At this point it is unclear whether secretion is impaired in ANDV–infected endothelial cells, or whether decreased or aberrant secretion might play a role in regulating cellular activation or immune recognition of ANDV–infected endothelial cells. However, the dramatic reduction in miR–410 suggests that downregulating this prominently expressed endothelial miRNA may play an important role in the success of hantaviruses within their unique endothelial cell niche. This provocative finding may prove interesting as specific miR–410 targets are defined and the role of miR–410 in regulating endothelial cell functions are disclosed. The mechanism by which ANDV downregulates miR–410 also remains to be defined.

Microarray analysis further revealed a 129–fold decrease in miR–218 in ANDV–infected endothelial cells (Figure 10B). A recent paper has determined that miR–218 specifically downregulates the expression of Robo1, a cell surface receptor that enhances angiogenesis by inhibiting the normal VEGF regulatory responses of another endothelial cell receptor, Robo4 (2, 182, 192). Robo4 normally stabilizes the vasculature by counteracting VEGF signaling responses that result in endothelial cell hyperpermeability (2, 97). In contrast, increased Robo1 expression results in the formation of heterodimeric Robo1–Robo4 complexes which decrease cell–cell adherence and enhance endothelial cell

migration (28, 91, 182, 198). This finding suggests that in ANDV infected ECs, decreased miR–218 levels may enhance VEGF directed permeability by increasing Robo1 and thereby decreasing Robo4 regulation. However, roles for miR–218, Robo1, and Robo4, in the enhanced VEGF directed permeability of ANDV–infected endothelial cells, require further investigation.

Similarly, miR–126 is an endothelial cell–specific miRNA which regulates VEGF–induced vascular permeability by repressing the expression of SPRED1 (46, 47, 204). SPRED1 induces actin turnover and is tied to the increased paracellular permeability of endothelial cells. SPRED1 functions by binding TESK1 and blocking TESK1 phosphorylation of cofilin (46, 94). Unphosphorylated cofilin increases the disassembly of actin filaments, resulting in the internalization of VE–cadherin and the disassembly of adherens junctions that maintain a paracellular fluid barrier (191, 204, 205). In fact, over–expressing SPRED1 or knocking out miR–126 results in increased endothelial cell permeability in response to VEGF (46, 94, 204). Curiously, we observed only a small increase in miR–126 (2–fold) within ANDV infected endothelial cells but this did not result in a decrease in SPRED1 mRNA levels. In fact, counter to increased miR–126 levels (Figure 11), we observed a 10–fold increase in SPRED1 mRNA following ANDV infection (Figure 13), which is consistent with the enhanced permeability of ANDV–infected endothelial cells.

Decreased cofilin phosphorylation within ANDV– versus TULV–infected endothelial cells (Figure 14) was also consistent with observed increases in SPRED1 and suggested that ANDV interfered with normal miR–126 regulation of SPRED1 following infection. In fact, the response to SPRED1 overexpression is similar to the enhanced permeability of endothelial cells infected by pathogenic hantaviruses (46, 57). When we analyzed the effect of SPRED1 downregulation on the permeability of ANDV infected cells we found that SPRED1 siRNAs both reduced SPRED1 mRNA levels (Figure 15A) and inhibited endothelial cell permeability following ANDV infection (Figure 15B). Increased SPRED1 levels in ANDV–infected endothelial cells may increase cofilin activity and enhance adherens junction disassembly responses (46, 47, 66, 94). This data demonstrates that increased SPRED1 contributes to the permeability of ANDV–infected endothelial cells. As a result our findings link alterations in cellular VEGF responses to a potential mechanism for the enhanced paracellular permeability of hantavirus–infected endothelial cells.

Recently published data also tie miR–503 to altered regulation of cofilin responses, and thereby decreased adherence junction stability, within ANDV–infected endothelial cells (92, 120). ANDV infection resulted in a 77–fold decrease in miR–503 within endothelial cells (Figures 10B and 11) and miR–503 regulates the expression of cyclin D1 (92). While cyclin D1 knockouts display increased cellular adherence, increased cyclin D1 expression decreases cellular

adherence and enhances cell migration by inhibiting Rho/ROCK signaling responses (120). LIM kinase, which phosphorylates cofilin, is a key ROCK substrate and, thus, a reduction in miR–503 levels could also contribute to the enhanced cofilin activity and enhanced EC permeability observed in ANDV–infected endothelial cells (120). These findings suggest that additional microRNAs may contribute to hantavirus induced endothelial cell permeability and provide additional targets for therapeutic consideration (120).

Our results indicate that ANDV interferes with both microRNA expression and the ability of microRNAs to regulate their cognate target mRNAs within endothelial cells. Based on studies presented here we propose a model for a potential mechanism by which ANDV infection induces permeability in infected endothelial cells (Figure 16). Under normal conditions miR–126 inhibits SPRED1 and PIK3R2 levels resulting in increased vascular integrity (204). In contrast, knockout of miR–126 in endothelial cells results in increased SPRED1 and PIK3R2 levels and increased vascular permeability (46, 205). Similar to miR–126 knockouts, ANDV infection of ECs results in the upregulation of SPRED1 and PIK3R2 levels, however miR–126 levels were not reduced. Increased SPRED1 levels results in decreased TESK1 activity and, consequently, increased levels of active cofilin leading to the depolymerization of actin filaments and adherens junction disassembly (94, 151, 196). The ability of the hantavirus nucleocapsid protein to bind RNA and localize to cytoplasmic P–

bodies (133) provides a potential means for the nucleocapsid protein to interfere with the function of miR–126, and other microRNAs, within ANDV–infected endothelial cells. However, the ability of the hantavirus nucleocapsid protein or other viral proteins to regulate miRNA functions remains to be explored.

These studies suggest the potential for blocking hantavirus diseases by directly targeting SPRED1 or PIK3R2 or their pathway–specific responses. Figure 15B demonstrates that siRNA knockdown of SPRED1 blocks ANDV induced permeability responses in infected endothelial cells. Further experiments will be required to identify pathway–specific components that are necessary to block ANDV–directed vascular permeability responses. Additionally, experiments presented here suggest the possible application of blocking microRNA responses to mitigate cancer, angiogenesis, and cardiopulmonary diseases where endothelial cell dysfunction and miRNA regulation are central to the disease process (145, 174, 205).

Chapter 4:

Hantavirus Reverse Genetics

Introduction:

Reverse genetics is a term coined for the generation of recombinant RNA viruses from DNA clones. Reverse genetics systems permit the study of RNA viruses through modification of their genome via cloned complimentary DNA (cDNA) (154). This approach was first successfully applied to generate recombinant DNA viruses when a Simian virus 40 (SV40) containing λ phage DNA was rescued following transfection of CV–1 monkey kidney cells (64). The first reverse genetics system developed for RNA viruses was for poliovirus, a positive–sense RNA virus (166). In this system, cDNA constructs containing segments of the poliovirus genome were joined to generate a full–length cDNA clone. Transfection of the full–length cDNA clone into CV–1 or HeLa cells produced infectious poliovirus (166).

The ability to rescue negative–sense RNA viruses has been more difficult. While the genome of positive–sense RNA viruses is infectious, this is not the case for negative–sense RNA viruses. Moreover, negative–sense RNA viruses require an RNA–dependent RNA polymerase to generate a positive–sense RNA intermediate for translation of viral proteins and which serve as templates for genome replication (154). Rescue of a negative–sense RNA virus first occurred when the neuraminidase (NA) gene of influenza virus was incorporated into a helper influenza virus lacking the gene. *In vitro* transcribed NA RNA was mixed with purified influenza nucleoprotein and polymerase to generate a

ribonucleoprotein (RNP) complex which was transfected into cells. Cells were then infected with helper virus and reassortant virus was isolated by selection. Subsequently, rescue of influenza viruses containing site–specific mutations within the NA gene established the approach as a means to study distinct aspects of influenza virus biology (41).

The preparation of RNP complexes requires the synthesis of RNA and purification of viral proteins *in vitro* to form biologically active RNP complexes (154). This approach for rescuing virus was improved through the use of plasmids to amplify and express viral genes and proteins within cells. In this approach, a construct containing the RNA polymerase I (Pol I) promoter and hepatitis delta virus ribozyme elements flanking a viral gene was transfected into cells along with RNA polymerase II (Pol II) driven constructs expressing viral proteins required for genome replication (ie, nucleoprotein and polymerase). Following infection with helper virus, recombinant virus was selected. This approach was the first to be used to rescue influenza virus through the use of plasmids (162). Similar plasmid–based approaches have been used to generate other negative–sense RNA viruses including rabies virus (178), vesicular stomatitis virus (115, 208), measles virus (167), respiratory syncytial virus (31), and Sendai virus (31, 100).

The use of this approach to rescue segmented negative–sense RNA viruses is limited by the need to infect transfected cells with helper virus to provide the

other viral gene segments. This requires strong selection techniques to isolate recombinants from helper viruses which hampers the study of growth–inhibiting mutations (147). The Pol I promoter driven approach was further developed into a completely plasmid–based system to rescue recombinant influenza virus obviating the need for helper virus infection (48, 147).

To establish the plasmid–based system, plasmids were created with a Pol I promoter upstream and hepatitis delta ribozyme element downstream of each of the eight influenza gene segments (48, 147). Since the viral polymerase requires specific end terminal sequences for recognition of the gene segments, the ribozyme element is included to generate precise RNA ends. Four protein expression vectors encoding PB1, PB2, PA (the influenza polymerase subunits), and NP (nucleoprotein) were co–transfected with the eight Pol I constructs to rescue virus (48, 147). The plasmid–based system was further optimized through the use of bidirectional constructs that generate Pol I–driven vRNAs and Pol II–driven mRNAs, decreasing the number of required vectors to eight (80). An additional improvement has been the use of a single construct containing eight Pol I transcription cassettes encoding each gene segment (146). The success of influenza reverse genetics suggested that reverse genetics systems could be developed for other negative–sense RNA viruses.

Efficient reverse genetics systems have been developed using T7 RNA polymerase to drive transcription of viral RNAs (34). Rabies virus was the first

virus to be rescued entirely from cloned cDNAs utilizing T7 polymerase transcriptional elements (178). Subsequently, the T7–driven system has been used to rescue other negative–sense viruses including those within the *Paramyxoviridae*, *Rhabdoviridae*, *Filoviridae*, *Arenaviridae*, and *Bunyaviridae* families (34).

Reverse genetics systems were developed for Bunyamwera (BUN) virus which, like hantaviruses, is a member of the *Bunyaviridae* family and contains a tripartite negative–sense genome. Each BUN gene segment was cloned into a vector with a T7 RNA polymerase promoter upstream and a Hepatitis Delta virus ribozyme downstream (16). T7 RNA polymerase expression was used to transcribe RNAs with specific termini, determined by the T7 RNA polymerase transcription start site (three guanine nucleotides immediately downstream of the T7 promoter) and the auto–catalytic Hepatitis Delta ribozyme element, which are required for viral transcription and replication. In addition, three helper constructs used to express BUN proteins were also provided in *trans*. Following co–transfection of all six vectors into cells, BUN was successfully rescued (16). Further experiments revealed that virus could be rescued without expression of helper BUN proteins and that transfection of plasmids encoding anti–genomic sense RNAs alone was sufficient to rescue virus (124). While a number of systems have been established to rescue negative–sense RNA viruses , the success

of the BUN approach provides a model for establishing hantavirus reverse genetics systems.

Results:

Reverse genetics systems have been developed for numerous viruses including influenza viruses and bunyaviruses (34, 124, 147). The ability to manipulate the genomes of negative–sense RNA viruses has permitted the generation of attenuated viruses for use in vaccine development and the study of determinants of viral pathogenesis (31, 147, 154, 157). The success of Bunyavirus reverse genetics suggests that similar approaches can be used for hantaviruses.

To rescue recombinant ANDV, cDNAs encoding anti–genome sense RNAs (cRNAs) corresponding to the L, M, and S segments were generated by PCR using primers containing BsmBI restriction sites generating unique overhangs following restriction digestion. Digested PCR products were cloned into BsmBI–digested pT7HR2 (containing Hammerhead and Hepatitis Delta ribozyme elements) (Figure 17C) or pT7HR1 (containing only the downstream Hepatitis Delta ribozyme element) vectors (Figure 17D). To distinguish recombinant ANDV from the wild–type lab strain, a BamHI restriction site was introduced in the N protein ORF within the S segment construct by site–directed mutagenesis (pT7HR1–ANDV–S–Marker; Figure 18A). Introduced mutations are silent and do not alter the N protein amino acid sequence. Additionally,

helper constructs were generated to express ANDV proteins to facilitate replication and packaging of viral RNAs. The ANDV polymerase, G_NG_C, and N protein ORFs were cloned into pTM1 downstream of an IRES element (Figure 17E) to permit high–level expression of these proteins.

Expression of ANDV Proteins From pT7HR2, pT7HR1, and pTM1 Vectors

To monitor N protein expression from pT7HR2–ANDV–S, pT7HR1–ANDV–S–Marker, and pTM1–ANDV–S, VeroE6 cells were co–transfected with each construct individually and a T7 polymerase expression plasmid (pCAGGS–T7) (155) and assayed by immunoperoxidase staining for N protein 36 hours post transfection. Figures 18B–D demonstrate that N protein was expressed within VeroE6 cells transfected with either pT7HR2–ANDV–S, pT7HR1–ANDV–S–Marker, or pTM1–ANDV–S, respectively. These data indicate that ANDV N protein can be expressed from anti–genomic (positive) sense RNAs with or without the presence of an IRES. However, the presence of the upstream IRES in pTM1–S substantially enhanced protein expression (Figure 18C and D). Further experiments using pT7HR2–ANDV–S consistently resulted in a lower expression of N protein when compared to cells transfected with the pT7HR1–ANDV–S–Marker. Consequently, further studies were performed using pT7HR1 constructs which lack the upstream ribozyme.

Protein expression from ANDV M segment constructs was monitored by Western blot of ANDV G_C following co–transfection of VeroE6 cells with

pT7HR1–ANDV–M or pTM1–ANDV–M and pCAGGS–T7. Thirty–six hours post transfection cells were lysed, protein separated by 12% SDS–PAGE, and G_C detected using rabbit polyclonal anti–G_C antibody (U.S. Biological). Figure 19 illustrates that G_C is expressed from both pT7HR1–ANDV–M and pTM1–ANDV–M. Comparison with G_C from ANDV infected cells suggests that the observed G_C protein is identical in size to wild–type ANDV G_C.

There are currently no available antibodies to the ANDV polymerase. To evaluate polymerase expression from pT7HR1 and pTM1 vectors, a reporter construct was generated to monitor polymerase activity. The enhanced green fluorescent protein (GFP) ORF was inserted into pT7HR1 in the antisense orientation flanked by ANDV L segment UTRs (pT7HR1–GFP–rev) (Figure 20A). Expression of GFP from this construct requires a functional ANDV polymerase to generate positive–sense GFP RNA which can serve as a template for translation. Figure 20 illustrates that GFP–expressing VeroE6 cells were present only following co–transfection of pT7HR1–ANDV–L (Figure 20C) or pTM1–ANDV–L (Figure 20D) compared to cells transfected with only pT7HR1–GFP–rev (Figure 20B). Moreover, GFP expression was enhanced in the presence of the nucleocapsid protein (Figure 20E).

Plasmid–based Rescue of Recombinant Andes Virus

Our data suggests that ANDV proteins are expressed from both pT7HR1 and pTM1 constructs. Therefore, we attempted to rescue recombinant ANDV

following co–transfection of pT7HR1–ANDV–L, –M, –S–Marker with or without helper pTM1 plasmids. Cells were co–transfected with equal amounts (1 μg) of pT7HR1–ANDV–L, –M, –S–Marker, pCAGGS–T7, with or without helper pTM1 plasmids using Lipofectamine 2000. Five days post transfection, media from transfected VeroE6 cells was passaged on VeroE6 cells and the presence of recombinant ANDV–infected cells was assayed by immunoperoxidase staining for nucleocapsid protein. Despite the presence N protein–expressing VeroE6 cells following transfection (Figure 21A), only a few VeroE6 cells were found to be expressing N protein (Figure 21B) after this first passage. However, subsequent passage using media collected from VeroE6 cells infected in the first passage failed to produce any infected cells as determined by immunoperoxidase staining. This suggests that recombinant viruses produced following transfection were not able to replicate after being passaged.

In Vitro Transcription of ANDV Gene Segments

In addition to plasmid–based rescue of recombinant ANDV, we evaluated transfection of *in vitro* transcribed ANDV gene segments cRNAs as an alternative approach. To generate templates for *in vitro* transcription, a unique ApaI restriction enzyme site was inserted downstream of the 3' UTR within the pT7HR1–ANDV–L, –M, and –S–Marker vectors by site–directed mutagenesis (pT7HR1–ANDV–Segment–ApaI; Table II). Following digestion by ApaI, the linearized vectors were used as templates for *in vitro* transcription. Figure 22

illustrates that L, M, and S segment cRNAs were efficiently transcribed from the linearized vectors and, based on their relative migration to one another, each transcript was the expected length (approximate ratio: 3:2:1, L:M:S).

To evaluate whether the *in vitro* transcribed RNAs could serve as templates for translation, ApaI–digested pT7HR1–ANDV–S–Marker was used as a template for *in vitro* transcription/translation. Figure 23 demonstrates that the nucleocapsid protein was generated *in vitro* from the linearized ANDV–S–Marker construct. These data suggest that *in vitro* transcribed ANDV gene segment RNAs can be used as templates to express ANDV proteins following transfection of the RNAs into cells. *In vitro* transcribed ANDV gene segment cRNAs are currently being evaluated for their ability to generate recombinant ANDVs using several approaches including microinjection, electroporation, and *in vitro* virus synthesis using clarified cell lysates as has been accomplished for poliovirus (138).

Discussion:

Our data show that hantavirus proteins can be expressed from constructs generating anti–genome sense cRNAs (Figures 17–19). Following transfection of VeroE6 cells with pT7HR1–ANDV–M or pT7HR1–ANDV–S–Marker ANDV, G_C and N could be detected by Western blot (G_C; Figure 19) or immunoperoxidase staining (N, Figure 18C). This suggests that ANDV cRNAs

contain *cis*–acting elements that facilitate translation of viral proteins by the cellular translation machinery. Moreover, *in vitro* transcription of hantavirus cRNAs from ApaI–linearized pT7HR1 gene segment constructs results in the generation of RNA transcripts (Figure 22) which can be translated *in vitro* (Figure 23).

In ANDV–infected cells, G_C is expressed as part of a G_NG_C glycoprotein precursor which is co–translationally cleaved. Expression of individual G_N and G_C requires the presence of the "WAASA" pentapeptide located between the G_N and G_C which is recognized by a cellular signal peptidase that cleaves the precursor (122). Analysis of G_C expression (Figure 19) indicates that the G_NG_C pro–protein encoded by pT7HR1–ANDV–M and pTM1–ANDV–M is synthesized during translation and that the G_C protein expressed from these vectors is the same size as the wild–type ANDV G_C (Figure 19). Additionally, since the mature G_N is cleaved from a G_NG_C precursor, this data also suggests that proper cotranslational processing occurred and that the G_N protein is co–expressed.

Despite initial success expressing GFP from a reporter construct containing ANDV L segment ends (Figure 20), further experiments involving transfection of codon–optimized ANDV L construct (pTM1–ANDV–L–Opt) resulted in decreased N protein expression in transfected cells. The hantavirus polymerase binds RNA (110) and, therefore, overexpression of the ANDV

polymerase using a codon–optimized ORF may result in deleterious interactions between the viral polymerase and cellular RNAs resulting in increased cytotoxicity. To address this problem, a pTM1 construct encoding the wild–type ANDV polymerase ORF was generated and subsequently used in experiments to generate recombinant ANDV.

Attempts to rescue recombinant ANDV following transfection of pT7HR1 gene segment constructs, with or without the co–transfection of pTM1 helper constructs, have not been successful. While a few attempts resulted in the presence of a small number of nucleocapsid protein containing cells following the passage of media from transfected cells (Figure 21B), subsequent passage did not result in the detection of any N protein expressing cells.

Generation of recombinant virus requires efficient packaging of viral gene segments which is dependent upon the presence of properly terminated gene segment ends. While the auto–catalytic activity of the Hepatitis delta ribozyme is reported to be highly efficient (25), it is possible that the 3' ends of the transcribed ANDV gene segments cRNAs are not being processed effectively by the ribozyme. This could be the result of localized interactions of the transcribed cRNA 3' ends with the Hepatitis delta ribozyme which might obstruct the self–cleaving ability of the ribozyme. Under this condition, the cRNA transcripts could still serve as templates for translation of viral protein, as illustrated in Figures 17–19. However, the ability of the ANDV polymerase to use the

transcripts as templates to generate vRNAs would likely be blocked since panhandle structures formed by interactions of the 5' and 3' gene segment UTRs would be severely diminished due the presence of the un–cleaved ribozyme. Replication of the hantavirus genome requires the presence of the panhandle structures formed by the interaction of the UTRs which interacts with the nucleocapsid to facilitate viral polymerase activity (110, 136).

To address the possibility that inefficient processing by the Hepatitis delta ribozyme may be preventing the generation of vRNAs from transcribed cRNAs, *in vitro* transcription of ANDV cRNAs was investigated to rescue recombinant ANDV. A unique ApaI restriction enzyme site was inserted into the pT7HR1 gene segment constructs downstream of the 3' UTR to facilitate the generation of a properly terminated end. Following digestion with ApaI, the constructs can serve as templates for *in vitro* transcription and contain a precisely defined end (Figure 22). Thus far, attempts to rescue virus following transfection of *in vitro* transcribed cRNAs, with or without co–transfection of helper pTM1 constructs, have failed to result in the production of recombinant virus beyond more than one passage.

The success of hantavirus reverse genetics requires continued efforts to evaluate components being used to rescue recombinant ANDV. A key element that requires further investigation is the ANDV polymerase. As discussed previously, the hantavirus polymerase binds RNAs (110) and experiments in

which a codon–optimized polymerase vector has been used have resulted in deleterious effects on the expression of the nucleocapsid protein. This may be due to interaction of the ANDV polymerase with cellular mRNAs and/or miRNAs which disrupts normal cellular functions or an effect on translational machinery. Additionally, the viral polymerase likely contains endonuclease activity that directs cap splicing on viral RNAs, but which could inactivate cellular mRNAs. During the course of hantavirus infection the levels of the polymerase are relatively low compared to G_N, G_C, and the nucleocapsid protein. This suggests that high level expression of the polymerase may be disadvantageous for virus viability. Further experiments are required to elucidate the function of the viral polymerase within infected, or transfected, cells. However, the lack of effective tools such as antibodies directed against the hantavirus polymerase has thus far hindered such studies.

References

1. **Acevedo, L. M., S. Barillas, S. M. Weis, J. R. Gothert, and D. A. Cheresh.** 2008. Semaphorin 3A suppresses VEGF-mediated angiogenesis yet acts as a vascular permeability factor. Blood **111:**2674-80.
2. **Acevedo, L. M., S. M. Weis, and D. A. Cheresh.** 2008. Robo4 counteracts VEGF signaling. Nat Med **14:**372-3.
3. **Alff, P. J., I. N. Gavrilovskaya, E. Gorbunova, K. Endriss, Y. Chong, E. Geimonen, N. Sen, N. C. Reich, and E. R. Mackow.** 2006. The pathogenic NY-1 hantavirus G1 cytoplasmic tail inhibits RIG-I- and TBK-1-directed interferon responses. J Virol **80:**9676-86.
4. **Alff, P. J., N. Sen, E. Gorbunova, I. N. Gavrilovskaya, and E. R. Mackow.** 2008. The NY-1 hantavirus Gn cytoplasmic tail coprecipitates TRAF3 and inhibits cellular interferon responses by disrupting TBK1-TRAF3 complex formation. J Virol **82:**9115-22.
5. **Avsic-Zupanc, T., S. Y. Xiao, R. Stojanovic, A. Gligic, G. van der Groen, and J. W. LeDuc.** 1992. Characterization of Dobrava virus: a Hantavirus from Slovenia, Yugoslavia. J Med Virol **38:**132-7.
6. **Baker, E. K., E. C. Tozer, M. Pfaff, S. J. Shattil, J. C. Loftus, and M. H. Ginsberg.** 1997. A genetic analysis of integrin function: Glanzmann thrombasthenia in vitro. Proc Natl Acad Sci U S A **94:**1973-8.
7. **Banno, A., and M. H. Ginsberg.** 2008. Integrin activation. Biochem Soc Trans **36:**229-34.
8. **Bartel, D. P.** 2004. MicroRNAs: genomics, biogenesis, mechanism, and function. Cell **116:**281-97.
9. **Bates, D. O., and S. J. Harper.** 2002. Regulation of vascular permeability by vascular endothelial growth factors. Vascul Pharmacol **39:**225-37.
10. **Baumgartner-Parzer, S. M., and W. K. Waldhausl.** 2001. The endothelium as a metabolic and endocrine organ: its relation with insulin resistance. Exp Clin Endocrinol Diabetes **109 Suppl 2:**S166-79.
11. **Berger, M. M., C. Hesse, C. Dehnert, H. Siedler, P. Kleinbongard, H. J. Bardenheuer, M. Kelm, P. Bartsch, and W. E. Haefeli.** 2005. Hypoxia impairs systemic endothelial function in individuals prone to high-altitude pulmonary edema. Am J Respir Crit Care Med **172:**763-7.
12. **Bernatchez, P. N., S. Soker, and M. G. Sirois.** 1999. Vascular endothelial growth factor effect on endothelial cell proliferation, migration, and platelet-activating factor synthesis is Flk-1-dependent. J Biol Chem **274:**31047-54.
13. **Bernshtein, A. D., N. S. Apekina, T. V. Mikhailova, Y. A. Myasnikov, L. A. Khlyap, Y. S. Korotkov, and I. N. Gavrilovskaya.** 1999.

Dynamics of Puumala hantavirus infection in naturally infected bank voles (Clethrinomys glareolus). Arch Virol **144:**2415-28.

14. **Borges, E., Y. Jan, and E. Ruoslahti.** 2000. Platelet-derived growth factor receptor beta and vascular endothelial growth factor receptor 2 bind to the beta 3 integrin through its extracellular domain. J Biol Chem **275:**39867-73.
15. **Brakenhielm, E.** 2007. Substrate matters: reciprocally stimulatory integrin and VEGF signaling in endothelial cells. Circ Res **101:**536-8.
16. **Bridgen, A., and R. M. Elliott.** 1996. Rescue of a segmented negative-strand RNA virus entirely from cloned complementary DNAs. Proc Natl Acad Sci U S A **93:**15400-4.
17. **Brummer-Korvenkontio, M., A. Vaheri, T. Hovi, C. H. von Bonsdorff, J. Vuorimies, T. Manni, K. Penttinen, N. Oker-Blom, and J. Lahdevirta.** 1980. Nephropathia epidemica: detection of antigen in bank voles and serologic diagnosis of human infection. J Infect Dis **141:**131-4.
18. **Byzova, T. V., C. K. Goldman, N. Pampori, K. A. Thomas, A. Bett, S. J. Shattil, and E. F. Plow.** 2000. A mechanism for modulation of cellular responses to VEGF: activation of the integrins. Mol Cell **6:**851-60.
19. **Byzova, T. V., R. Rabbani, S. E. D'Souza, and E. F. Plow.** 1998. Role of integrin alpha(v)beta3 in vascular biology. Thromb Haemost **80:**726-34.
20. **Chang, B., M. Crowley, M. Campen, and F. Koster.** 2007. Hantavirus cardiopulmonary syndrome. Semin Respir Crit Care Med **28:**193-200.
21. **Chaparro, J., J. Vega, W. Terry, J. L. Vera, B. Barra, R. Meyer, C. J. Peters, A. S. Khan, and T. G. Ksiazek.** 1998. Assessment of person-to-person transmission of hantavirus pulmonary syndrome in a Chilean hospital setting. J Hosp Infect **40:**281-5.
22. **Chen, J. P., and T. M. Cosgriff.** 2000. Hemorrhagic fever virus-induced changes in hemostasis and vascular biology. Blood Coagul Fibrinolysis **11:**461-83.
23. **Chen, K., and N. Rajewsky.** 2007. The evolution of gene regulation by transcription factors and microRNAs. Nat Rev Genet **8:**93-103.
24. **Childs, J. E., T. G. Ksiazek, C. F. Spiropoulou, J. W. Krebs, S. Morzunov, G. O. Maupin, K. L. Gage, P. E. Rollin, J. Sarisky, R. E. Enscore, and et al.** 1994. Serologic and genetic identification of Peromyscus maniculatus as the primary rodent reservoir for a new hantavirus in the southwestern United States. J Infect Dis **169:**1271-80.
25. **Chowrira, B. M., P. A. Pavco, and J. A. McSwiggen.** 1994. In vitro and in vivo comparison of hammerhead, hairpin, and hepatitis delta virus self-processing ribozyme cassettes. J Biol Chem **269:**25856-64.

26. **Choy, E. Y., K. L. Siu, K. H. Kok, R. W. Lung, C. M. Tsang, K. F. To, D. L. Kwong, S. W. Tsao, and D. Y. Jin.** 2008. An Epstein-Barr virus-encoded microRNA targets PUMA to promote host cell survival. J Exp Med **205:**2551-60.
27. **Christou, H., A. Yoshida, V. Arthur, T. Morita, and S. Kourembanas.** 1998. Increased vascular endothelial growth factor production in the lungs of rats with hypoxia-induced pulmonary hypertension. Am J Respir Cell Mol Biol **18:**768-76.
28. **Cirulli, V., and M. Yebra.** 2007. Netrins: beyond the brain. Nat Rev Mol Cell Biol **8:**296-306.
29. **Clement, J. P.** 2003. Hantavirus. Antiviral Res **57:**121-7.
30. **Coller, B.** 1997. GPIIb/IIIa Antagonists: Pathophysiologic and Therapeutic insights from studies of c7E3 Fab. Thrombosis and Haemostasis **78:**730-35.
31. **Collins, P. L., M. G. Hill, E. Camargo, H. Grosfeld, R. M. Chanock, and B. R. Murphy.** 1995. Production of infectious human respiratory syncytial virus from cloned cDNA confirms an essential role for the transcription elongation factor from the 5' proximal open reading frame of the M2 mRNA in gene expression and provides a capability for vaccine development. Proc Natl Acad Sci U S A **92:**11563-7.
32. **Cosgriff, T. M., H. W. Lee, A. F. See, D. B. Parrish, J. S. Moon, D. J. Kim, and R. M. Lewis.** 1991. Platelet dysfunction contributes to the haemostatic defect in haemorrhagic fever with renal syndrome. Trans R Soc Trop Med Hyg **85:**660-3.
33. **Cosgriff, T. M., and R. M. Lewis.** 1991. Mechanisms of disease in hemorrhagic fever with renal syndrome. Kidney Int Suppl **35:**S72-9.
34. **de Wit, E., M. I. Spronken, G. Vervaet, G. F. Rimmelzwaan, A. D. Osterhaus, and R. A. Fouchier.** 2007. A reverse-genetics system for Influenza A virus using T7 RNA polymerase. J Gen Virol **88:**1281-7.
35. **Dejana, E., F. Orsenigo, and M. G. Lampugnani.** 2008. The role of adherens junctions and VE-cadherin in the control of vascular permeability. J Cell Sci **121:**2115-22.
36. **Duchin, J. S., F. T. Koster, C. J. Peters, G. L. Simpson, B. Tempest, S. R. Zaki, T. G. Ksiazek, P. E. Rollin, S. Nichol, E. T. Umland, and et al.** 1994. Hantavirus pulmonary syndrome: a clinical description of 17 patients with a newly recognized disease. The Hantavirus Study Group. N Engl J Med **330:**949-55.
37. **Dvorak, H. F.** 2006. Discovery of vascular permeability factor (VPF). Exp Cell Res **312:**522-6.
38. **Dvorak, H. F., L. F. Brown, M. Detmar, and A. M. Dvorak.** 1995. Vascular permeability factor/vascular endothelial growth factor,

microvascular hyperpermeability, and angiogenesis. Am J Pathol **146:**1029-39.

39. **Dvorak, H. F., T. M. Sioussat, L. F. Brown, B. Berse, J. A. Nagy, A. Sotrel, E. J. Manseau, L. Van de Water, and D. R. Senger.** 1991. Distribution of vascular permeability factor (vascular endothelial growth factor) in tumors: concentration in tumor blood vessels. J Exp Med **174:**1275-8.
40. **Elwell, M. R., G. S. Ward, M. Tingpalapong, and J. W. LeDuc.** 1985. Serologic evidence of Hantaan-like virus in rodents and man in Thailand. Southeast Asian J Trop Med Public Health **16:**349-54.
41. **Enami, M., W. Luytjes, M. Krystal, and P. Palese.** 1990. Introduction of site-specific mutations into the genome of influenza virus. Proc Natl Acad Sci U S A **87:**3802-5.
42. **Enria, D. A., A. M. Briggiler, N. Pini, and S. Levis.** 2001. Clinical manifestations of New World hantaviruses. Curr Top Microbiol Immunol **256:**117-34.
43. **Espinoza, R., P. Vial, L. M. Noriega, A. Johnson, S. T. Nichol, P. E. Rollin, R. Wells, S. Zaki, E. Reynolds, and T. G. Ksiazek.** 1998. Hantavirus pulmonary syndrome in a Chilean patient with recent travel in Bolivia. Emerg Infect Dis **4:**93-5.
44. **Esser, S., M. G. Lampugnani, M. Corada, E. Dejana, and W. Risau.** 1998. Vascular endothelial growth factor induces VE-cadherin tyrosine phosphorylation in endothelial cells. J Cell Sci **111 (Pt 13):**1853-65.
45. **Eulalio, A., I. Behm-Ansmant, D. Schweizer, and E. Izaurralde.** 2007. P-body formation is a consequence, not the cause, of RNA-mediated gene silencing. Mol Cell Biol **27:**3970-81.
46. **Fish, J. E., M. M. Santoro, S. U. Morton, S. Yu, R. F. Yeh, J. D. Wythe, K. N. Ivey, B. G. Bruneau, D. Y. Stainier, and D. Srivastava.** 2008. miR-126 regulates angiogenic signaling and vascular integrity. Dev Cell **15:**272-84.
47. **Fish, J. E., and D. Srivastava.** 2009. MicroRNAs: opening a new vein in angiogenesis research. Sci Signal **2:**pe1.
48. **Fodor, E., L. Devenish, O. G. Engelhardt, P. Palese, G. G. Brownlee, and A. Garcia-Sastre.** 1999. Rescue of influenza A virus from recombinant DNA. J Virol **73:**9679-82.
49. **Forsythe, J. A., B. H. Jiang, N. V. Iyer, F. Agani, S. W. Leung, R. D. Koos, and G. L. Semenza.** 1996. Activation of vascular endothelial growth factor gene transcription by hypoxia-inducible factor 1. Mol Cell Biol **16:**4604-13.
50. **Frenette, P. S., and D. D. Wagner.** 1996. Adhesion molecules--Part II: Blood vessels and blood cells. N Engl J Med **335:**43-5.

51. **Fulhorst, C. F., M. N. Cajimat, A. Utrera, M. L. Milazzo, and G. M. Duno.** 2004. Maporal virus, a hantavirus associated with the fulvous pygmy rice rat (Oligoryzomys fulvescens) in western Venezuela. Virus Res **104:**139-44.
52. **Gamble, J. R., J. Drew, L. Trezise, A. Underwood, M. Parsons, L. Kasminkas, J. Rudge, G. Yancopoulos, and M. A. Vadas.** 2000. Angiopoietin-1 is an antipermeability and anti-inflammatory agent in vitro and targets cell junctions. Circ Res **87:**603-7.
53. **Gavard, J., and J. S. Gutkind.** 2006. VEGF controls endothelial-cell permeability by promoting the beta-arrestin-dependent endocytosis of VE-cadherin. Nat Cell Biol **8:**1223-34.
54. **Gavard, J., V. Patel, and J. S. Gutkind.** 2008. Angiopoietin-1 prevents VEGF-induced endothelial permeability by sequestering Src through mDia. Dev Cell **14:**25-36.
55. **Gavrilovskaya, I. N., E. J. Brown, M. H. Ginsberg, and E. R. Mackow.** 1999. Cellular entry of hantaviruses which cause hemorrhagic fever with renal syndrome is mediated by beta3 integrins. J Virol **73:**3951-9.
56. **Gavrilovskaya, I. N., E. E. Gorbunova, and E. R. Mackow.** 2010. Pathogenic hantaviruses direct the adherence of quiescent platelets to infected endothelial cells. J Virol **84:**4832-9.
57. **Gavrilovskaya, I. N., E. E. Gorbunova, N. A. Mackow, and E. R. Mackow.** 2008. Hantaviruses direct endothelial cell permeability by sensitizing cells to the vascular permeability factor VEGF, while angiopoietin 1 and sphingosine 1-phosphate inhibit hantavirus-directed permeability. J Virol **82:**5797-806.
58. **Gavrilovskaya, I. N., T. Peresleni, E. Geimonen, and E. R. Mackow.** 2002. Pathogenic hantaviruses selectively inhibit beta3 integrin directed endothelial cell migration. Arch Virol **147:**1913-31.
59. **Gavrilovskaya, I. N., M. Shepley, R. Shaw, M. H. Ginsberg, and E. R. Mackow.** 1998. beta3 Integrins mediate the cellular entry of hantaviruses that cause respiratory failure. Proc Natl Acad Sci U S A **95:**7074-9.
60. **Geimonen, E., I. Fernandez, I. N. Gavrilovskaya, and E. R. Mackow.** 2003. Tyrosine residues direct the ubiquitination and degradation of the NY-1 hantavirus G1 cytoplasmic tail. J Virol **77:**10760-868.
61. **Geimonen, E., R. LaMonica, K. Springer, Y. Farooqui, I. N. Gavrilovskaya, and E. R. Mackow.** 2003. Hantavirus pulmonary syndrome-associated hantaviruses contain conserved and functional ITAM signaling elements. J Virol **77:**1638-43.
62. **Geimonen, E., S. Neff, T. Raymond, S. S. Kocer, I. N. Gavrilovskaya, and E. R. Mackow.** 2002. Pathogenic and nonpathogenic hantaviruses

differentially regulate endothelial cell responses. Proc Natl Acad Sci U S A **99:**13837-42.

63. **Glass, G. E., J. E. Childs, G. W. Korch, and J. W. LeDuc.** 1988. Association of intraspecific wounding with hantaviral infection in wild rats (Rattus norvegicus). Epidemiol Infect **101:**459-72.
64. **Goff, S. P., and P. Berg.** 1976. Construction of hybrid viruses containing SV40 and lambda phage DNA segments and their propagation in cultured monkey cells. Cell **9:**695-705.
65. **Gorbunova, E., I. Gavrilovskaya, T. Pepini, and E. R. Mackow.** 2010. VEGFR2 and Src Kinase Inhibitors Suppress ANDV Induced Endothelial Cell Permeability. J Virol.
66. **Gorbunova, E., I. N. Gavrilovskaya, and E. R. Mackow.** 2010. Pathogenic hantaviruses Andes virus and Hantaan virus induce adherens junction disassembly by directing vascular endothelial cadherin internalization in human endothelial cells. J Virol **84:**7405-11.
67. **Grassmann, R., and K. T. Jeang.** 2008. The roles of microRNAs in mammalian virus infection. Biochim Biophys Acta **1779:**706-11.
68. **Groeneveld, A. B.** 2002. Vascular pharmacology of acute lung injury and acute respiratory distress syndrome. Vascul Pharmacol **39:**247-56.
69. **He, L., and G. J. Hannon.** 2004. MicroRNAs: small RNAs with a big role in gene regulation. Nat Rev Genet **5:**522-31.
70. **Hennessy, E., M. Clynes, P. B. Jeppesen, and L. O'Driscoll.** 2010. Identification of microRNAs with a role in glucose stimulated insulin secretion by expression profiling of MIN6 cells. Biochem Biophys Res Commun **396:**457-62.
71. **Hepojoki, J., T. Strandin, A. Vaheri, and H. Lankinen.** 2010. Interactions and oligomerization of hantavirus glycoproteins. J Virol **84:**227-42.
72. **Hepojoki, J., T. Strandin, H. Wang, O. Vapalahti, A. Vaheri, and H. Lankinen.** 2010. Cytoplasmic tails of hantavirus glycoproteins interact with the nucleocapsid protein. J Gen Virol **91:**2341-50.
73. **Heusschen, R., M. van Gink, A. W. Griffioen, and V. L. Thijssen.** 2010. MicroRNAs in the tumor endothelium: novel controls on the angioregulatory switchboard. Biochim Biophys Acta **1805:**87-96.
74. **Heyman, P., A. Plyusnina, P. Berny, C. Cochez, M. Artois, M. Zizi, J. P. Pirnay, and A. Plyusnin.** 2004. Seoul hantavirus in Europe: first demonstration of the virus genome in wild Rattus norvegicus captured in France. Eur J Clin Microbiol Infect Dis **23:**711-7.
75. **Hippenstiel, S., M. Krull, A. Ikemann, W. Risau, M. Clauss, and N. Suttorp.** 1998. VEGF induces hyperpermeability by a direct action on endothelial cells. Am J Physiol **274:**L678-84.

76. **Hiscott, J., J. Lacoste, and R. Lin.** 2006. Recruitment of an interferon molecular signaling complex to the mitochondrial membrane: disruption by hepatitis C virus NS3-4A protease. Biochem Pharmacol **72:**1477-84.
77. **Hiscott, J., and R. Lin.** 2006. Inhibition of the interferon antiviral response by hepatitis C virus. Expert Rev Clin Immunol **2:**49-58.
78. **Hjelle, B., S. W. Lee, W. Song, N. Torrez-Martinez, J. W. Song, R. Yanagihara, I. Gavrilovskaya, and E. R. Mackow.** 1995. Molecular linkage of hantavirus pulmonary syndrome to the white-footed mouse, Peromyscus leucopus: genetic characterization of the M genome of New York virus. J Virol **69:**8137-41.
79. **Hodivala-Dilke, K. M., K. P. McHugh, D. A. Tsakiris, H. Rayburn, D. Crowley, M. Ullman-Cullere, F. P. Ross, B. S. Coller, S. Teitelbaum, and R. O. Hynes.** 1999. Beta3-integrin-deficient mice are a model for Glanzmann thrombasthenia showing placental defects and reduced survival. J Clin Invest **103:**229-38.
80. **Hoffmann, E., G. Neumann, Y. Kawaoka, G. Hobom, and R. G. Webster.** 2000. A DNA transfection system for generation of influenza A virus from eight plasmids. Proc Natl Acad Sci U S A **97:**6108-13.
81. **Hooper, J. W., A. M. Ferro, and V. Wahl-Jensen.** 2008. Immune serum produced by DNA vaccination protects hamsters against lethal respiratory challenge with Andes virus. J Virol **82:**1332-8.
82. **Hooper, J. W., T. Larsen, D. M. Custer, and C. S. Schmaljohn.** 2001. A lethal disease model for hantavirus pulmonary syndrome. Virology **289:**6-14.
83. **Huggins, J. W., C. M. Hsiang, T. M. Cosgriff, M. Y. Guang, J. I. Smith, Z. O. Wu, J. W. LeDuc, Z. M. Zheng, J. M. Meegan, Q. N. Wang, and et al.** 1991. Prospective, double-blind, concurrent, placebo-controlled clinical trial of intravenous ribavirin therapy of hemorrhagic fever with renal syndrome. J Infect Dis **164:**1119-27.
84. **Humphries, M. J., P. A. McEwan, S. J. Barton, P. A. Buckley, J. Bella, and A. P. Mould.** 2003. Integrin structure: heady advances in ligand binding, but activation still makes the knees wobble. Trends Biochem Sci **28:**313-20.
85. **Hussain, M., R. J. Taft, and S. Asgari.** 2008. An insect virus-encoded microRNA regulates viral replication. J Virol **82:**9164-70.
86. **Hynes, R. O.** 2002. Integrins: bidirectional, allosteric signaling machines. Cell **110:**673-87.
87. **Hynes, R. O., and K. M. Hodivala-Dilke.** 1999. Insights and questions arising from studies of a mouse model of Glanzmann thrombasthenia. Thromb Haemost **82:**481-5.

88. **Igarashi, J., P. A. Erwin, A. P. Dantas, H. Chen, and T. Michel.** 2003. VEGF induces S1P1 receptors in endothelial cells: Implications for cross-talk between sphingolipid and growth factor receptors. Proc Natl Acad Sci U S A **100:**10664-9.
89. **Jaaskelainen, K. M., P. Kaukinen, E. S. Minskaya, A. Plyusnina, O. Vapalahti, R. M. Elliott, F. Weber, A. Vaheri, and A. Plyusnin.** 2007. Tula and Puumala hantavirus NSs ORFs are functional and the products inhibit activation of the interferon-beta promoter. J Med Virol **79:**1527-36.
90. **Jaaskelainen, K. M., A. Plyusnina, A. Lundkvist, A. Vaheri, and A. Plyusnin.** 2008. Tula hantavirus isolate with the full-length ORF for nonstructural protein NSs survives for more consequent passages in interferon-competent cells than the isolate having truncated NSs ORF. Virol J **5:**3.
91. **Jain, R. K., E. di Tomaso, D. G. Duda, J. S. Loeffler, A. G. Sorensen, and T. T. Batchelor.** 2007. Angiogenesis in brain tumours. Nat Rev Neurosci **8:**610-22.
92. **Jiang, Q., M. G. Feng, and Y. Y. Mo.** 2009. Systematic validation of predicted microRNAs for cyclin D1. BMC Cancer **9:**194.
93. **Jin, M., J. Park, S. Lee, B. Park, J. Shin, K. J. Song, T. I. Ahn, S. Y. Hwang, B. Y. Ahn, and K. Ahn.** 2002. Hantaan virus enters cells by clathrin-dependent receptor-mediated endocytosis. Virology **294:**60-9.
94. **Johne, C., D. Matenia, X. Y. Li, T. Timm, K. Balusamy, and E. M. Mandelkow.** 2008. Spred1 and TESK1--two new interaction partners of the kinase MARKK/TAO1 that link the microtubule and actin cytoskeleton. Mol Biol Cell **19:**1391-403.
95. **Johnson, A. M., L. T. de Souza, I. B. Ferreira, L. E. Pereira, T. G. Ksiazek, P. E. Rollin, C. J. Peters, and S. T. Nichol.** 1999. Genetic investigation of novel hantaviruses causing fatal HPS in Brazil. J Med Virol **59:**527-35.
96. **Johnson, K. M.** 2001. Hantaviruses: History and Overview, p. pp. 1-14. *In* C. a. N. Schmaljohn, S. (ed.), Hantaviruses, vol. 256. Springer-Verlag.
97. **Jones, C. A., N. R. London, H. Chen, K. W. Park, D. Sauvaget, R. A. Stockton, J. D. Wythe, W. Suh, F. Larrieu-Lahargue, Y. S. Mukouyama, P. Lindblom, P. Seth, A. Frias, N. Nishiya, M. H. Ginsberg, H. Gerhardt, K. Zhang, and D. Y. Li.** 2008. Robo4 stabilizes the vascular network by inhibiting pathologic angiogenesis and endothelial hyperpermeability. Nat Med **14:**448-53.
98. **Jonsson, C. B., J. Hooper, and G. Mertz.** 2008. Treatment of hantavirus pulmonary syndrome. Antiviral Res **78:**162-9.

99. **Jopling, C. L., K. L. Norman, and P. Sarnow.** 2006. Positive and negative modulation of viral and cellular mRNAs by liver-specific microRNA miR-122. Cold Spring Harb Symp Quant Biol **71:**369-76.
100. **Kato, A., Y. Sakai, T. Shioda, T. Kondo, M. Nakanishi, and Y. Nagai.** 1996. Initiation of Sendai virus multiplication from transfected cDNA or RNA with negative or positive sense. Genes Cells **1:**569-79.
101. **Khan, A. S., C. F. Spiropoulou, S. Morzunov, S. R. Zaki, M. A. Kohn, S. R. Nawas, L. McFarland, and S. T. Nichol.** 1995. Fatal illness associated with a new hantavirus in Louisiana. J Med Virol **46:**281-6.
102. **Kim, V. N., J. Han, and M. C. Siomi.** 2009. Biogenesis of small RNAs in animals. Nat Rev Mol Cell Biol **10:**126-39.
103. **Kim, Y. S., C. Ahn, J. S. Han, S. Kim, J. S. Lee, and P. W. Lee.** 1995. Hemorrhagic fever with renal syndrome caused by the Seoul virus. Nephron **71:**419-27.
104. **Klempa, B., M. Stanko, M. Labuda, R. Ulrich, H. Meisel, and D. H. Kruger.** 2005. Central European Dobrava Hantavirus isolate from a striped field mouse (Apodemus agrarius). J Clin Microbiol **43:**2756-63.
105. **Kobayashi, M., M. Nishita, T. Mishima, K. Ohashi, and K. Mizuno.** 2006. MAPKAPK-2-mediated LIM-kinase activation is critical for VEGF-induced actin remodeling and cell migration. EMBO J **25:**713-26.
106. **Kohl, A., R. F. Clayton, F. Weber, A. Bridgen, R. E. Randall, and R. M. Elliott.** 2003. Bunyamwera virus nonstructural protein NSs counteracts interferon regulatory factor 3-mediated induction of early cell death. J Virol **77:**7999-8008.
107. **Kraus, A. A., M. J. Raftery, T. Giese, R. Ulrich, R. Zawatzky, S. Hippenstiel, N. Suttorp, D. H. Kruger, and G. Schonrich.** 2004. Differential antiviral response of endothelial cells after infection with pathogenic and nonpathogenic hantaviruses. J Virol **78:**6143-50.
108. **Kuehbacher, A., C. Urbich, A. M. Zeiher, and S. Dimmeler.** 2007. Role of Dicer and Drosha for endothelial microRNA expression and angiogenesis. Circ Res **101:**59-68.
109. **Kuhnert, F., M. R. Mancuso, J. Hampton, K. Stankunas, T. Asano, C. Z. Chen, and C. J. Kuo.** 2008. Attribution of vascular phenotypes of the murine Egfl7 locus to the microRNA miR-126. Development **135:**3989-93.
110. **Kukkonen, S. K., A. Vaheri, and A. Plyusnin.** 2005. L protein, the RNA-dependent RNA polymerase of hantaviruses. Arch Virol **150:**533-56.
111. **Lamalice, L., F. Le Boeuf, and J. Huot.** 2007. Endothelial cell migration during angiogenesis. Circ Res **100:**782-94.

112. **Lampugnani, M. G., and E. Dejana.** 2007. Adherens junctions in endothelial cells regulate vessel maintenance and angiogenesis. Thromb Res **120 Suppl 2:**S1-6.
113. **Lampugnani, M. G., and E. Dejana.** 2007. The control of endothelial cell functions by adherens junctions. Novartis Found Symp **283:**4-13; discussion 13-7, 238-41.
114. **Lampugnani, M. G., F. Orsenigo, M. C. Gagliani, C. Tacchetti, and E. Dejana.** 2006. Vascular endothelial cadherin controls VEGFR-2 internalization and signaling from intracellular compartments. J Cell Biol **174:**593-604.
115. **Lawson, N. D., E. A. Stillman, M. A. Whitt, and J. K. Rose.** 1995. Recombinant vesicular stomatitis viruses from DNA. Proc Natl Acad Sci U S A **92:**4477-81.
116. **Lee, H. W.** 1989. Hemorrhagic fever with renal syndrome in Korea. Rev Infect Dis **11 Suppl 4:**S864-76.
117. **Lee, H. W., P. W. Lee, and K. M. Johnson.** 1978. Isolation of the etiologic agent of Korean Hemorrhagic fever. J Infect Dis **137:**298-308.
118. **Lee, P. W., H. L. Amyx, R. Yanagihara, D. C. Gajdusek, D. Goldgaber, and C. J. Gibbs, Jr.** 1985. Partial characterization of Prospect Hill virus isolated from meadow voles in the United States. J Infect Dis **152:**826-9.
119. **Levis, S., S. P. Morzunov, J. E. Rowe, D. Enria, N. Pini, G. Calderon, M. Sabattini, and S. C. St Jeor.** 1998. Genetic diversity and epidemiology of hantaviruses in Argentina. J Infect Dis **177:**529-38.
120. **Li, Z., C. Wang, G. C. Prendergast, and R. G. Pestell.** 2006. Cyclin D1 functions in cell migration. Cell Cycle **5:**2440-2.
121. **Liu, B., X. C. Peng, X. L. Zheng, J. Wang, and Y. W. Qin.** 2009. MiR-126 restoration down-regulate VEGF and inhibit the growth of lung cancer cell lines in vitro and in vivo. Lung Cancer **66:**169-75.
122. **Lober, C., B. Anheier, S. Lindow, H. D. Klenk, and H. Feldmann.** 2001. The Hantaan virus glycoprotein precursor is cleaved at the conserved pentapeptide WAASA. Virology **289:**224-9.
123. **Lopez, N., P. Padula, C. Rossi, M. E. Lazaro, and M. T. Franze-Fernandez.** 1996. Genetic identification of a new hantavirus causing severe pulmonary syndrome in Argentina. Virology **220:**223-6.
124. **Lowen, A. C., C. Noonan, A. McLees, and R. M. Elliott.** 2004. Efficient bunyavirus rescue from cloned cDNA. Virology **330:**493-500.
125. **Lundkvist, A., V. Vasilenko, I. Golovljova, A. Plyusnin, and A. Vaheri.** 1998. Human Dobrava hantavirus infections in Estonia. Lancet **352:**369.

126. **Mackow, E. R., and I. N. Gavrilovskaya.** 2001. Cellular receptors and hantavirus pathogenesis. Curr Top Microbiol Immunol **256:**91-115.
127. **Mackow, E. R., and I. N. Gavrilovskaya.** 2009. Hantavirus regulation of endothelial cell functions. Thromb Haemost **102:**1030-41.
128. **Maes, P., E. Keyaerts, J. Clement, V. Bonnet, A. Robert, and M. Van Ranst.** 2004. Detection of Puumala hantavirus antibody with ELISA using a recombinant truncated nucleocapsid protein expressed in Escherichia coli. Viral Immunol **17:**315-21.
129. **Matsumoto, T., S. Bohman, J. Dixelius, T. Berge, A. Dimberg, P. Magnusson, L. Wang, C. Wikner, J. H. Qi, C. Wernstedt, J. Wu, S. Bruheim, H. Mugishima, D. Mukhopadhyay, A. Spurkland, and L. Claesson-Welsh.** 2005. VEGF receptor-2 Y951 signaling and a role for the adapter molecule TSAd in tumor angiogenesis. EMBO J **24:**2342-53.
130. **Matthys, V. S., E. Gorbunova, I. Gavrilovskaya, T. Pepini, and E. R. Mackow.** 2010. The C-Terminal 42 Residues of the TULV Gn Protein Regulate Interferon Induction. J Virol.
131. **Matthys, V. S., E. E. Gorbunova, I. N. Gavrilovskaya, and E. R. Mackow.** 2010. Andes virus recognition of human and Syrian hamster beta3 integrins is determined by an L33P substitution in the PSI domain. J Virol **84:**352-60.
132. **McCaughey, C., and C. A. Hart.** 2000. Hantaviruses. J Med Microbiol **49:**587-99.
133. **Mir, M. A., W. A. Duran, B. L. Hjelle, C. Ye, and A. T. Panganiban.** 2008. Storage of cellular 5' mRNA caps in P bodies for viral cap-snatching. Proc Natl Acad Sci U S A **105:**19294-9.
134. **Mir, M. A., and A. T. Panganiban.** 2006. Characterization of the RNA chaperone activity of hantavirus nucleocapsid protein. J Virol **80:**6276-85.
135. **Mir, M. A., and A. T. Panganiban.** 2008. A protein that replaces the entire cellular eIF4F complex. EMBO J **27:**3129-39.
136. **Mir, M. A., and A. T. Panganiban.** 2004. Trimeric hantavirus nucleocapsid protein binds specifically to the viral RNA panhandle. J Virol **78:**8281-8.
137. **Mir, M. A., S. Sheema, A. Haseeb, and A. Haque.** 2010. Hantavirus nucleocapsid protein has distinct m7G cap- and RNA-binding sites. J Biol Chem **285:**11357-68.
138. **Molla, A., A. V. Paul, and E. Wimmer.** 1991. Cell-free, de novo synthesis of poliovirus. Science **254:**1647-51.
139. **Morzunov, S. P., H. Feldmann, C. F. Spiropoulou, V. A. Semenova, P. E. Rollin, T. G. Ksiazek, C. J. Peters, and S. T. Nichol.** 1995. A newly recognized virus associated with a fatal case of hantavirus pulmonary syndrome in Louisiana. J Virol **69:**1980-3.

140. **Moss, B., O. Elroy-Stein, T. Mizukami, W. A. Alexander, and T. R. Fuerst.** 1990. Product review. New mammalian expression vectors. Nature **348:**91-2.
141. **Mukhopadhyay, D., L. Tsiokas, X. M. Zhou, D. Foster, J. S. Brugge, and V. P. Sukhatme.** 1995. Hypoxic induction of human vascular endothelial growth factor expression through c-Src activation. Nature **375:**577-81.
142. **Mustonen, J., O. Vapalahti, H. Henttonen, A. Pasternack, and A. Vaheri.** 1998. Epidemiology of hantavirus infections in Europe. Nephrol Dial Transplant **13:**2729-31.
143. **Nagy, J. A., L. Benjamin, H. Zeng, A. M. Dvorak, and H. F. Dvorak.** 2008. Vascular permeability, vascular hyperpermeability and angiogenesis. Angiogenesis **11:**109-19.
144. **Nair, V., and M. Zavolan.** 2006. Virus-encoded microRNAs: novel regulators of gene expression. Trends Microbiol **14:**169-75.
145. **Negrini, M., M. S. Nicoloso, and G. A. Calin.** 2009. MicroRNAs and cancer--new paradigms in molecular oncology. Curr Opin Cell Biol **21:**470-9.
146. **Neumann, G., K. Fujii, Y. Kino, and Y. Kawaoka.** 2005. An improved reverse genetics system for influenza A virus generation and its implications for vaccine production. Proc Natl Acad Sci U S A **102:**16825-9.
147. **Neumann, G., T. Watanabe, H. Ito, S. Watanabe, H. Goto, P. Gao, M. Hughes, D. R. Perez, R. Donis, E. Hoffmann, G. Hobom, and Y. Kawaoka.** 1999. Generation of influenza A viruses entirely from cloned cDNAs. Proc Natl Acad Sci U S A **96:**9345-50.
148. **Nichol, S. T., C. F. Spiropoulou, S. Morzunov, P. E. Rollin, T. G. Ksiazek, H. Feldmann, A. Sanchez, J. Childs, S. Zaki, and C. J. Peters.** 1993. Genetic identification of a hantavirus associated with an outbreak of acute respiratory illness. Science **262:**914-7.
149. **Nicoloso, M. S., R. Spizzo, M. Shimizu, S. Rossi, and G. A. Calin.** 2009. MicroRNAs--the micro steering wheel of tumour metastases. Nat Rev Cancer **9:**293-302.
150. **Nolte, K. B., R. M. Feddersen, K. Foucar, S. R. Zaki, F. T. Koster, D. Madar, T. L. Merlin, P. J. McFeeley, E. T. Umland, and R. E. Zumwalt.** 1995. Hantavirus pulmonary syndrome in the United States: a pathological description of a disease caused by a new agent. Human Pathology **26:**110-20.
151. **Nonami, A., T. Taketomi, A. Kimura, K. Saeki, H. Takaki, T. Sanada, K. Taniguchi, M. Harada, R. Kato, and A. Yoshimura.** 2005. The Sprouty-related protein, Spred-1, localizes in a lipid raft/caveola and

inhibits ERK activation in collaboration with caveolin-1. Genes Cells **10:**887-95.

152. **Olsson, A. K., A. Dimberg, J. Kreuger, and L. Claesson-Welsh.** 2006. VEGF receptor signalling - in control of vascular function. Nat Rev Mol Cell Biol **7:**359-71.
153. **Padula, P. J., A. Edelstein, S. D. Miguel, N. M. Lopez, C. M. Rossi, and R. D. Rabinovich.** 1998. Hantavirus pulmonary syndrome outbreak in Argentina: molecular evidence for person-to-person transmission of Andes virus. Virology **241:**323-30.
154. **Palese, P., H. Zheng, O. G. Engelhardt, S. Pleschka, and A. Garcia-Sastre.** 1996. Negative-strand RNA viruses: genetic engineering and applications. Proc Natl Acad Sci U S A **93:**11354-8.
155. **Paterson, R. G., C. J. Russell, and R. A. Lamb.** 2000. Fusion protein of the paramyxovirus SV5: destabilizing and stabilizing mutants of fusion activation. Virology **270:**17-30.
156. **Pauley, K. M., T. Eystathioy, A. Jakymiw, J. C. Hamel, M. J. Fritzler, and E. K. Chan.** 2006. Formation of GW bodies is a consequence of microRNA genesis. EMBO Rep **7:**904-10.
157. **Pekosz, A., B. He, and R. A. Lamb.** 1999. Reverse genetics of negative-strand RNA viruses: closing the circle. Proc Natl Acad Sci U S A **96:**8804-6.
158. **Pensiero, M. N., and J. Hay.** 1992. The Hantaan virus M-segment glycoproteins G1 and G2 can be expressed independently. J Virol **66:**1907-14.
159. **Pensiero, M. N., J. B. Sharefkin, C. W. Dieffenbach, and J. Hay.** 1992. Hantaan virus infection of human endothelial cells. J Virol **66:**5929-36.
160. **Pepini, T., E. E. Gorbunova, I. N. Gavrilovskaya, J. E. Mackow, and E. R. Mackow.** 2010. Andes Virus Regulation of Cellular MicroRNAs Contributes to Hantavirus-Induced Endothelial Cell Permeability. J Virol **84:**11929-36.
161. **Peters, C. J., G. L. Simpson, and H. Levy.** 1999. Spectrum of hantavirus infection: hemorrhagic fever with renal syndrome and hantavirus pulmonary syndrome. Annu Rev Med **50:**531-45.
162. **Pleschka, S., R. Jaskunas, O. G. Engelhardt, T. Zurcher, P. Palese, and A. Garcia-Sastre.** 1996. A plasmid-based reverse genetics system for influenza A virus. J Virol **70:**4188-92.
163. **Plyusnin, A., and S. P. Morzunov.** 2001. Virus evolution and genetic diversity of hantaviruses and their rodent hosts. Curr Top Microbiol Immunol **256:**47-75.
164. **Plyusnin, A., O. Vapalahti, H. Lankinen, H. Lehvaslaiho, N. Apekina, Y. Myasnikov, H. Kallio-Kokko, H. Henttonen, A. Lundkvist, M.**

Brummer-Korvenkontio, and et al. 1994. Tula virus: a newly detected hantavirus carried by European common voles. J Virol **68:**7833-9.

165. **Plyusnin, A., O. Vapalahti, and A. Vaheri.** 1996. Hantaviruses: genome structure, expression and evolution. J Gen Virol **77 (Pt 11):**2677-87.
166. **Racaniello, V. R., and D. Baltimore.** 1981. Cloned poliovirus complementary DNA is infectious in mammalian cells. Science **214:**916-9.
167. **Radecke, F., P. Spielhofer, H. Schneider, K. Kaelin, M. Huber, C. Dotsch, G. Christiansen, and M. A. Billeter.** 1995. Rescue of measles viruses from cloned DNA. EMBO J **14:**5773-84.
168. **Ravkov, E. V., P. E. Rollin, T. G. Ksiazek, C. J. Peters, and S. T. Nichol.** 1995. Genetic and serologic analysis of Black Creek Canal virus and its association with human disease and Sigmodon hispidus infection. Virology **210:**482-9.
169. **Raymond, T., E. Gorbunova, I. N. Gavrilovskaya, and E. R. Mackow.** 2005. Pathogenic hantaviruses bind plexin-semaphorin-integrin domains present at the apex of inactive, bent alphavbeta3 integrin conformers. Proc Natl Acad Sci U S A **102:**1163-8.
170. **Reynolds, L. E., L. Wyder, J. C. Lively, D. Taverna, S. D. Robinson, X. Huang, D. Sheppard, R. O. Hynes, and K. M. Hodivala-Dilke.** 2002. Enhanced pathological angiogenesis in mice lacking beta3 integrin or beta3 and beta5 integrins. Nat Med **8:**27-34.
171. **Robinson, S. D., L. E. Reynolds, L. Wyder, D. J. Hicklin, and K. M. Hodivala-Dilke.** 2004. Beta3-integrin regulates vascular endothelial growth factor-A-dependent permeability. Arterioscler Thromb Vasc Biol **24:**2108-14.
172. **Rollin, P. E., T. G. Ksiazek, L. H. Elliott, E. V. Ravkov, M. L. Martin, S. Morzunov, W. Livingstone, M. Monroe, G. Glass, S. Ruo, and et al.** 1995. Isolation of black creek canal virus, a new hantavirus from Sigmodon hispidus in Florida. J Med Virol **46:**35-9.
173. **Sand, M., T. Gambichler, D. Sand, M. Skrygan, P. Altmeyer, and F. G. Bechara.** 2009. MicroRNAs and the skin: tiny players in the body's largest organ. J Dermatol Sci **53:**169-75.
174. **Sarnow, P., C. L. Jopling, K. L. Norman, S. Schutz, and K. A. Wehner.** 2006. MicroRNAs: expression, avoidance and subversion by vertebrate viruses. Nat Rev Microbiol **4:**651-9.
175. **Schmaljohn, C., and B. Hjelle.** 1997. Hantaviruses: a global disease problem. Emerg Infect Dis **3:**95-104.
176. **Schmaljohn, C. S.** 2001. Bunyaviridae and their Replication, p. 1581-1602. *In* D. M. Knipe, P. M. Howley, and e. al. (ed.), Fields Virology 4ed, vol. 1. Lippincott Williams & Wilkins, Philadelphia.

177. **Schneider, U., M. Schwemmle, and P. Staeheli.** 2005. Genome trimming: a unique strategy for replication control employed by Borna disease virus. Proc Natl Acad Sci U S A **102:**3441-6.
178. **Schnell, M. J., T. Mebatsion, and K. K. Conzelmann.** 1994. Infectious rabies viruses from cloned cDNA. EMBO J **13:**4195-203.
179. **Schonrich, G., A. Rang, N. Lutteke, M. J. Raftery, N. Charbonnel, and R. G. Ulrich.** 2008. Hantavirus-induced immunity in rodent reservoirs and humans. Immunol Rev **225:**163-89.
180. **Sen, N., A. Sen, and E. R. Mackow.** 2007. Degrons at the C terminus of the pathogenic but not the nonpathogenic hantavirus G1 tail direct proteasomal degradation. J Virol **81:**4323-30.
181. **Severson, W. E., C. S. Schmaljohn, A. Javadian, and C. B. Jonsson.** 2003. Ribavirin causes error catastrophe during Hantaan virus replication. J Virol **77:**481-8.
182. **Sheldon, H., M. Andre, J. A. Legg, P. Heal, J. M. Herbert, R. Sainson, A. S. Sharma, J. K. Kitajewski, V. L. Heath, and R. Bicknell.** 2009. Active involvement of Robo1 and Robo4 in filopodia formation and endothelial cell motility mediated via WASP and other actin nucleation-promoting factors. FASEB J **23:**513-22.
183. **Shi, X., and R. M. Elliott.** 2002. Golgi localization of Hantaan virus glycoproteins requires coexpression of G1 and G2. Virology **300:**31-8.
184. **Sibold, C., S. Sparr, A. Schulz, M. Labuda, O. Kozuch, J. Lysy, D. H. Kruger, and H. Meisel.** 1995. Genetic characterization of a new hantavirus detected in Microtus arvalis from Slovakia. Virus Genes **10:**277-81.
185. **Somanath, P. R., N. L. Malinin, and T. V. Byzova.** 2009. Cooperation between integrin alphavbeta3 and VEGFR2 in angiogenesis. Angiogenesis **12:**177-85.
186. **Song, J. W., L. J. Baek, D. C. Gajdusek, R. Yanagihara, I. Gavrilovskaya, B. J. Luft, E. R. Mackow, and B. Hjelle.** 1994. Isolation of pathogenic hantavirus from white-footed mouse (Peromyscus leucopus). Lancet **344:**1637.
187. **Spiropoulou, C. F.** 2001. Hantavirus maturation. Curr Top Microbiol Immunol **256:**33-46.
188. **Suurna, M. V., S. L. Ashworth, M. Hosford, R. M. Sandoval, S. E. Wean, B. M. Shah, J. R. Bamburg, and B. A. Molitoris.** 2006. Cofilin mediates ATP depletion-induced endothelial cell actin alterations. Am J Physiol Renal Physiol **290:**F1398-407.
189. **Takagi, J., B. M. Petre, T. Walz, and T. A. Springer.** 2002. Global conformational rearrangements in integrin extracellular domains in outside-in and inside-out signaling. Cell **110:**599-11.

190. **Tang, N., L. Wang, J. Esko, F. J. Giordano, Y. Huang, H. P. Gerber, N. Ferrara, and R. S. Johnson.** 2004. Loss of HIF-1alpha in endothelial cells disrupts a hypoxia-driven VEGF autocrine loop necessary for tumorigenesis. Cancer Cell **6:**485-95.
191. **Taniguchi, K., R. Kohno, T. Ayada, R. Kato, K. Ichiyama, T. Morisada, Y. Oike, Y. Yonemitsu, Y. Maehara, and A. Yoshimura.** 2007. Spreds are essential for embryonic lymphangiogenesis by regulating vascular endothelial growth factor receptor 3 signaling. Mol Cell Biol **27:**4541-50.
192. **Tie, J., Y. Pan, L. Zhao, K. Wu, J. Liu, S. Sun, X. Guo, B. Wang, Y. Gang, Y. Zhang, Q. Li, T. Qiao, Q. Zhao, Y. Nie, and D. Fan.** 2010. MiR-218 inhibits invasion and metastasis of gastric cancer by targeting the Robo1 receptor. PLoS Genet **6:**e1000879.
193. **Tischler, N. D., A. Gonzalez, T. Perez-Acle, M. Rosemblatt, and P. D. Valenzuela.** 2005. Hantavirus Gc glycoprotein: evidence for a class II fusion protein. J Gen Virol **86:**2937-47.
194. **Torrez-Martinez, N., and B. Hjelle.** 1995. Enzootic of Bayou hantavirus in rice rats (Oryzomys palustris) in 1983. Lancet **346:**780-1.
195. **Toshima, J., J. Y. Toshima, T. Amano, N. Yang, S. Narumiya, and K. Mizuno.** 2001. Cofilin phosphorylation by protein kinase testicular protein kinase 1 and its role in integrin-mediated actin reorganization and focal adhesion formation. Mol Biol Cell **12:**1131-45.
196. **Tsumura, Y., J. Toshima, O. C. Leeksma, K. Ohashi, and K. Mizuno.** 2005. Sprouty-4 negatively regulates cell spreading by inhibiting the kinase activity of testicular protein kinase. Biochem J **387:**627-37.
197. **Urbich, C., A. Kuehbacher, and S. Dimmeler.** 2008. Role of microRNAs in vascular diseases, inflammation, and angiogenesis. Cardiovasc Res **79:**581-8.
198. **Urbich, C., L. Rossig, D. Kaluza, M. Potente, J. N. Boeckel, A. Knau, F. Diehl, J. G. Geng, W. K. Hofmann, A. M. Zeiher, and S. Dimmeler.** 2009. HDAC5 is a repressor of angiogenesis and determines the angiogenic gene expression pattern of endothelial cells. Blood **113:**5669-79.
199. **Valbuena, G., and D. H. Walker.** 2006. The endothelium as a target for infections. Annu Rev Pathol **1:**171-98.
200. **Valdivieso, F., P. Vial, M. Ferres, C. Ye, D. Goade, A. Cuiza, and B. Hjelle.** 2006. Neutralizing antibodies in survivors of Sin Nombre and Andes hantavirus infection. Emerg Infect Dis **12:**166-8.
201. **Vapalahti, O., A. Lundkvist, S. K. Kukkonen, Y. Cheng, M. Gilljam, M. Kanerva, T. Manni, M. Pejcoch, J. Niemimaa, A. Kaikusalo, H. Henttonen, A. Vaheri, and A. Plyusnin.** 1996. Isolation and

characterization of Tula virus, a distinct serotype in the genus Hantavirus, family Bunyaviridae. J Gen Virol **77 (Pt 12):**3063-7.

202. **Voelkel, N. F., R. W. Vandivier, and R. M. Tuder.** 2006. Vascular endothelial growth factor in the lung. Am J Physiol Lung Cell Mol Physiol **290:**L209-21.
203. **Wahl-Jensen, V., J. Chapman, L. Asher, R. Fisher, M. Zimmerman, T. Larsen, and J. W. Hooper.** 2007. Temporal analysis of Andes virus and Sin Nombre virus infections of Syrian hamsters. J Virol **81:**7449-62.
204. **Wang, S., A. B. Aurora, B. A. Johnson, X. Qi, J. McAnally, J. A. Hill, J. A. Richardson, R. Bassel-Duby, and E. N. Olson.** 2008. The endothelial-specific microRNA miR-126 governs vascular integrity and angiogenesis. Dev Cell **15:**261-71.
205. **Wang, S., and E. N. Olson.** 2009. AngiomiRs--key regulators of angiogenesis. Curr Opin Genet Dev **19:**205-11.
206. **Weber, F., A. Bridgen, J. K. Fazakerley, H. Streitenfeld, N. Kessler, R. E. Randall, and R. M. Elliott.** 2002. Bunyamwera bunyavirus nonstructural protein NSs counteracts the induction of alpha/beta interferon. J Virol **76:**7949-55.
207. **Wells, R. M., S. Sosa Estani, Z. E. Yadon, D. Enria, P. Padula, N. Pini, J. N. Mills, C. J. Peters, and E. L. Segura.** 1997. An unusual hantavirus outbreak in southern Argentina: person-to-person transmission? Hantavirus Pulmonary Syndrome Study Group for Patagonia. Emerg Infect Dis **3:**171-4.
208. **Whelan, S. P., L. A. Ball, J. N. Barr, and G. T. Wertz.** 1995. Efficient recovery of infectious vesicular stomatitis virus entirely from cDNA clones. Proc Natl Acad Sci U S A **92:**8388-92.
209. **Whitehouse, C. A.** 2004. Crimean-Congo hemorrhagic fever. Antiviral Res **64:**145-60.
210. **Wiesner, S., K. R. Legate, and R. Fassler.** 2005. Integrin-actin interactions. Cell Mol Life Sci **62:**1081-99.
211. **Winter, J., S. Jung, S. Keller, R. I. Gregory, and S. Diederichs.** 2009. Many roads to maturity: microRNA biogenesis pathways and their regulation. Nat Cell Biol **11:**228-34.
212. **Xiao, S. Y., J. W. Leduc, Y. K. Chu, and C. S. Schmaljohn.** 1994. Phylogenetic analyses of virus isolates in the genus Hantavirus, family Bunyaviridae. Virology **198:**205-17.
213. **Xiong, J. P., T. Stehle, S. L. Goodman, and M. A. Arnaout.** 2004. A novel adaptation of the integrin PSI domain revealed from its crystal structure. J Biol Chem **279:**40252-4.
214. **Xiong, J. P., T. Stehle, R. Zhang, A. Joachimiak, M. Frech, S. L. Goodman, and M. A. Arnaout.** 2002. Crystal structure of the

extracellular segment of integrin alpha Vbeta3 in complex with an Arg-Gly-Asp ligand. Science **296:**151-5.

215. **Yanagihara, R.** 1990. Hantavirus infection in the United States: epizootiology and epidemiology. Rev Infect Dis **12:**449-57.

216. **Zaki, S., P. Greer, L. Coffield, C. Goldsmith, K. Nolte, K. Foucar, R. Feddersen, R. Zumwalt, G. Miller, P. Rollin, T. Ksiazek, S. Nichol, and C. Peters.** 1995. Hantavirus Pulmonary Syndrome: pathogenesis of an emerging infectious disease. Am J. Pathol. **146:**552-79.

Appendix I:

TULV and PHV Differentially Regulate Early Interferon Responses (130)

Introduction:

At least two nonpathogenic hantaviruses have been identified that are not associated with any human disease, Prospect Hill Virus (PHV) and Tula virus (TULV) (96, 164, 175). Contrasting functions of pathogenic and nonpathogenic hantaviruses permits analysis of protein–encoded virulence determinants that contribute to hantavirus pathogenesis.

Interestingly, both pathogenic and nonpathogenic hantaviruses infect human endothelial cells, however PHV fails to regulate early cellular interferon (IFN) responses and as a result both PHV replication and the pathogenic potential of PHV are restricted in human endothelial cells (3, 4, 62, 175). Integrin receptor regulation further distinguishes pathogenic from non-pathogenic hantaviruses and is associated with increased vascular permeability (57, 58, 169). Only pathogenic hantaviruses use $\alpha_v\beta_3$ integrin endothelial cell receptors, while TULV and PHV use $\alpha_5\beta_1$ integrins for cell entry (55, 59, 169). β_3 receptors on platelets and endothelial cells regulate fluid barrier functions of the vasculature as well as permeability induced by vascular endothelial growth factor (VEGF) (56, 57, 66). These responses clearly differentiate pathogenic hantaviruses from nonpathogenic PHV and TULV (57, 58), and are likely to contribute, at least in part, to endothelial cell permissivity and hantavirus pathogenesis.

In pathogenic hantaviruses the G_N cytoplasmic tail (G_N–T) has been shown to regulate RIGI– and TBK1–directed IFN induction, disrupt TRAF3–

TBK1 complexes, and mediate binding to TRAF3 and Src (3, 4, 61). The G_N–T is 142 amino acids long and mediates several functions, including interactions with the viral nucleocapsid protein that presumably nucleates viral budding into the cis–Golgi (71). However, consistent with the failure to replicate successfully in human endothelial cells, the G_N–T of nonpathogenic PHV fails to regulate RIGI– and TBK1–directed IFN responses (3, 4). Interestingly, although TULV is nonpathogenic, TULV replicates in human endothelial cells to titers similar to those of pathogenic hantaviruses (57). This points out a fundamental difference in endothelial cell regulation by nonpathogenic TULV and PHV, and suggests that TULV has the ability to regulate IFN induction within human endothelial cells.

Results:

TULV Regulates Early ISG Induction in Infected Endothelial Cells

Here we demonstrate that PHV and TULV similarly infect >95% of human endothelial cells 1 day post infection. In contrast, by 3 days p.i. there is a substantial reduction in the presence of nucleocapsid protein within PHV–infected endothelial cells in comparison to TULV–infected cells (Figure 24A). In fact, titers of TULV increase 3 logs from 1–3 days post–infection of human endothelial cells while PHV titers remain at input levels during this period (data not shown).

These findings suggest that TULV regulates IFN responses of endothelial cells which restrict PHV replication.

In order to determine whether TULV regulates the early induction of ISGs within human endothelial cells, we comparatively evaluated MxA and ISG56 mRNA levels following infection by TULV and PHV. PHV infection of human endothelial cells resulted in a 400– and 800–fold induction of MxA and ISG56, respectively, while TULV only increased MxA and ISG56 10– to 30–fold 1 day post–infection (Figure 24B). These findings demonstrate a dramatic difference in the induction of ISGs in human endothelial cells by two nonpathogenic hantaviruses 1 day post–infection. In contrast, 2–3 days post–infection, both TULV and PHV induce MxA and ISG56 >500–fold. These findings are nearly identical to the pattern of IFN responses previously observed following pathogenic hantavirus infection of human endothelial cells, resulting in little or no ISG responses 1 day p.i. (3). As a result, nonpathogenic TULV also inhibits the early induction of ISGs within human endothelial cells.

Discussion:

Although both PHV and TULV are considered nonpathogenic, both hantaviruses enter and synthesize viral proteins within human endothelial cells (29, 127, 159, 175, 215). Interestingly, PHV is not amplified within human endothelial cells while TULV replicates to similar levels as pathogenic NY–1V

and HTNV following infection of human endothelial cells (Figure 24A) (3, 57, 120, 201). However, previous studies demonstrate that PHV replicates within IFN–locus deficient VeroE6 cells, while PHV infection of endothelial cells results in the high–level induction of ISGs which restricts PHV replication (3, 62, 107, 187). In fact, both pathogenic and nonpathogenic hantaviruses are sensitive to IFN pretreatment or the addition of IFN at early times post–infection (3). However, pathogenic NY–1V, HTNV, and ANDV hantaviruses successfully replicate within human endothelial cells by blocking early IFN responses (3, 62). Figure 25 demonstrates that, similar to pathogenic hantaviruses, TULV proteins regulate cellular IFN responses, and thus nonpathogenic TULV differs from PHV at a fundamental level.

While replication within endothelial cells and evasion of early IFN responses is a requirement for hantavirus pathogenesis, TULV replication within human endothelial cells demonstrates that blocking early IFN responses is not sufficient for a hantavirus to be pathogenic. However, β_3 integrin receptor interactions have also been associated with hantavirus pathogenesis, and β_3 integrins are critical regulators of vascular barrier functions and prominent on the surface of endothelial cells and platelets (14, 15, 55, 57-59, 66, 169). Pathogenic hantaviruses uniquely bind platelets and cell–associated hantaviruses recruit quiescent platelets to the surface of infected endothelial cells, fundamentally altering the surface of infected endothelium at late times post–infection (56). β_3

integrins also play an important role in stabilizing fluid barrier functions of the endothelium by regulating permeabilizing responses of VEGF. In contrast to nonpathogenic TULV and PHV, only pathogenic hantaviruses enhance VEGF–directed endothelial cell permeability which may contribute to pathogenesis (55, 57-59, 66, 169).

Appendix II:

Figures and Legends

Hantavirus	Host	Place of Isolation	Disease	Reference
Hantaan (HTNV)	*Apodemus agrarius*	Asia	HFRS	116, 117
Dobrava–Belgrade (DOBV)	*Apodemus agrarius, Apodemus flavicollis*	Balkans, Europe	HFRS	5, 104
Thailand (THAV)	*Bandicota indica*	S.E. Asia	HFRS	40, 212
Puumala (PUUV)	*Myodes glareolus*	Europe	HFRS	17, 142
Seoul (SEOV)	*Rattus norvegicus*	Worldwide	HFRS	74, 103
Sin Nombre (SNV)	*Peromyscus maniculatus*	S.W. US	HPS	24, 148
New York–1 (NY–1V)	*Peromyscus leucopus*	N.E. US	HPS	78, 186
Bayou (BAYV)	*Oryzomys palustris*	S.E. US	HPS	101, 139, 194
Black Creek Canal (BCCV)	*Sigmodon hispidus*	Florida (US)	HPS	168, 172
Andes (ANDV)	*Oligoryzomys longicaudatus*	Argentina, Chile	HPS	42, 119, 123, 153
Maporal (MAPV)	*Oligoryzomys fulvescens*	Venezuela	HPS	51
Tula (TULV)	*Microtus arvalis*	Europe	None	164, 184
Prospect Hill (PHV)	*Microtus pennsylvanicus*	US	None	118

Table I Hantaviruses, Hosts, Place of Isolation, and Associated Disease (adapted from 179).

Name	Primers (5′ – 3′)
pT7HR1–ANDV–L	5′ Half: TTGGATCCGTCTCAGACTCCGGGATAGAAAAAGTTAGAAAAATGGAAAAGTATAGAGAGA TTTTCGTCTCCAATGAAAGTTTCCTGCCTGTATCTGCTGTGATAC 3′ Half: TTTTCGTCTCTCATTGGCATGCTATAAATCAAGAGATGTGGAAGAGC TTTTCGTCTCAACCCTAGTAGTATGCTCCGGGAAAAGAACACTACAATATAC
pT7HR1–ANDV–M	TTGGATCCGTCTCAGACTCCGCAAGAAGAAGCAAAAAATTAAAGAAGTGAGTTTAAAATG TTTTCGTCTCAACCCTAGTAGTATGCTCCGCAGGAACAAAAGCCTCGGTAAG
pT7HR1–ANDV–S	TTTTCGTCTCTGACTCCTTGAGAAGCTACTGCTGCGAAAGCTGGAATG TTTTCGTCTCAACCCTAGTAGTATGCTCCTTGAAAAGCAATCAAG
pT7HR1–ANDV–S–Marker	GTGAAAGACAACAAAGGAACCAGGATCCGGTTTAAGGATGATTCTTCC GGAAGAATCATCCTTAAACCGGATCCTGGTTCCTTTGTTGTCTTTCAC
pTM1–ANDV–L	TAGTAGTAGACTCCGGGATAGAAAAAGTTAGAAAACGTCTCCCATGGAAAAGTACAGAGAGATTCATCAGAGAGTTAGG CCTAACTCTCTGATGAATCTCTCTGTACTTTTCCATGGGAGACGTTTTCTAACTTTTTCTATCCCGGAGTCTACTACTA
pTM1–ANDV–M	TTCTCGTCTCCCATGGGAAGGCTGGTATCTGGTTGCTCTTGGAATCTGC CGGCTCAGCGTCTCGGATCCCTAGACAGTTTTCTTGTGTCCTCTCCTGGGGCACAGAACACTG
pTM1–ANDV–S	TTTTCGTCTCCCAATGAGCACCCTCCAAGAATTACAAGAAAACATC TTTGGATCCTTACAACTTAAGTGGCTCTTGGTTGGAGATC
pT7HR1–ANDV–L–ApaI	GACCATACTACTAGGGCCCTCGGCATGGCATCTCC GGAGATGCCATGCCGAGGGCCCTAGTAGTATGCTC
pT7HR1–ANDV–M–ApaI	GAGCATACTACTAGGGCCCTCGGCATGGCATCTCC GGAGATGCCATGCCGAGGGCCCTAGTAGTATGCTC
pT7HR1–ANDV–S–ApaI	GAGCATACTACTAGGGCCCTCGGCATGGCATCTCC GGAGATGCCATGCCGAGGGCCCTAGTAGTATGCTC

Table II ANDV Reverse Genetics Cloning Primers Primer sequences used to generate PCR products representing ANDV L (GenBank Accession: AY228239.1), M (GenBank Accession: AY228238.1), or S (GenBank Accession: AY228237.1) anti–genome sense cDNAs or encoding ANDV protein ORFs are presented.

Figure 1 New World Hantavirus Distribution (adapted from Zina Deretsky, NSF; CDC). Andes virus (red font) has been reported to be spread from person–to–person (21, 153, 207). Prospect Hill virus (yellow font) is a nonpathogenic hantavirus.

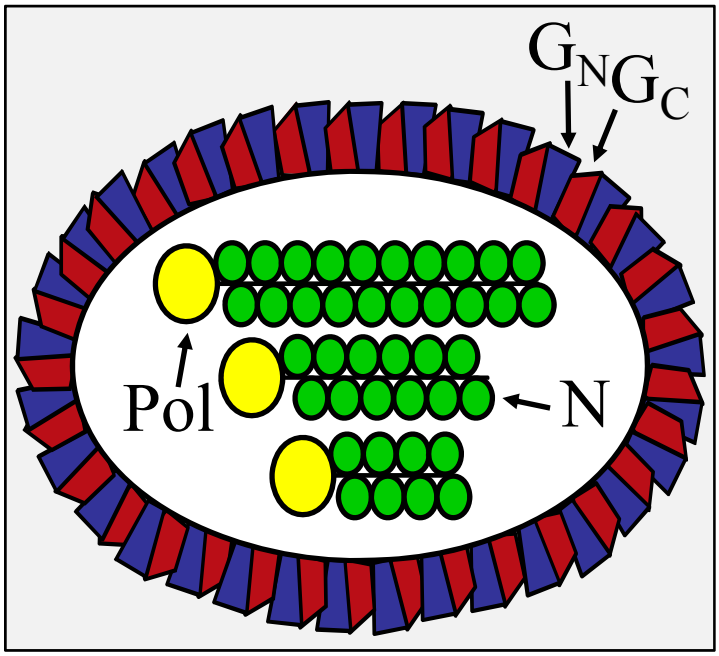

Figure 2 Schematic Diagram of a Hantavirus Particle. Hantaviruses are spherical enveloped viruses with a tri–segmented single–stranded, negative–sense RNA genome. The small (S) segment encodes the nucleocapsid (N) protein. The medium (M) segment encodes the viral surface glycoproteins G_N and G_C which are expressed as a precursor that is co–translationally cleaved (132, 179). The large (L) segment encodes the RNA–dependent RNA polymerase (Pol).

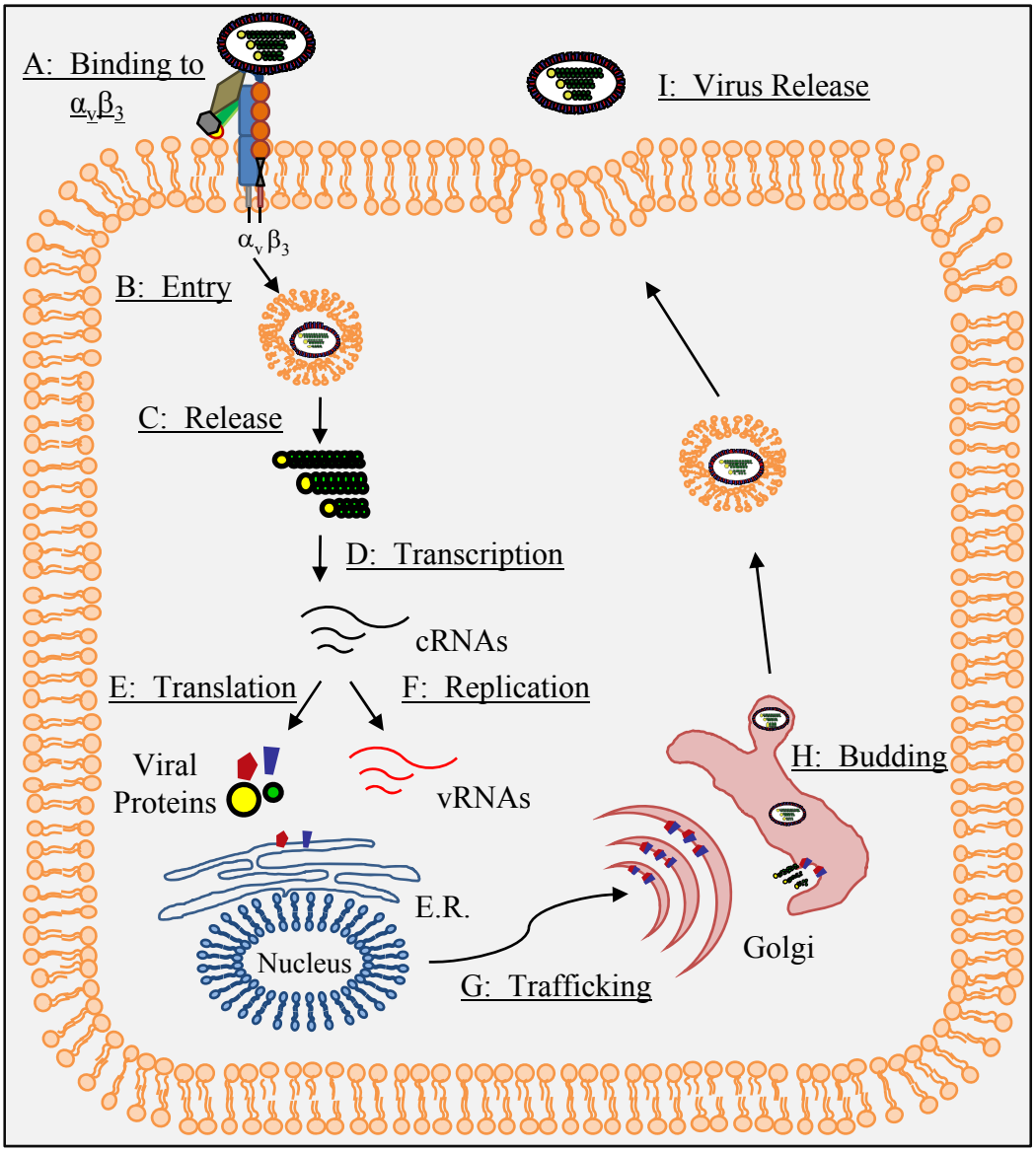

Figure 3 **Hantavirus Life Cycle (adapted from 208) (175).** Pathogenic hantaviruses bind $\alpha_v\beta_3$ integrins expressed on the surface of endothelial cells (55, 59, 168), it's primary cellular target (55, 58, 59) (A). Following entry (B), viral RNAs are released into the cytoplasm (C) where viral cRNAs are generated by the polymerase (D) and used as templates for translating viral proteins (E) and RNA replication (F). The viral glycoproteins, G_N and G_C, are trafficked (G) to the cis–Golgi where viral budding occurs (176) (H). Hantaviruses exit cells through an unknown secretory process (I).

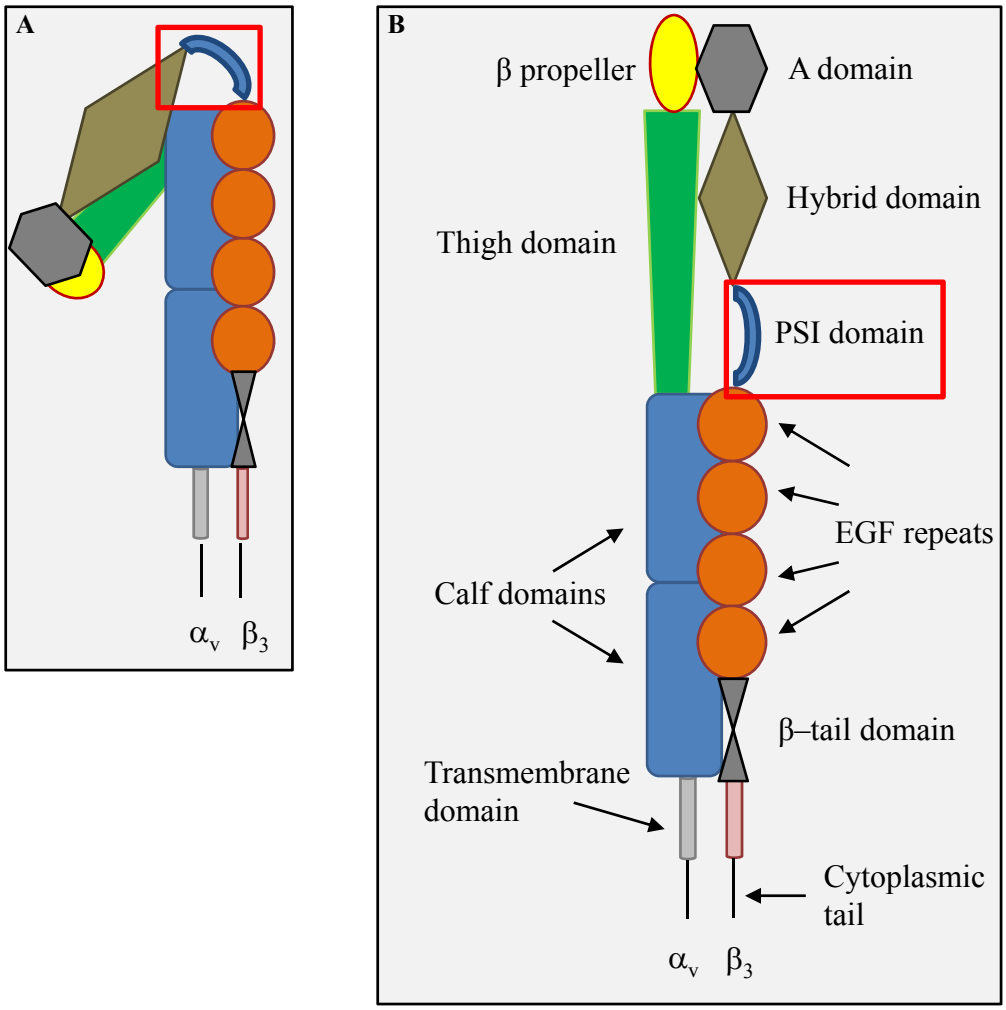

Figure 4 Schematic Representation of the (A) Bent, Inactive and (B) Extended, Active $\alpha_v\beta_3$ Integrin Conformations (adapted from 84). The α subunit comprises a β propeller at the top, followed by three sandwich modules (thigh and calf domains), a transmembrane domain and a short cytoplasmic tail (84). The β subunit is comprised of an A domain, followed by a β–sandwich hybrid domain, four epidermal growth factor (EGF) repeats and a β–tail domain (84). The PSI domain which directs interaction with pathogenic hantaviruses is located at the apex of the bent, inactive integrin (A) and highlighted (red box) (169).

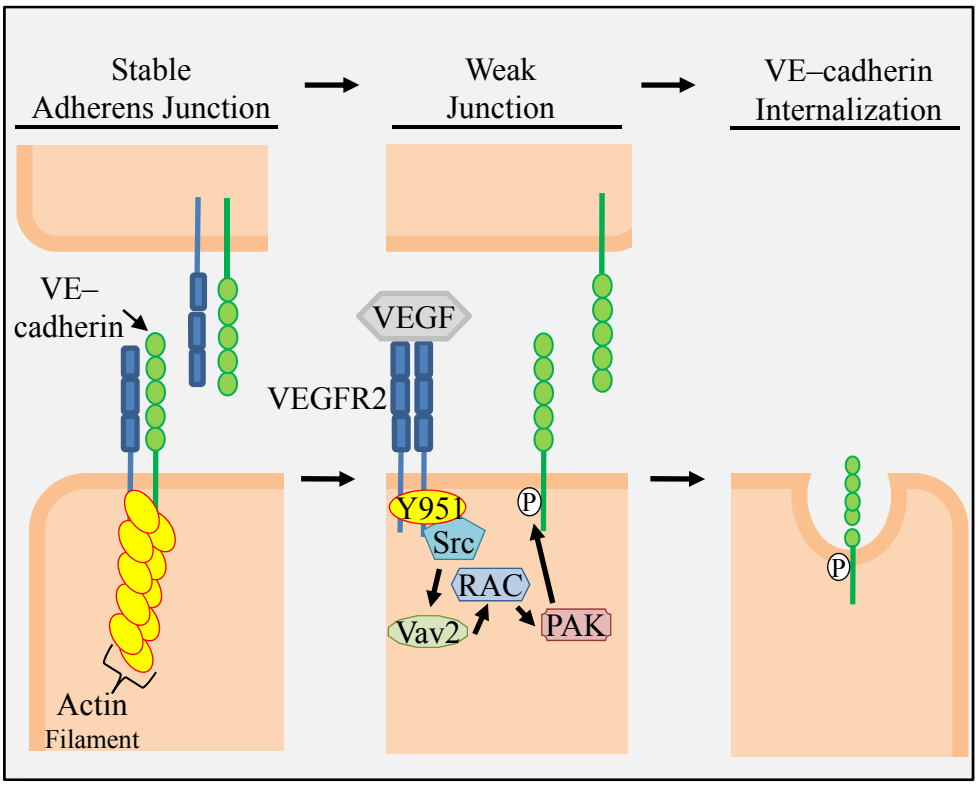

Figure 5 Adherens Junction Disassembly. Binding of VEGF to VEGFR2 causes receptor dimerization, subsequent autophosphorylation of the VEGFR2 cytoplasmic tail, and the activation of a number of signaling responses (129). A Src–directed signaling cascade leads to the phosphorylation of VE–cadherin (54) which results in VE–cadherin internalization and destabilization of the adherens junction (53, 152). Regulation of vascular barrier functions, therefore, is achieved through coordination of multiple factors and signaling events including integrins and VEGF–directed responses (35, 52, 54, 111, 114, 143).

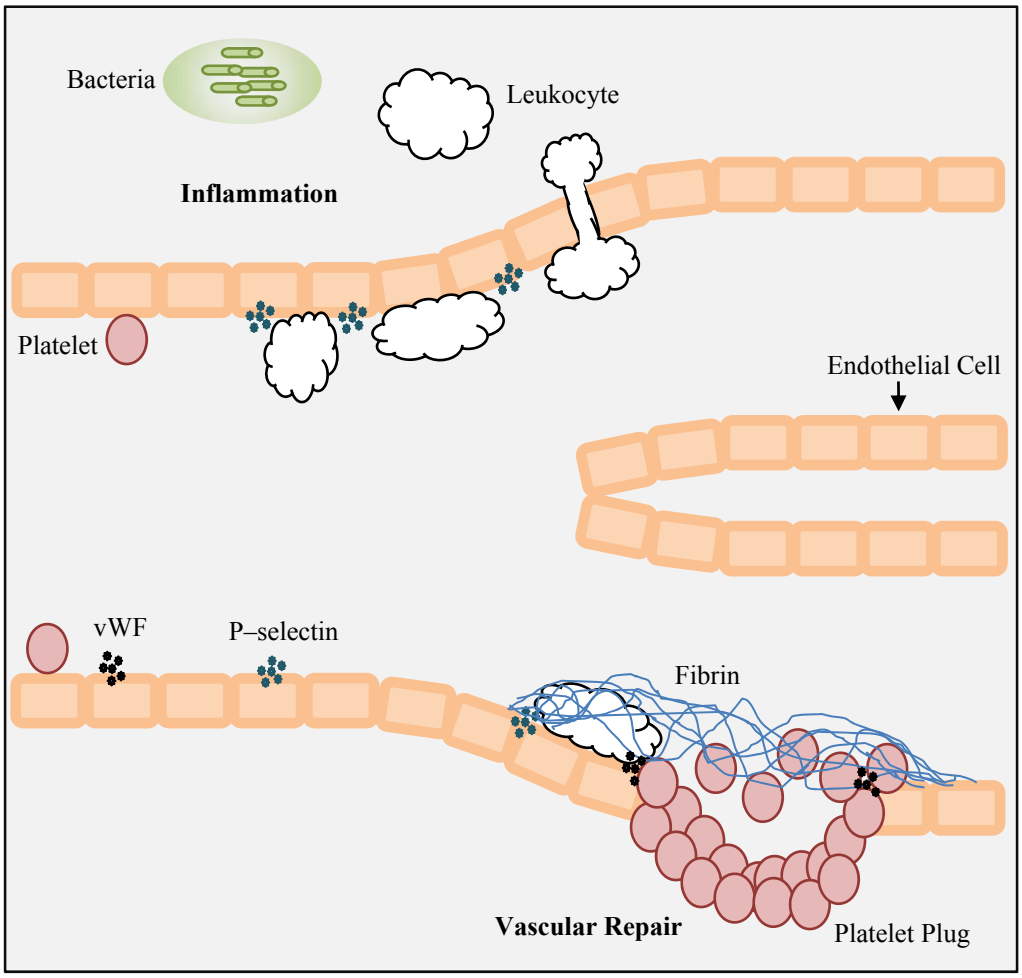

Figure 6 Regulation of Immune Cell Responses and EC Barrier Integrity (adapted from 50). The endothelium regulates a number of important functions which require their ability to move. To allow the extravasation of leukocytes (in response to bacterial infection, for example), endothelial cells induce rolling of leukocytes before they migrate to sites of inflammation or vascular injury. This is facilitated by selectins expressed by ECs. After activation, strong adherence of leukocytes to ECs results from interactions between β_2 integrins on leukocytes with specific immunoglobulin superfamily receptors on the endothelium. Following extravasation, leukocytes migrate toward the site of infection/inflammation along a chemoattractant gradient. Additionally, ECs need to move in response to vascular injury. Immediately after injury, ECs release factors including P–selectin and von Willebrand factor (vWF). Von Willebrand factor and P–selectin direct rolling and adhesion of platelets to the site of injury. Once at the site of injury, platelet $\alpha_{IIb}\beta_3$ integrin activation and platelet degranulation result in platelet aggregation which recruits leukocytes that participate in repair. The platelet plug formed by the aggregated platelets is stabilized by the accumulation of fibrin strands.

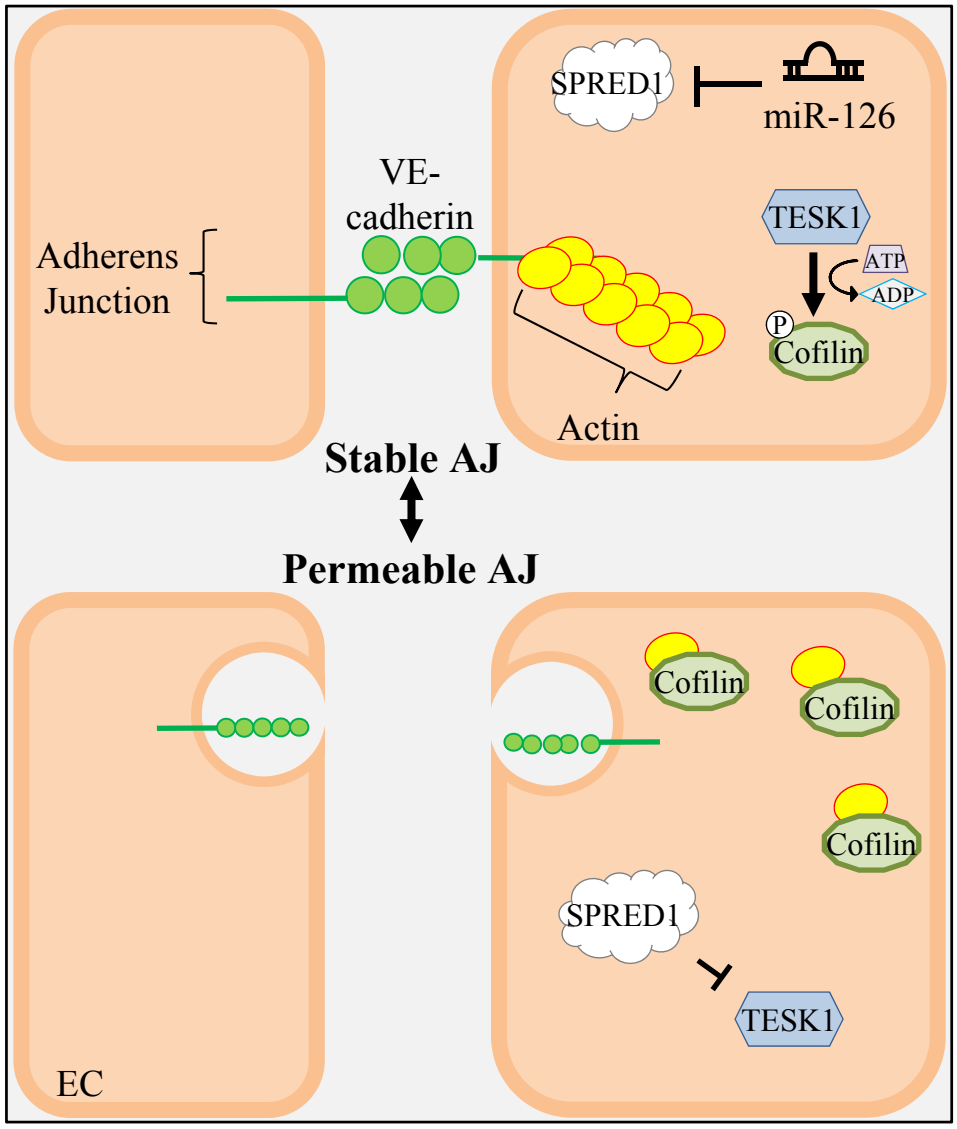

Figure 7: MiR–126 and SPRED1 Regulation of Vascular Permeability. MiR–126 is specifically expressed at high levels in ECs, and knockdown of miR–126 causes the loss of vascular integrity, inhibits VEGF induced EC migration, alters cytoskeletal organization and results in hemorrhage during embryonic development and in adult mice (46, 205). MiR–126 regulates VEGF directed EC responses by downregulating SPRED1 and PIK3R2. SPRED1 binds to TESK1 and prevents TESK1 phosphorylation of cofilin. This destabilizes actin filaments required for VE–cadherin assembly within AJs (94, 151, 196). SPRED1 overexpression alone increases EC permeability (46), and thus changes in SPRED1 and miR–126 may directly regulate EC sensitivity to VEGF activation (46, 121, 197, 204, 205).

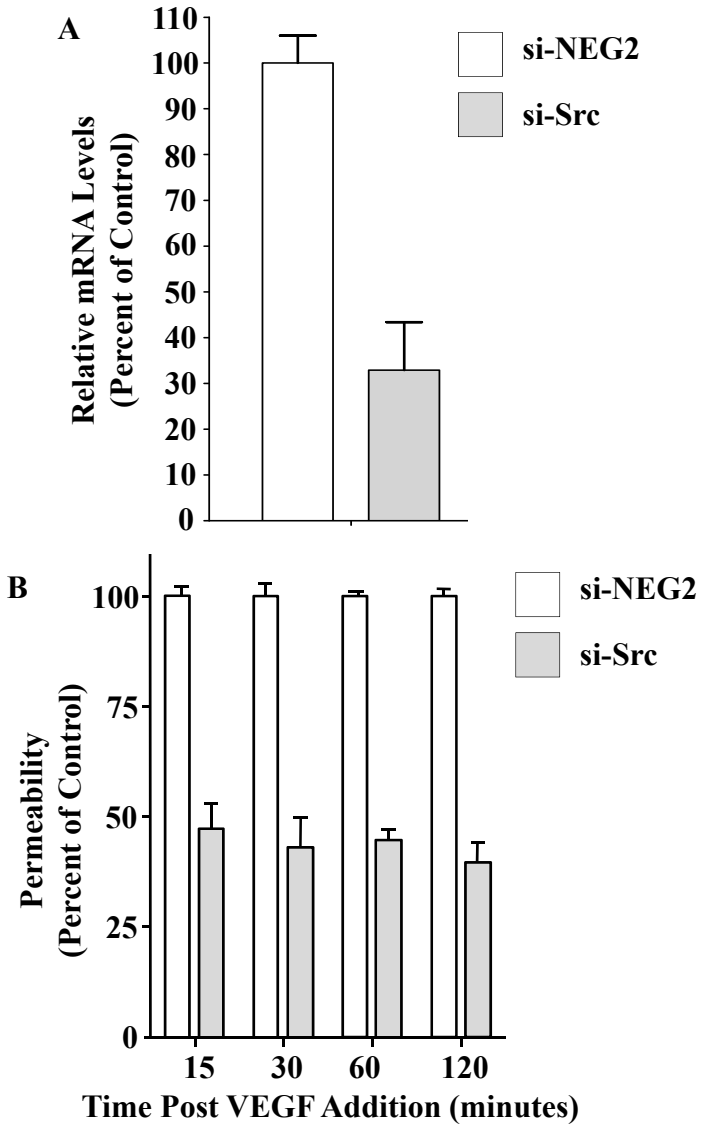

Figure 8 Src Knockdown Inhibits ANDV–Induced EC Permeability (65). (A) ECs were transfected with Src siRNA or a scrambled siRNA (si–NEG2), and the levels of Src mRNA were analyzed by qRT–PCR (159) three days post transfection. Total cellular RNA was purified and Src mRNA levels were standardized to constant GAPDH mRNA levels. Data are presented as the fold change in mRNA levels relative to those of mock infected controls using the $2^{-\Delta CT}$ method (108). (B) EC permeability was determined as previously described (57). One day after transfection with Src or scrambled siRNAs, ECs were infected with ANDV or were mock infected. Three days p.i., FITC–dextran and VEGF were added to media in the upper chamber, and the presence of FITC–dextran in the lower chamber was quantitated after 15, 30, 60, or 120 min as a measure of EC permeability (57). Results are expressed as the percent monolayer permeability relative to the basal permeability levels of controls (57). Experiments in (B) were performed in collaboration with Dr. Gavrilovskaya and Dr. Gorbunova in the lab. Experiments were performed in duplicate and plotted as the means ± SEM using GraphPad Prism 5 software.

A

miR-142-5p 2.17	miR-16 2.27	miR-142-3p 2.20	miR-21 3.06	miR-15a 1.52	miR-29b 1.86	let-7a 2.03	miR-126 2.47	miR-143 -1.19	let-7b 4.04	miR-27a 2.37	let-7f 1.26
miR-9 4.42	miR-26a 2.21	miR-24 2.35	miR-30e 1.95	miR-181a 2.58	miR-29a 2.65	miR-124 2.51	miR-144 1.29	miR-30d 1.48	miR-19b 2.34	miR-22 2.47	miR-122 1.20
miR-150 2.90	miR-32 2.49	miR-155 6.70	miR-140-5p 2.40	miR-125b 1.95	miR-141 2.34	miR-92a 1.68	miR-424 2.74	miR-191 1.65	miR-17 1.64	miR-130a 1.56	miR-20a 1.65
miR-27b 3.17	miR-26b 1.95	miR-146a 4.42	miR-200c 2.78	miR-99a 2.02	miR-19a 2.76	miR-23a 1.55	miR-30a 2.44	let-7i 3.17	miR-93 1.71	let-7c 2.92	miR-106b 1.89
miR-101 4.45	let-7g 2.44	miR-425 1.80	miR-15b 2.15	miR-28-5p 2.40	miR-18a 2.35	miR-25 2.44	miR-23b 1.81	miR-302a 6.34	miR-186 2.70	miR-29c 3.99	miR-7 5.76
let-7d 13.32	miR-30c -1.42	miR-181b 2.14	miR-223 -2.94	miR-320 3.24	miR-374a 2.29	let-7e 12899.25	miR-151-5p 2.84	miR-374b 1.95	miR-196b 2.39	miR-140-3p 2.94	miR-100 2.31
miR-103 2.44	miR-96 1.59	miR-302b -1.12	miR-194 3.06	miR-125a-5p 1.97	miR-423-5p 1.89	miR-376c 2.29	miR-195 1.99	miR-222 3.13	miR-28-3p 2.76	miR-128a 1.78	miR-302c 1.95
miR-423-3p 11.27	miR-185 2.39	miR-30b 1.22	miR-210 1.70								

B

mir-375 8.00	mir-182 2.23	mir-196a 1.26	mir-10a 2.58	mir-324-5p 1.21	mir-137 1.91	mir-378 2.81	mir-135b 1.13	mir-342-3p 1.05	mir-205 -1.27	mir-192 2.22	mir-10b -38.85
mir-744 2.46	mir-363 4.23	mir-503 -76.64	mir-130b 1.09	mir-151-3p 2.95	mir-214 1.07	mir-454 1.71	mir-379 2.36	mir-301a 1.47	mir-98 -1.41	mir-34a 1.84	mir-33a -9.99
mir-339-3p 5.70	mir-301b 2.11	mir-193b 1.30	mir-652 1.66	mir-20b 1.06	mir-138 1.40	mir-199a-3p 3.23	mir-183 -2.58	mir-134 1.32	mir-132 1.83	mir-148a 1.64	mir-218 -128.89
mir-365 1.58	mir-339-5p 1.10	mir-497 1.68	mir-193a-5p 1.85	mir-625 -1.44	mir-488 -3.12	mir-129-5p 1.22	mir-345 1.79	mir-518b -1.49	mir-517a 1.13	mir-421 1.09	mir-197 -5.94
mir-17* 3.12	mir-18b -1.95	mir-335 -1.05	mir-376a 1.55	mir-361-5p -1.51	mir-505 1.34	mir-877 -4.44	mir-203 4.86	mir-411 1.46	mir-152 2.16	mir-532-5p 4.26	mir-342-5p -2.75
mir-373 1.09	mir-135a 1.42	mir-202 1.84	mir-340 1.55	mir-139-5p 2.22	mir-129-3p 1.21	mir-545 2.85	mir-338-3p 2.53	mir-127-3p 1.44	mir-455-3p -2.04	mir-484 1.69	mir-500 -1.04
mir-518c 24.25	mir-1 -1.53	mir-590-3p 2.43	mir-372 1.27	mir-148b 1.99	mir-181c 1.84	mir-188-5p 1.46	mir-149 -2.11	mir-410 -3396.89	mir-431 2.19	mir-331-3p 2.00	mir-548c-5p 3.03
mir-486-5p -1.71	mir-34c-5p 1.80	mir-629 1.99	mir-452 3.23								

Figure 9 A, B: MicroRNA Microarray Data – Plates 1 and 2 (SA Biosciences) (160). The fold change in expression of miRNAs 3 days post ANDV infection of HUVECs is presented. Green boxes represent miRNAs that were upregulated ≥3–fold and red boxes represent miRNAs that were downregulated ≥3–fold.

C

mir-574-5p 1.41	mir-184 2.14	mir-660 2.49	mir-337-5p 1.74	mir-146b-5p 11.27	mir-432 1.34	mir-370 1.93	mir-95 4.10	mir-206 4.30	mir-873 2.21	mir-532-3p 1.78	mir-139-3p 2.39
mir-524-5p 3.26	mir-188-3p -1.02	mir-590-5p 2.14	mir-455-5p 2.54	mir-331-5p 1.12	mir-429 1.98	mir-362-5p 1.15	mir-525-3p 3.67	mir-493 2.34	mir-526b 3.93	mir-190 2.06	mir-515-5p 4.16
mir-665 2.37	mir-147 2.12	mir-361-3p 4.01	mir-514 1.47	mir-376b 1.60	mir-582-5p 2.14	mir-187 2.67	mir-671-5p 2.02	mir-487b -1.06	mir-651 2.31	mir-219-5p 1.90	mir-299-3p 1.22
mir-449a 2.02	mir-369-3p 2.27	mir-219-2-3p 2.08	mir-105 2.26	mir-551b 3.49	mir-542-5p 1.65	mir-542-3p 2.59	mir-618 1.89	mir-502-3p 2.12	mir-519a 1.85	mir-181d 5.05	mir-382 2.12
mir-508-3p 1.19	mir-450a 1.98	mir-127-5p 1.52	mir-523 1.61	mir-589 1.77	mir-369-5p -1.41	mir-615-3p -2.74	mir-527 2.34	mir-576-3p -1.56	mir-337-3p 1.82	mir-362-3p 2.27	mir-515-3p 3.38
mir-518a-3p 1.90	mir-885-5p 1.28	mir-433 1.30	mir-512-3p 1.86	mir-548d-5p 1.38	mir-133b 2.31	mir-296-5p 1.07	mir-371-3p 1.05	mir-330-3p 1.90	mir-329 1.51	mir-495 1.22	mir-450b-5p 3.38
mir-758 -1.13	mir-522 1.37	mir-323-3p 1.56	mir-889 2.90	mir-208b 1.72	mir-487a 2.12	mir-628-3p 2.40	mir-628-5p 2.20	mir-671-3p 2.27	mir-485-3p -1.95	mir-548d-3p -1.09	mir-383 3.06
mir-548b-3p 1.50	mir-215 2.45	mir-520d-5p 2.20	mir-520d-3p 2.92								

D

mir-584 2.21	mir-513-5p 1.46	mir-579 1.52	mir-498 -1.38	mir-550 1.14	mir-556-5p 1.83	mir-380 -2.23	mir-491-3p -4.07	mir-576-5p 2.61	mir-597 1.01	mir-504 1.78	mir-520g 1.12
mir-642 1.06	mir-875-5p 1.11	mir-875-3p -1.39	mir-501-5p 2.51	mir-501-3p 1.41	mir-544 1.72	mir-548a-5p 1.81	mir-548a-3p -1.25	mir-422a 1.15	mir-489 1.13	mir-636 2.88	mir-198 1.46
mir-496 -2.12	mir-518d-3p 1.08	mir-524-3p 1.25	mir-519b-5p -1.20	mir-519c-3p -1.07	mir-516a-3p 1.74	mir-502-5p 2.82	mir-512-5p 1.32	mir-566 1.05	mir-548c-3p 1.02	mir-555 1.14	mir-492 -1.32
mir-638 1.11	mir-412 1.14	mir-588 1.39	mir-650 1.24	mir-619 1.91	mir-543 -1.15	mir-643 1.00	mir-603 1.02	mir-602 1.02	mir-563 1.11	mir-558 -1.39	mir-657 -1.36
mir-511 1.41	mir-595 1.43	mir-613 1.16	mir-802 1.04	mir-583 -1.20	mir-384 -1.36	mir-611 1.34	mir-575 1.08	mir-658 1.36	mir-637 1.40	mir-580 1.41	mir-564 1.34
mir-610 -2.65	mir-633 -1.10	mir-562 1.11	mir-614 1.95	mir-325 1.24	mir-600 1.01	mir-630 1.11	mir-298 -1.37	mir-622 1.31	mir-626 1.33	mir-659 1.37	mir-585 2.42
mir-639 1.57	mir-220c 1.04	mir-211 1.00	mir-623 1.47	mir-641 -1.98	mir-557 1.38	mir-212 1.40	mir-632 1.43	mir-567 -1.03	mir-605 2.11	mir-208 1.99	mir-448 1.97
mir-621 1.41	mir-648 1.14	mir-190b 4.71	mir-587 1.38								

Figure 9 C, D: MicroRNA Microarray Data – Plates 3 and 4 (SA Biosciences) (160). The fold change in expression of miRNAs 3 days post ANDV infection of HUVECs is presented. Green boxes represent miRNAs that were upregulated ≥3–fold and red boxes represent miRNAs that were downregulated ≥3–fold.

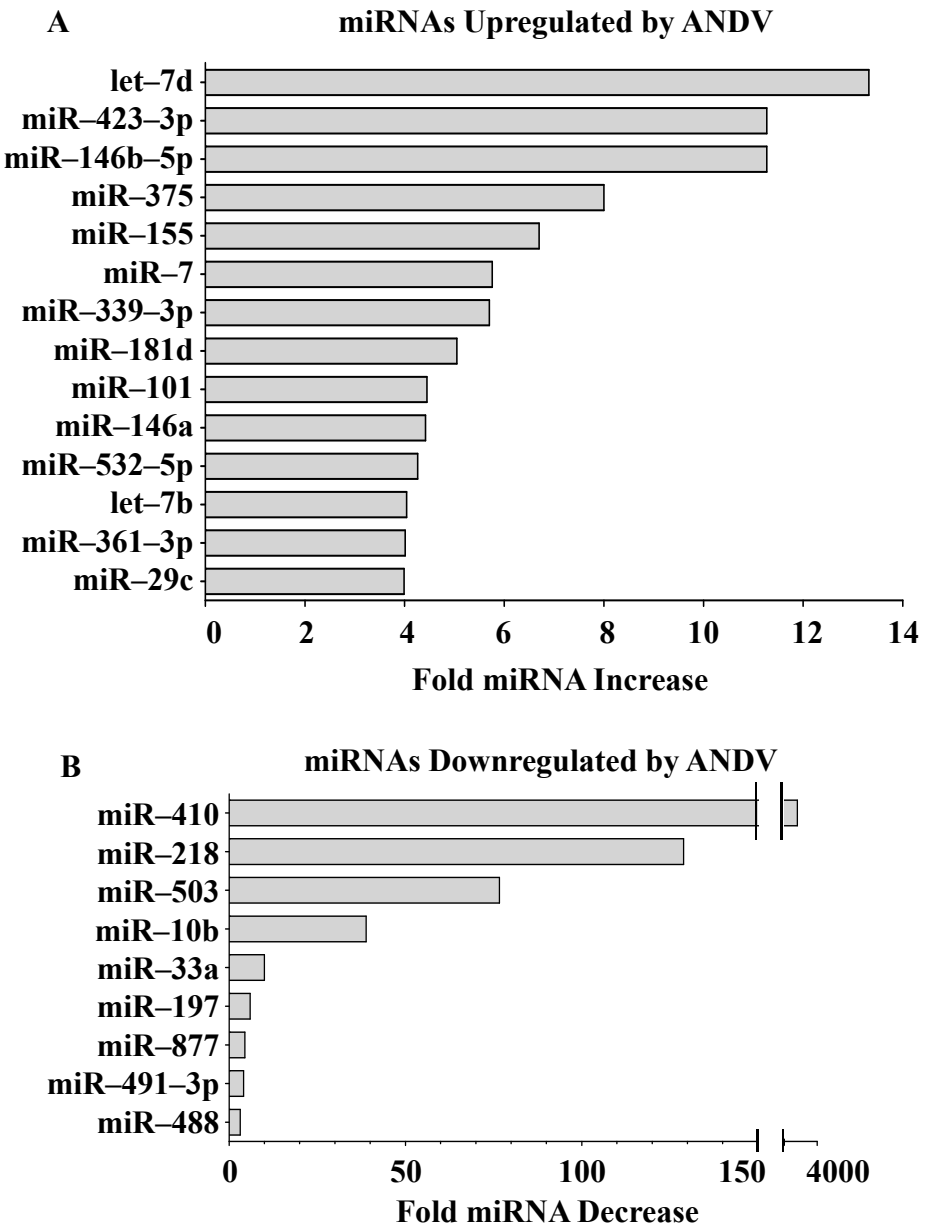

Figure 10 MiRNA qRT–PCR Microarray Analysis (160). EC monolayers were mock infected or infected with ANDV at an MOI of 1, and 3 days p.i., cells were lysed and small RNAs were purified (57). The level of 352 individual miRNAs was assessed by qRT–PCR on an Applied Biosystems 7300 RT–PCR machine (108). MiRNA levels from mock– and ANDV–infected cells were standardized to U6 RNA levels present in samples. The increase (A) or decrease (B) in miRNAs present in ANDV– versus mock–infected ECs was determined, and ≥4–fold changes in miRNA expression levels are presented.

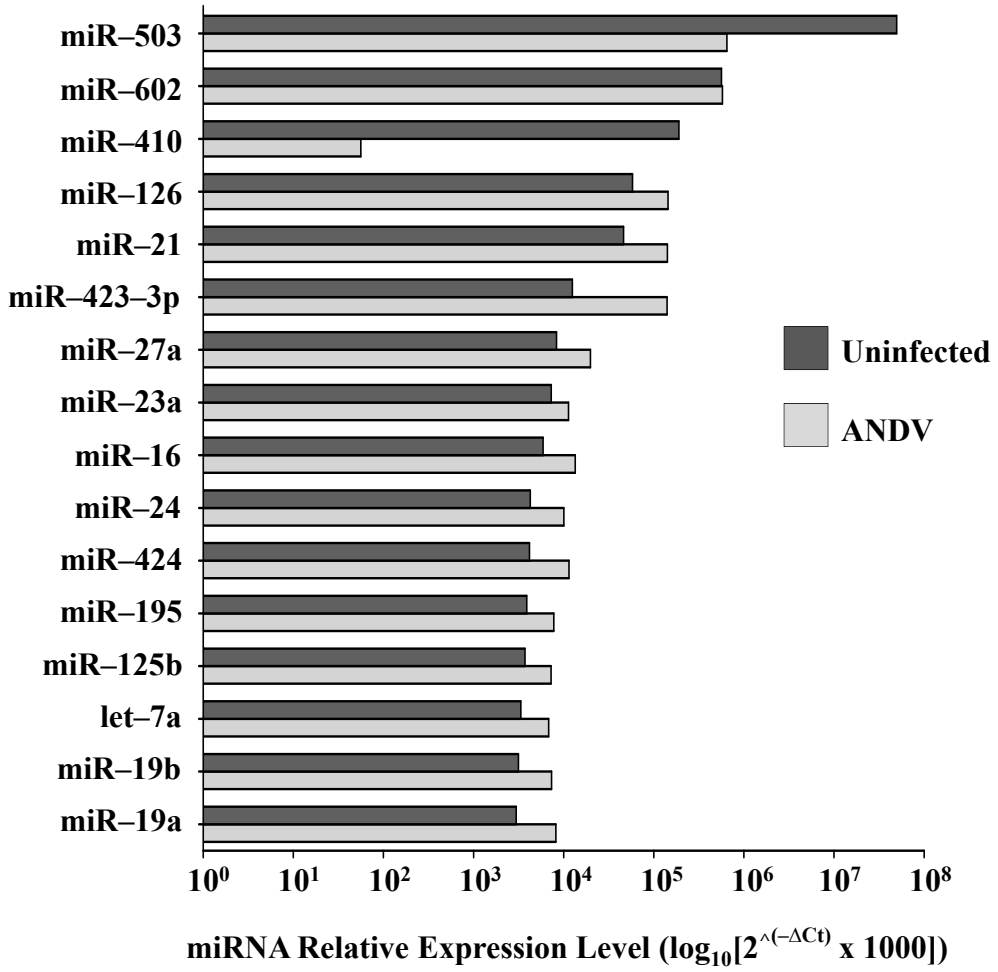

Figure 11 Relative miRNA Levels Following ANDV Infection (160). MiRNAs present in ANDV– and mock–infected controls were determined by qRT–PCR of cellular miRNAs as described in the legend to Figure 9 and standardized to U6 RNA levels (160). The relative levels of highly expressed EC miRNAs were determined using the $2^{\Delta C_t}$ method (108) and are comparatively presented.

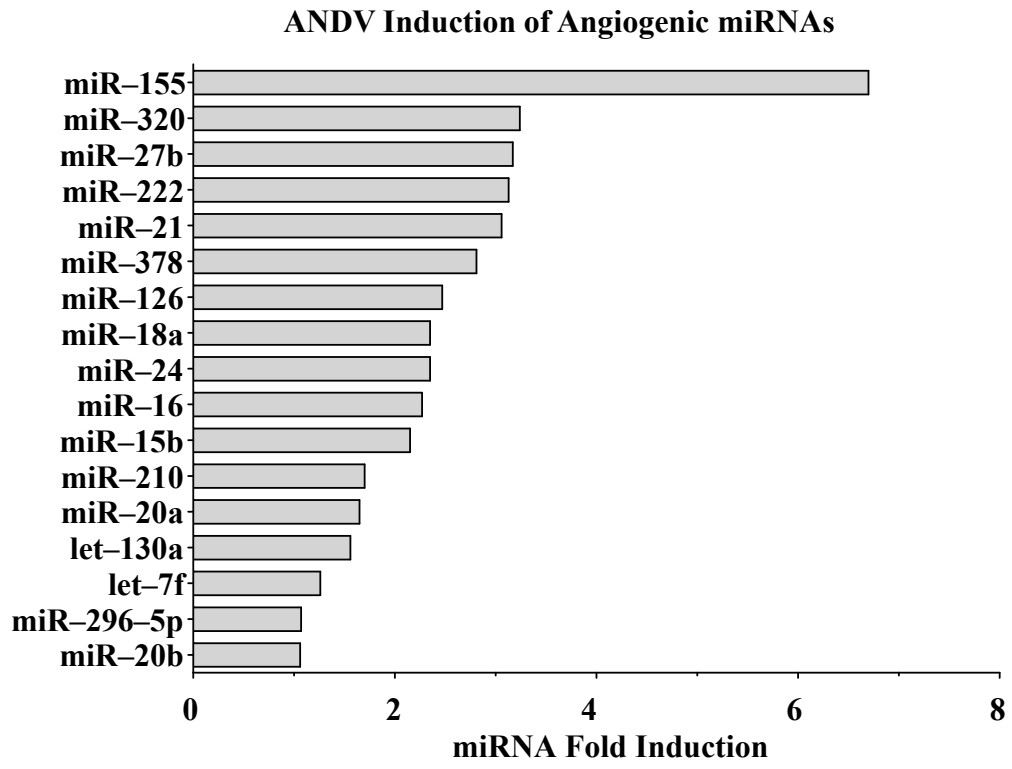

Figure 12 Angiogenic miRNAs Induced by ANDV Infection (160). The relative levels of cellular miRNAs present within ANDV– and mock–infected ECs were determined as described in the legend to Figure 10 (160). Changes in miRNAs reported to play a role in angiogenesis (205) are presented as the fold increase in miRNAs present in ANDV infected ECs relative to that in mock infected ECs.

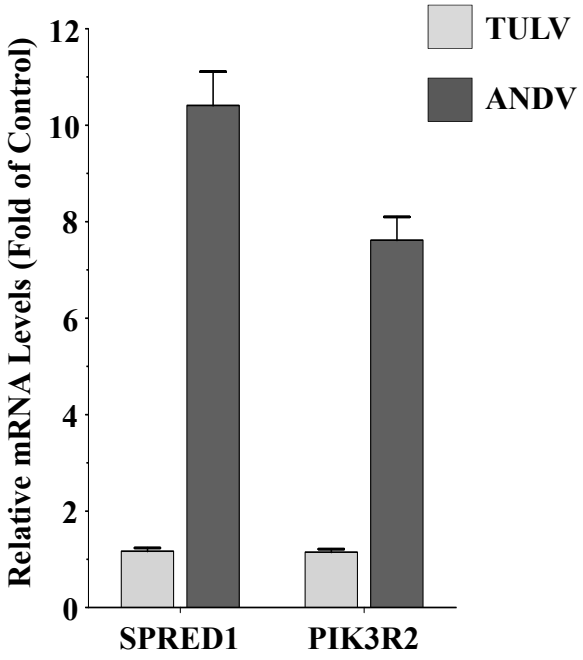

Figure 13 Sprouty–related EVH1 domain containing protein 1 (SPRED1) and Phosphoinositide–3–kinase, regulatory subunit 2 (PIK3R2) mRNA Induction Following ANDV Infection (160). HUVECs were infected with ANDV or TULV (MOI of 1) or were mock infected. Three days p.i., total cellular RNA was purified and SPRED1 and PIK3R2 mRNA levels were determined by quantitative real–time PCR (3). SPRED1 and PIK3R2 mRNA levels were standardized to constant GAPDH mRNA levels. Experiments were performed in duplicate and data are presented as the fold change in mRNA levels relative to those of mock infected controls using the $2^{-\Delta CT}$ method (108) and plotted as the means ± SEM using GraphPad Prism 5 software.

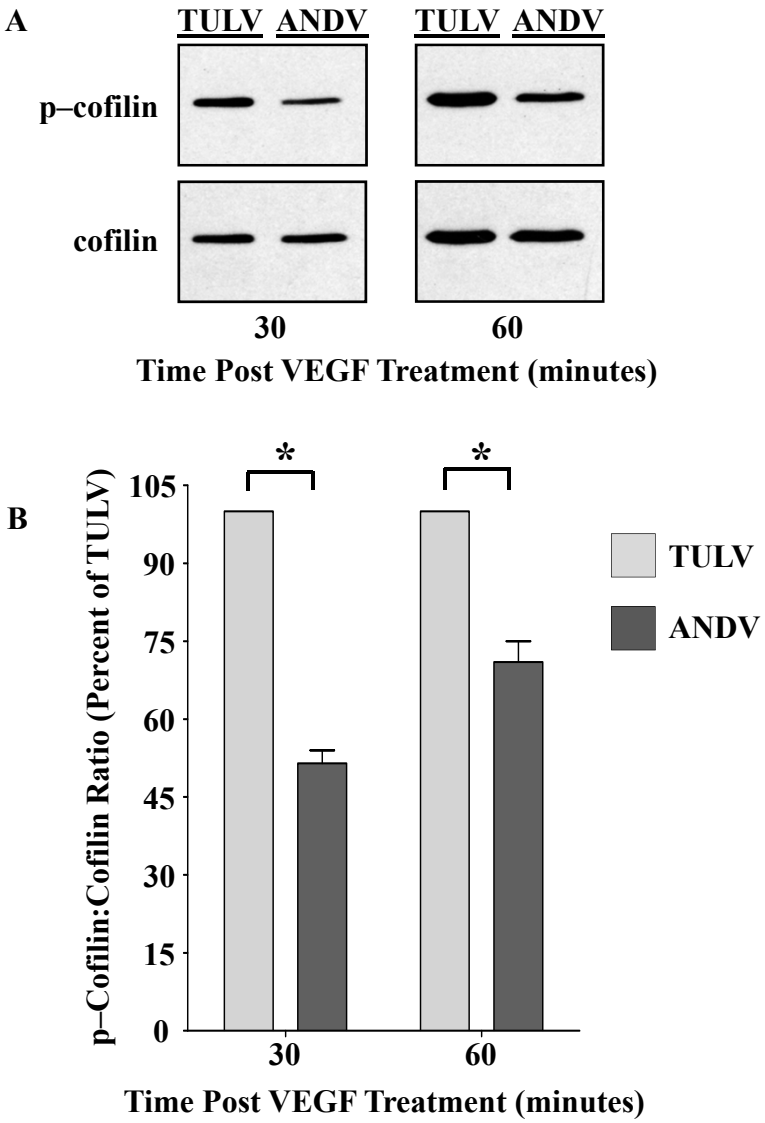

Figure 14 Decreased Cofilin Phosphorylation in ANDV–Infected ECs Following VEGF Treatment (160). (A) Cofilin phosphorylation within ANDV–infected ECs following VEGF treatment was assessed by Western blotting (60). HUVECs were infected with ANDV or TULV (MOI of 0.5) and 3 days p.i. cells were treated with VEGF for the indicated times (57). Equivalent amounts of total protein were separated by SDS polyacrylamide (15%) gel electrophoresis and analyzed by Western blotting using anti–cofilin or anti–phospho–cofilin rabbit polyclonal antibodies, HRP–conjugated anti–rabbit secondary antibody, and enhanced chemiluminescence. Ninety percent of cells were infected by ANDV and TULV, respectively, as determined by immunoperoxidase staining for N protein (59). (B) Densitometric analysis of cofilin and phospho–cofilin levels was performed using ImageJ (NIH) software, and data from four independent experiments were plotted as the means ± SEM using GraphPad Prism 5 software (*, $P < 0.005$).

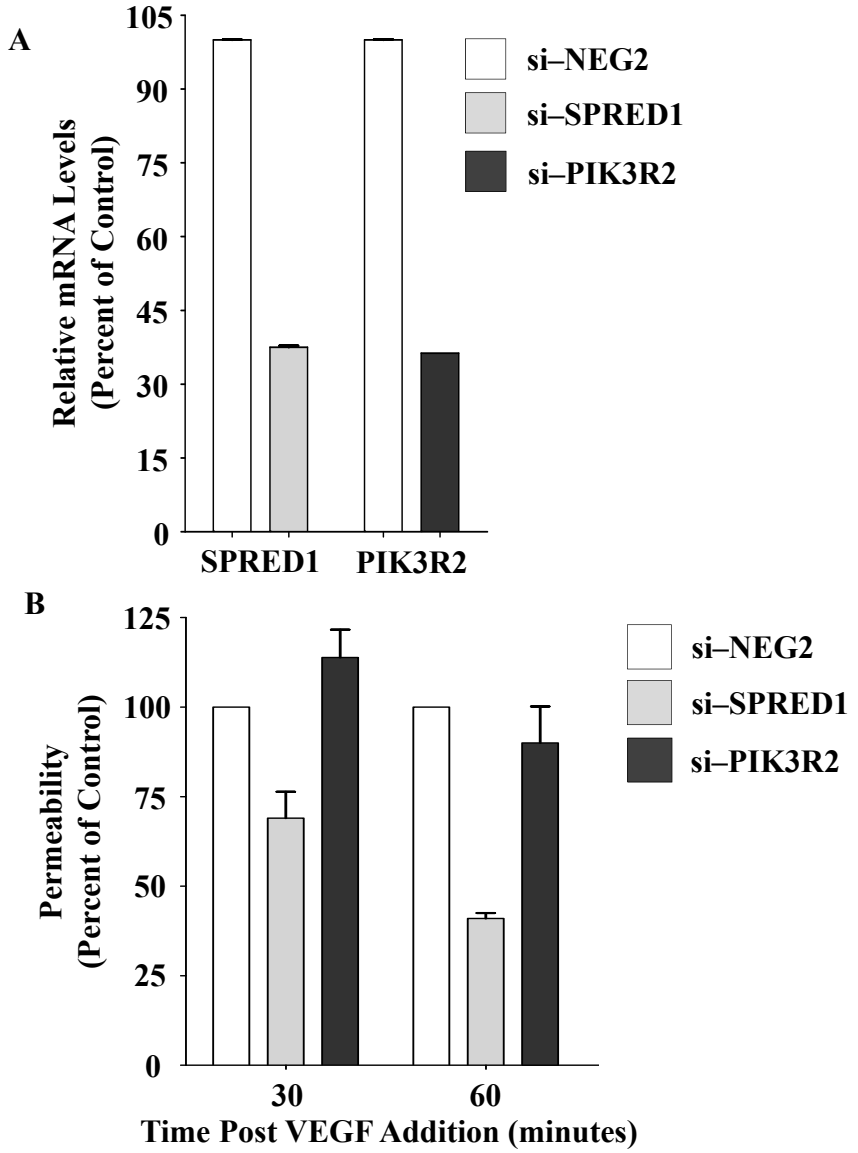

Figure 15 SPRED1 Knockdown Inhibits ANDV Induced EC Permeability (160). (A) ECs were transfected with siRNAs specific for SPRED1, PIK3R2, or a scrambled siRNA (si–NEG2) using SureFECT transfection reagent. The levels of SPRED1 and PIK3R2 mRNAs were analyzed by qRT–PCR three days post transfection (3). MRNA levels were quantitated and standardized as described in the legend to Figure 13 and are presented as a percentage of the levels of controls (3). (B) EC permeability was determined as previously described (57). One day after transfection with SPRED1, PIK3R2, or scrambled siRNAs, ECs were infected with ANDV or were mock infected. Three days p.i., FITC–dextran and VEGF were added to media in the upper chamber, and the presence of FITC–dextran in the lower chamber was quantitated after 30 or 60 min as a measure of EC permeability (57). Results are expressed as the percent monolayer permeability relative to the basal permeability levels of controls. Experiments in (B) were performed in collaboration with Dr. Gavrilovskaya and Dr. Gorbunova in the lab. Experiments were performed in triplicate and plotted as the means ± SEM using GraphPad Prism 5 software.

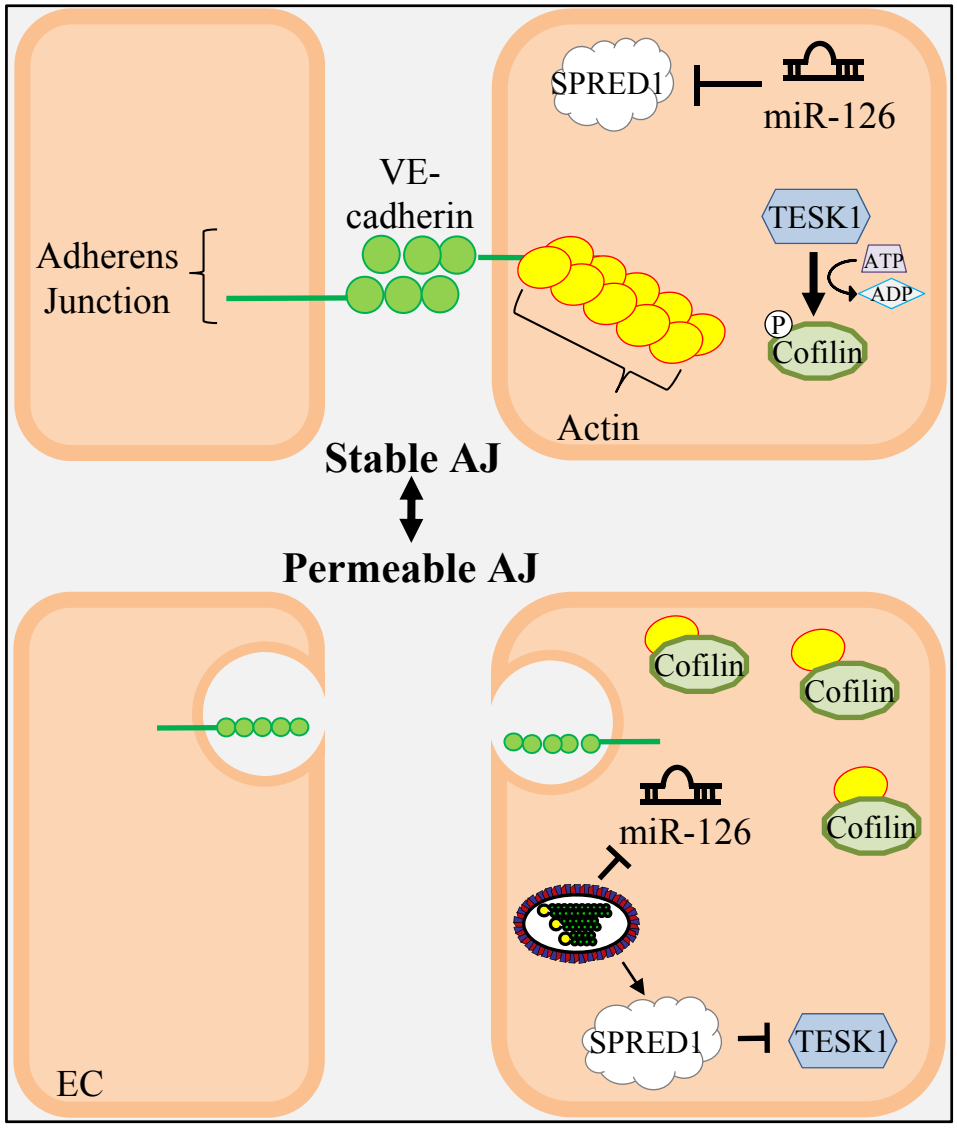

Figure 16: Model of ANDV–Induced Endothelial Cell Permeability. MiR–126 regulates VEGF directed EC responses by downregulating SPRED1 and PIK3R2 (204). ANDV infection of human endothelial cells blocks miR–126 regulation of SPRED1 mRNAs resulting in increased SPRED1 activity. This results in SPRED1 inhibition of TESK1 dephosphorylation of cofilin and increased cofilin actin filament turnover and adherens junction disassembly. The ability of the hantavirus nucleocapsid protein to bind RNA and localize to cytoplasmic P–bodies (133) provides a potential means for the nucleocapsid protein to interfere with the function of miR–126, and other microRNAs, within ANDV–infected endothelial cells.

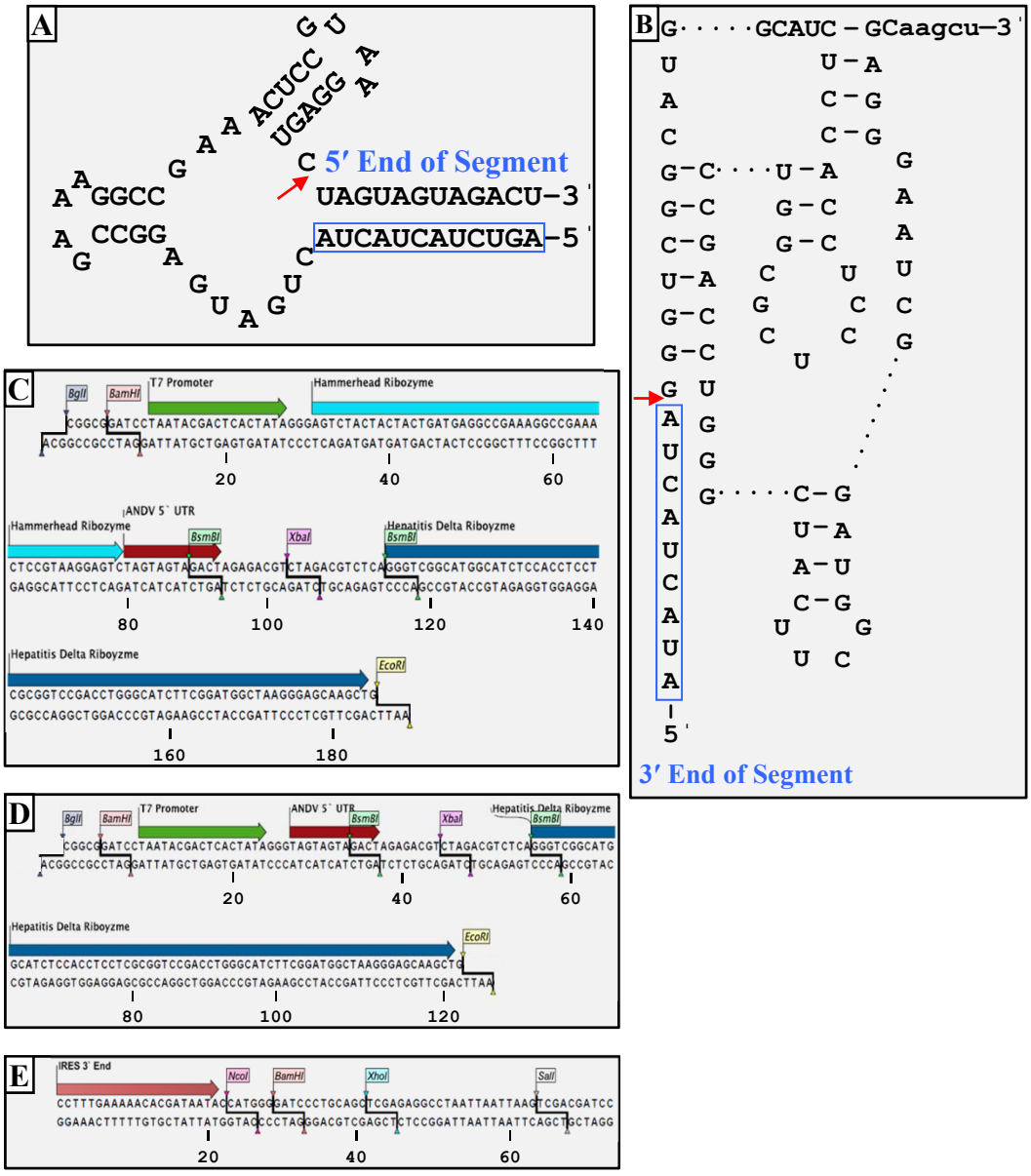

Figure 17 **Reverse Genetics Vectors.** To generate pT7HR2 (C), a cassette consisting of four ligated oligonucleotides containing the T7 RNA polymerase promoter, Hammerhead ribozyme (176) (A), Hepatitis Delta ribozyme (25) (B) (red arrows denote cleavage site), and cloning sites was synthesized and ligated into a BglI–EcoRI digested pET30a vector. (B) pT7HR1 was generated similarly to pT7HR2 except that the Hammerhead Ribozyme was not incorporated into the cassette and the T7 RNA polymerase was positioned so that transcription starts at the first base of the ANDV RNA segments (D). Andes virus L, M, and S anti–genomic cDNAs were generated by PCR using segment–specific oligonucleotides (Table II) containing a BsmBI restriction site on the 5' and 3' ends, digested with BsmBI, and cloned into pT7HR2 or pT7HR1 which had been linearized with BsmBI. ANDV protein expression vectors were generated by cloning of the Pol, G_NG_C, and N protein ORF's flanked by NcoI and BamHI restriction enzyme sites into a NcoI–BamHI digested pTM1 vector (140) (E).

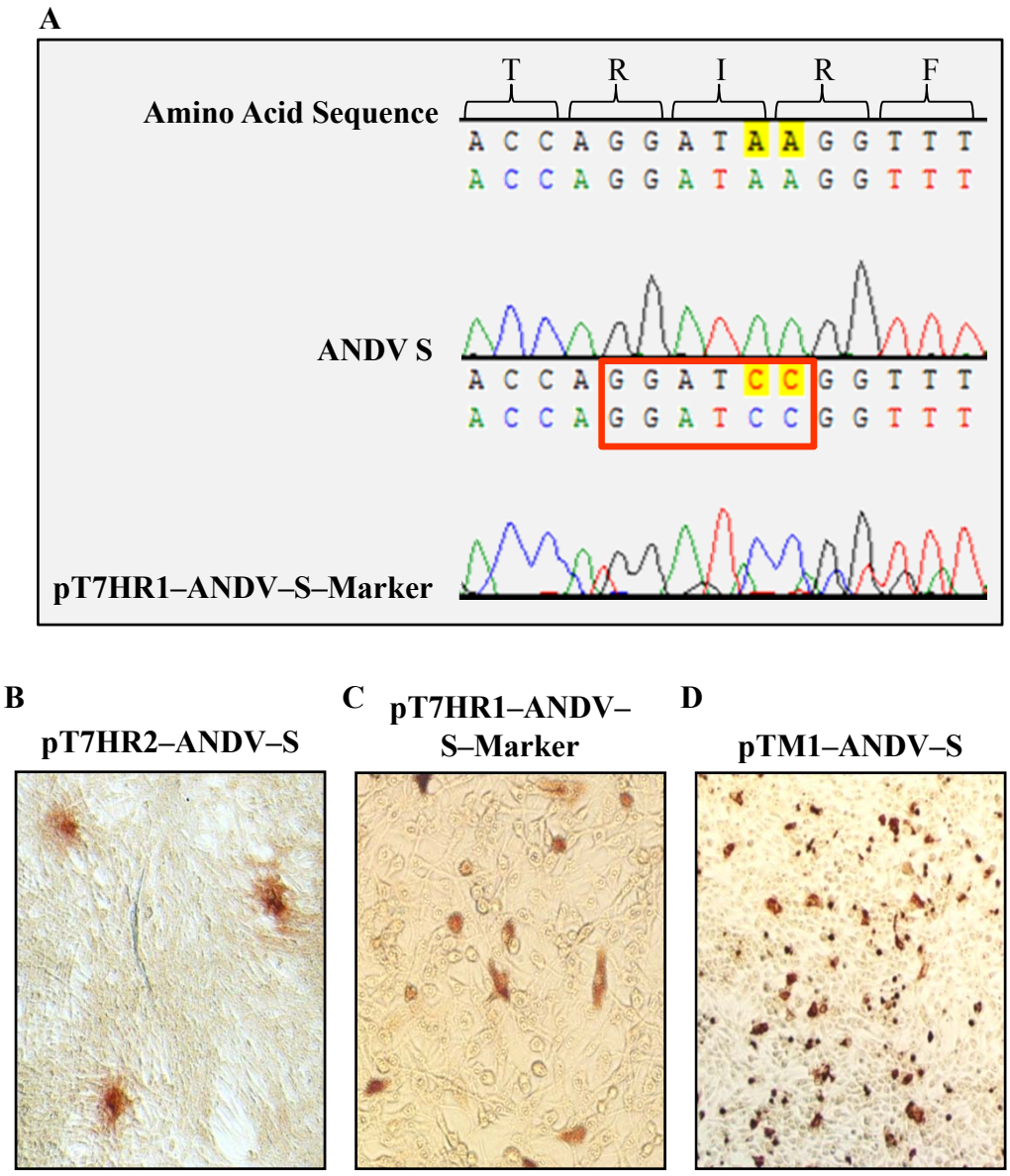

Figure 18 ANDV S Segment Marker Sequence and Nucleocapsid Protein Expression From pT7HR2, pT7HR1, and pTM1 Vectors. (A) To distinguish recombinant ANDV from the wild–type lab strain, a BamHI restriction site was introduced in the N protein ORF within the S segment construct by site–directed mutagenesis (Table II). The introduced silent mutations did not alter the N protein amino acid sequence. To monitor N protein expression from pT7HR2–ANDV–S (B), pT7HR1–ANDV–S–Marker (C), and pTM1–ANDV–S (D), VeroE6 cells were co–transfected with each construct individually and a T7 polymerase expression plasmid, pCAGGS–T7 (155), and assayed by immunoperoxidase staining for N protein 36 hours post transfection (59).

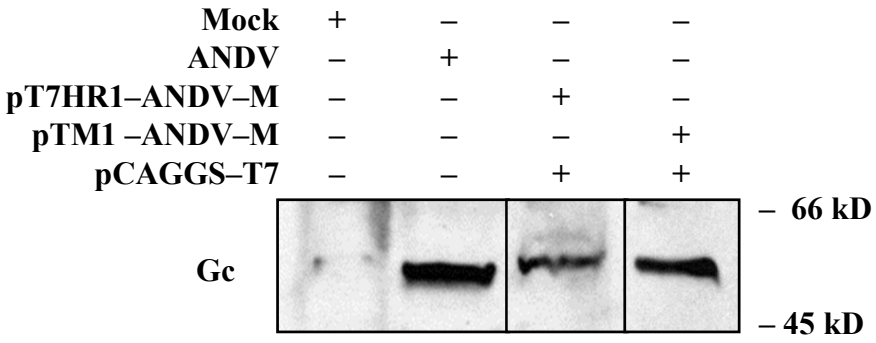

Figure 19 ANDV G_C Protein Expression From pT7HR1 and pTM1 Vectors. VeroE6 cells were co–transfected with pT7HR1–ANDV–M or pTM1–ANDV–M and the T7 RNA polymerase expression plasmid pCAGGS–T7 (155) (1 µg each) using FuGENE 6 transfection reagent. Thirty–six hours post transfection protein expression from ANDV M segment constructs was monitored by Western blot of ANDV G_C. Cells were lysed, protein separated by 12% SDS–PAGE, and G_C detected using a commercial rabbit polyclonal anti–G_C antibody. Lysates from ANDV– and mock–infected HUVECs were similarly resolved by 12% SDS–PAGE and G_C detected by Western blot (60).

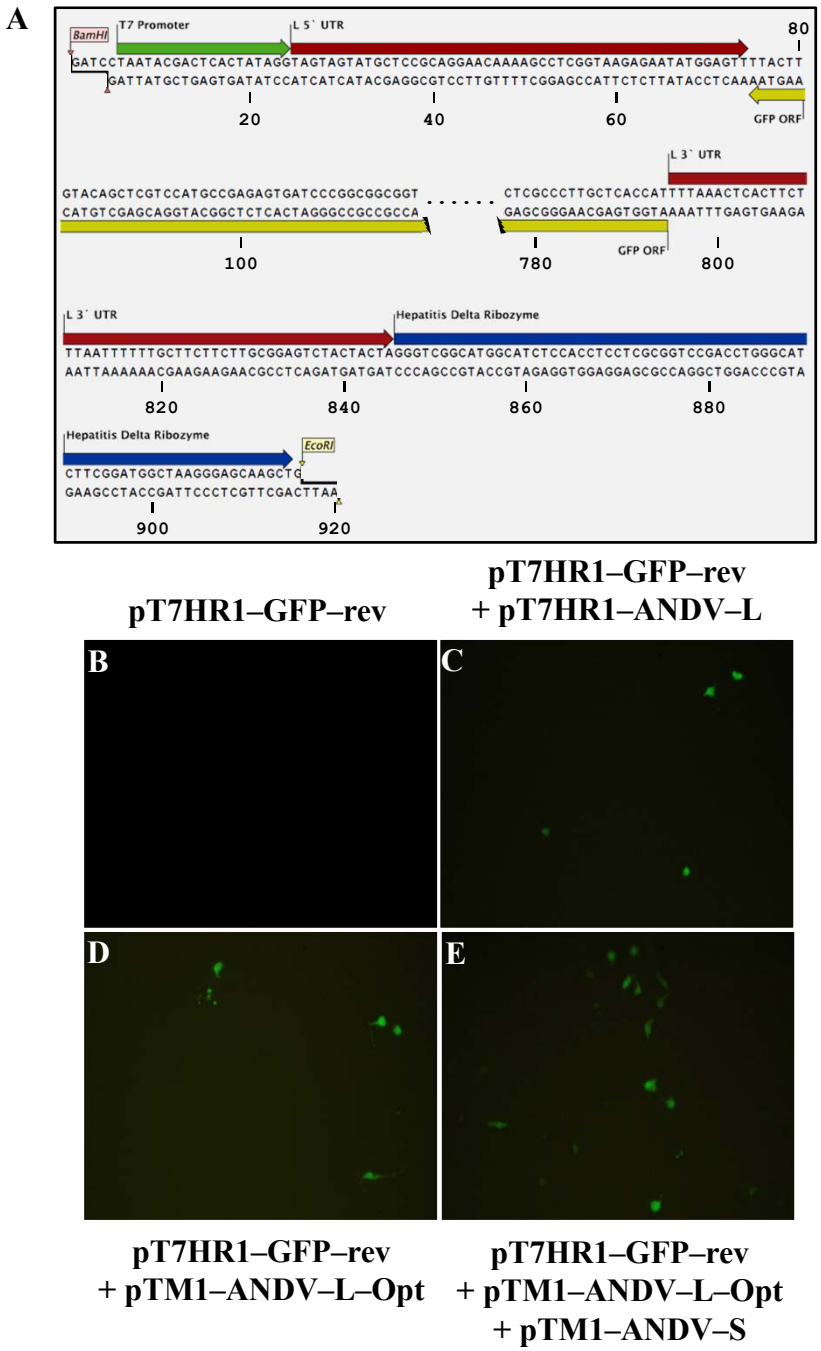

Figure 20 GFP Reporter Activity Following ANDV Polymerase Expression. To evaluate polymerase expression from pT7HR1 and pTM1 vectors, a GFP reporter construct was generated to monitor polymerase activity. The enhanced green fluorescent protein (GFP) ORF was inserted into pT7HR1 in the anti–genomic sense orientation flanked by ANDV L segment UTRs (pT7HR1–GFP–rev) (Figure A). VeroE6 cells were co–transfected with indicated vectors and GFP expression monitored 36 hours post–transfection using an Olympus IX51 microscope.

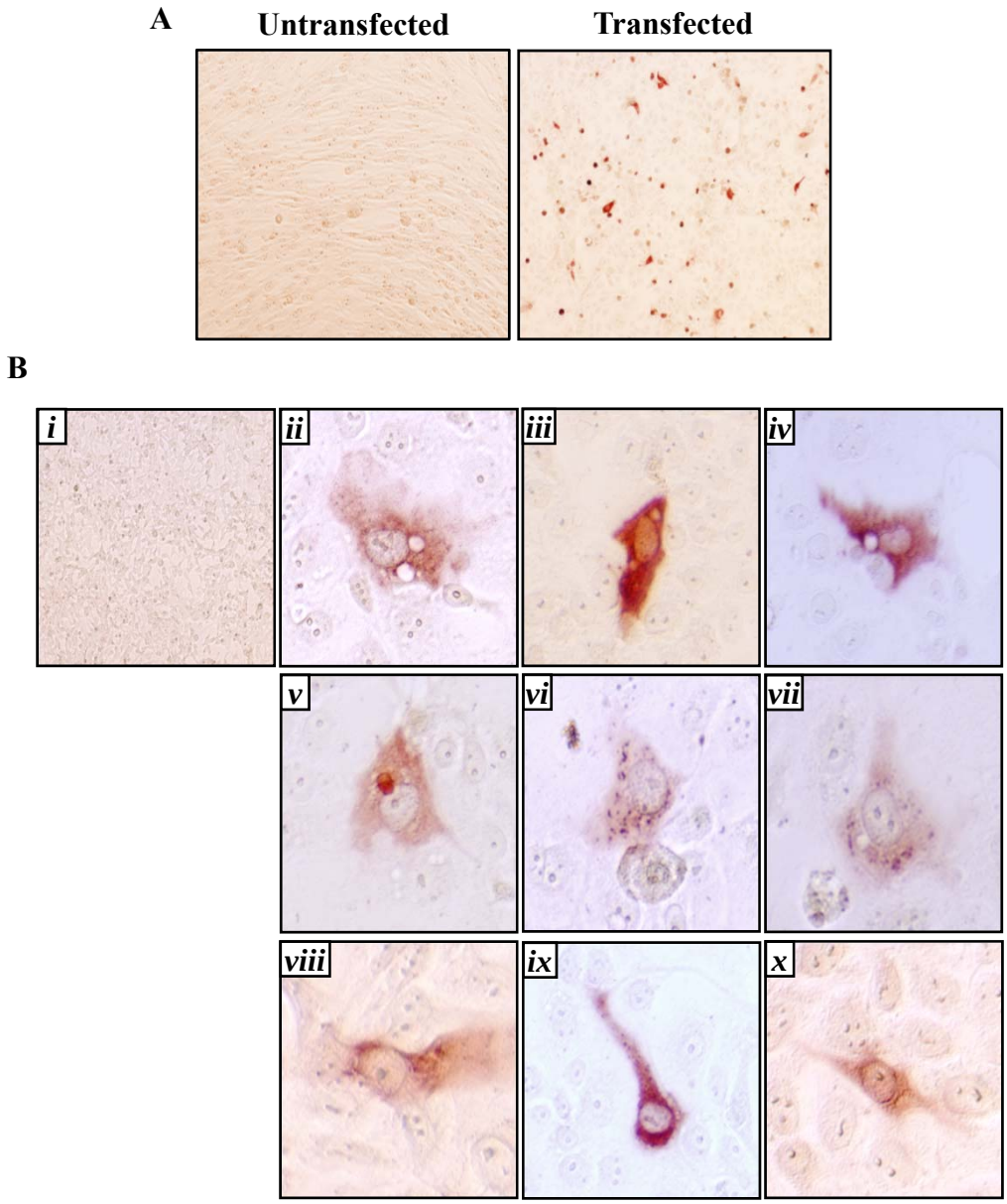

Figure 21 Rescue of ANDV. (A) To rescue recombinant ANDV, VeroE6 cells were co–transfected with equal amounts (1 µg) of pT7HR1–ANDV–L, –M, –S, pTM1 helper constructs, and 1 µg pCAGGS–T7 (155) or untransfected. VeroE6 cells were immunoperoxidase stained for N protein five days post transfection (59). Images are representative of multiple experiments. (B) Five days post transfection, media from untransfected (*i*) and transfected (*ii–x*) VeroE6 cells was passaged on VeroE6 and infected cells detected by immunoperoxidase staining for nucleocapsid protein 24 hours post infection (59). Images are representative of multiple experiments.

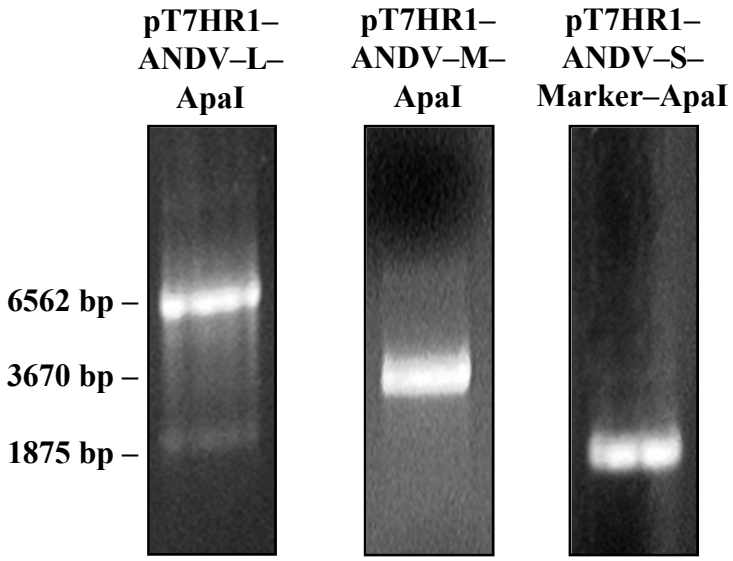

Figure 22 ***In Vitro*** **Transcription of ANDV L, M, and S Anti–genome Sense RNAs.** To generate templates for *in vitro* transcription, a unique ApaI restriction enzyme site was inserted downstream of the 3' UTR within the pT7HR1–ANDV–L, –M, and –S–Marker vectors by site–directed mutagenesis (Table II). Following digestion by ApaI, the linearized vectors were used as templates for T7 polymerase–driven *in vitro* transcription using the mMessage mMachine T7 kit. Reaction products were separated in a 1% agarose gel containing 0.5 μg/μl ethidium bromide.

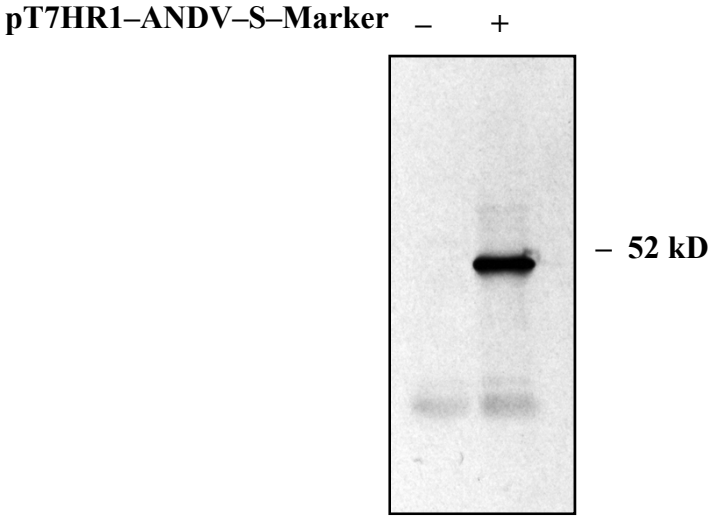

Figure 23 *In Vitro* Transcription/Translation of ANDV Nucleocapsid Protein. To evaluate whether *in vitro* transcribed RNAs could serve as templates for translation, ApaI–digested pT7HR1–ANDV–S–Marker (1 μg) was used as a template for *in vitro* transcription/translation using the TNT Quick Coupled Transcription/Translation System. Samples were resolved by 12% SDS–PAGE and nucleocapsid protein detected by Western blot using anti–nucleocapsid sera (60).

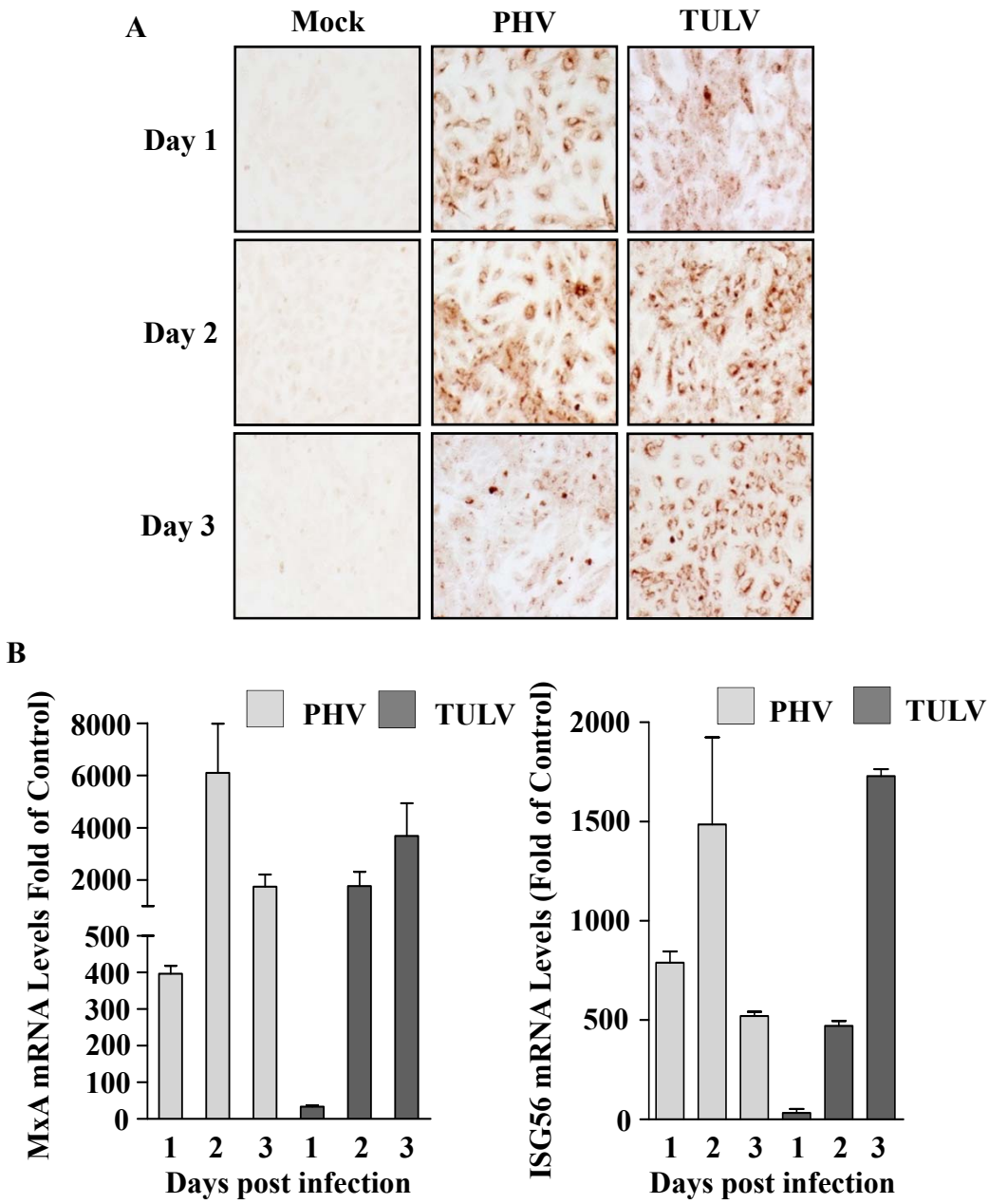

Figure 24 Nonpathogenic Hantavirus Infection of Endothelial Cells (130). HUVECs were infected with either PHV, TULV (MOI of 1) or mock infected. (A) Monolayers were fixed 1, 2, or 3 days post–infection and infected endothelial cells were detected by immunostaining using an anti–nucleocapsid antibody as previously described (55). (B) One day post–infection, total RNA was isolated using the RNeasy kit, cDNAs generated using the First Strand cDNA Synthesis kit, and MxA and ISG56 mRNA levels determined. Induction of ISGs, MxA and ISG56, was monitored by quantitative RT–PCR in duplicate using MxA– or ISG56–specific TaqMan primers and normalized to GAPDH mRNA levels within mock–infected controls (3).